An investigation and proposed integrated interaction law for moist agglomerate.

Ko, Cheuk Yin

An Investigation And Proposed Integrated Interaction Law For Moist Agglomerate

by

Cheuk Yin Ko, B.Eng (Wales)

Thesis submitted to the University of Wales
in candidature for the degree of Master of Philosophy.

Department of Civil Engineering,
University of Wales, Swansea

May, 2007

ProQuest LLC.
789 East Eisenhower Parkway
P.O. Box 1346
Ann Arbor, MI 48106 – 1346

DECLARATION

This work has not previously been accepted in substance for any degree and is not being concurrently submitted in candidature for any degree.

Signed..... .....(candidate)

Date.....16-05-2007.....

STATEMENT 1

This thesis is the result of my own investigations, expect where otherwise stated. Where correction services have been used, the extent and nature of the correction is clearly marked in a footnotes(s).

Other sources are acknowledged by footnotes giving explicit references. A bibliography is appended.

Signed.....(candidate)

Date.....16-05-2007.....

STATEMENT 2

I hereby give consent for my thesis, if accepted, to be available for photocopying and for inter-library loan, and for the title and summary to be made available to outside organisations.

Signed.....(candidate)

Date.....16-05-2007.....

University of Wales Swansea

AN INVESTIGATION AND PROPOSED INTEGRATED INTERACTION LAW FOR MOIST AGGLOMERATE

CHEUK YIN KO, BEng
Thesis submitted for the degree of Master of Philosophy
2007

Summary

In process industries powders are frequently granulated in order to promote their handleability and flowability. During these operations, a liquid binder is usually mixed with the powders to increase their cohesiveness. For binder granulation processed, coalescence and collision of moist agglomerate during the mixing process is the main concern. This thesis considers the computer simulation of moist agglomerate collisions using the discrete element method (DEM). The study is confined to pendular state moist agglomerate, at which liquid bridge is presented as a pendular liquid bridge and interparticle force is modeled as the adhesive contact force, the static liquid bridge force and the dynamic liquid bridge force.

This thesis briefly described various algorithms developed by other researchers for modelling the contact force due to surface adhesion and particle deformation and the pendular static liquid bridge force between mono-sized spherical particles due to hydrostatic pressure deficiency and surface tension.

A theoretical study of the pendular dynamic liquid bridge force between mono-sized spherical particles has been made and it has been found that a numerical instability occures from a DEM simulation with a fine time step size. As a result, an interaction law is proposed and implemented into a DEM code, DEMC, by specifying a minimum separation distance, namely the 'breakdown distance' two particles. It essentially avoids an infinite value of dynamic liquid bridge force predicted by typical expressions derived from lubrication theory for the dynamic liquid bridge, when two particles just contact.

Two dimensional computer simulations of a 'two particles head-on collision test' and 'agglomerate free falling tests' are reported. The results from the former simulation test demonstrate the effectiveness of adding viscous binder to prevent disintegration. Results of the agglomerate free falling test show that a repulsive liquid bridge force occurs between a pair of particles just about to contact. The magnitude of this repulsive force increases with a decreasing breakdown distance. It is also found that an excessive repulsive force occurs for agglomerate with too small value of breakdown distance. As a result, a range of appropriate value of the breakdown distance is recommended such that an appropriate amount of viscous effect is involved from the liquid bridge to the agglomerate system.

Acknowledgements

I wholeheartedly thank my research supervisor Dr. Y. Feng for his guidance and support throughout the entire research project. His invaluable comments, advice and discussion provided at every stage of the research are truly appreciated.

Besides, the helps and suggestions from Dr Colin Thornton, of University of Birmingham, Mr Jun Kato and Miss Su Sam Cheong, my research group colleagues, are also appreciated.

Finally, special thanks to my dear God for his supports, wisdoms and guidance, to my girlfriend and my parents.

CONTENTS

Chapter 1

Introduction

1.1 Background of the Project

Many different industries need to handle very fine grain granules and powders in their production processes, for example: the manufacturer of photocopying machine toner, the pharmaceuticals and even the chemical industries. They have to solve the difficulty on mobilizing and handling of fine particles due to their very light weight and fluffy nature.

Besides the handling problem during the product process, health and safety issue of the worker, working in such industries, is another issue that arises from the properties of fine powders. Fine powders have relatively little inertia and so they tend to travel with the flow and are suspended in the atmosphere for a very long time. The flow can be, for example, a breathe from a human that can bring the fine powders all the way to the lungs without expelling by the mucous along the trachea.

In order to reduce this hazard and difficulty in industrial handling, a liquid binder is often mixed into dry powders to promote a growth of small cluster and hence, an enhancement of process handling and health and safety measure. This introduction of liquid binder is based on the phenomenon of capillary action, which is one of the major components of the formation of small cluster.

1.2 Physical phenomena

Capillary action is an action of a narrow tube to draw liquid upward against the force of gravity. It occurs also as an adhesive intermolecular force among a pair or group of fine particles with closely-packed arrangement.

Agglomeration is a process that uses to promote the flowability and handleability of particulate materials, such as dust agricultural chemical and pharmaceuticals; to reduce the potential pollution hazard that the chemical dust imposes on the environment by, for example, purification of fine coal from ashes and sulphur [C.E.Capes et. al. (1984); R. Petela et al (1995)]; and to recover fine valuable minerals [Z. Sadowsky (1995); C. I. House et al (1992)].

The strength of agglomerate is identified as a combination of van der Waals adhesive forces, electrostatic and magnetic attractive forces, liquid bridge forces, solid sintering and crystallization forces. Among all these forces, adhesive force and liquid binding force are considered as the most important forces that hold particles together (Podczeck 1998).

In order to make use of agglomeration, it is necessary to understand these two forces. For the condition of normal loading, the London van der Waals theory for rigid spheres was established [H.C. Hamaker (1937)] and then followed by the JKR theory [K. L. Johnson et al (1971)], which considers not only the deformation of the area in contact, but also the deformation near the rim of the contact area, and is believed to be more appropriate for larger soft particles. Later, Derjauin [Derjauin et al (1975)] proposed the DMT model, which also takes the adhesive force into account, yet it ignores the deformation outside the contact area. The model is considered to be more appropriate for small hard spheres.

In order to make use of two theories properly, Tabor [D. Tabor (1977)] proposes a parameter (Tabor's parameter (ϕ)) to distinguish these two theories, which involves the comparison of the magnitude of elastic deformation with the range of surface forces. Later, Muller [V. M. Muller et al (1980)] proposed a more distinctive criterion (μ) : for

$\mu < 0.3$ the DMT- theory can be adopted, whereas for $\mu > 3.0$ the JKR- theory applies. These values are more accepted nowadays (F. Podczeck (1998)). Based on Tabor's parameter, D. Maugis (1992) shows that there exists a continuous transition from DMT to the JKR model, as the criterion rises from zero to infinity. He also concluded that it is not physically correct to assume tensile stresses in the area of contact without adhesion force outside (the JKR-theory), or to have no tensile stress inside the area of contact and considerable adhesion force outside (the DMT-theory). Finally, he extended the JKR-theory by using the exact expression of the profile of the sphere instead of the original parabolic approximation to calculate the contact radius under zero loads. His extended theory (Dugdale model) is proved to provide a better fit to experimental results (F. Podczeck (1998)). On the other hand, John and Greenwood (1997) construct an adhesion map which shows the transition between the various models. The elastic deformation of the surface caused by adhesion forces can be neglected, when a sufficiently high load is present. This implies that the Hertz theory [H. Hertz (1881,1896)] can be a reasonable model for high loading cases. In contrast, the JKR-model and the DMT-model could be considered as more appropriate for a low load case. For low loading cases that the elastic deformation will be small compared to the range of surface force, the DMT- theory could be applied. While for the case where elastic deformation caused by the adhesion forces is relatively large, in another words for softer materials, the JKR theory should be applied (F. Podczeck (1998)).

Besides the adhesive force due to elastic deformation of particle, the strength of an agglomeration will be further increased by the capillary effect of moisture, which is present in the gaps between particulates. A meniscus shaped liquid bridge can be formed by the influence of capillary action. Therefore, different theories were developed in the literature to resolve the profile of this meniscus shape, and hence the static liquid bridge forces acting between surfaces or spherical particles.

Young's Laplace equation is, to the best of the author's knowledge, the most common equation that is used to establish the profile of a liquid bridge. In order to solve this equation, it is often assumed, e.g.: G. Lian et. al. (1993), that the volume of liquid is

small to a degree that the influence of gravity can be neglected. Together with the approximation by Fisher (Fisher 1926), who proposed a simpler approach to estimating the liquid bridge force, the meridional profile of the liquid-gas interface is approximated as an arc of a circle, named the toroidal approximation. Consequently, the meridional profile can then be represented by the two principal radii of curvature.

No matter which approximation is concerned, the profile of liquid bridge and the magnitude of static liquid bridge force are also affected by other parameters, namely contact angle, filling angle, volume of the liquid bridge, etc. Authors [Weigert and Ripperger (1999), J. Meseguer et al (2003), Vafaei and Podowski (2005)] proposed certain findings and empirical equations on those parameters, so as to enhance the estimation of liquid bridge force. On the other hands, authors [Dai and Lu (1998), Pepin et al (2000), Pitois et al (2001), G. Lian et al (1993)] also reported the maximum elongation that a pendular liquid bridge can sustain. Among all these investigations, a widely accepted critical separation distance (rupture distance, S_c) is published by G. Lian et al (1993), in which he proposed that the rupture distance is given by the cube root of the liquid bridge volume.

Besides of the static liquid bridge force, authors, for example: [Y. Tatemoto et al (2005),S. S. Hsiau et al (2003), S.C. Yang at al (2001)] take the dynamic effect of the liquid bridge into account, which is the viscous force of the liquid in a dynamic particle collision system. These authors derive the governing equation of liquid viscous force from lubrication theory. This model may predict an infinite value of dynamic viscous force as the separation distance between two particle surfaces becomes zero. As some experimental results (Meurisse et al (2006)) show that there is a dramatically change of liquid bridge force as the separation distance approach zero, from attractive force to repulsive force.

1.3 Numerical Modeling

As granulation is one of the engineering problems that takes the discontinuous nature of materials and liquid binder behavior into account, it is necessary to establish an interaction law, either numerically or empirically, for the integration of both solid phase and liquid phase.

For numerical analysis, mathematical description of the above examples ought to take into account the shape, size and mass of individual particles, and also the interaction between the individual particles and liquid bridge. Depends on the nature of material being considered, different numerical analysis methods are used. For continuum problems, e.g.: heat transfer, a set of partial differential equations for conversation of mass, energy and momentum are used. For discontinuum, e.g.: granulation, a sets of governing equations for different particles are coupled through inter-particles interactions. The resulting global set of coupled governing equations describes the behavior of the particulate system as a whole.

Generally speaking, the mathematical formulation of problems with a discontinuum nature involves the interaction law between particles and balance principles. Analytical solutions of these equations are rarely available (A. Munjiza (2004)) and approximate numerical solution are sought instead.

For experimental analysis, there are also difficulties to experimentally obtain the behavior of some sophisticate discontinuum system. Such as a system with two particles squeeze an interstitial liquid bridge until they touch, deform slightly and eventually rebound from each other. This is believed, by the author, that the experiments for this 'load-deform-unload' process would be very complicated and expensive to obtain. The complicity comes from the precision of sample preparation, i.e.: the way to prepare identical elastic solid surfaces and identical profile of liquid bridge along different series of tests; experimental methodology, the way to measure the contact force and amount of elastic deformation of two surface; and unpredictable deformation of two solids surface due to inhomogeneous of materials.

As a matter of this, instead of doing experiment, a more economic and with reasonably accurate method is needed to find out the behavior of those engineering problems.

Numerical analysis provides a way to examine engineering problems. It does not seek exact answers, because they are sometimes impossible to obtain in practice. Instead, much of numerical analysis is concerned with obtaining approximate solutions while maintaining reasonable bounds on errors (A. Munjiza (2004)).

Depending of the nature of engineering problems, there are different types of numerical analysis available. They can be classified into continuum and discontinuum (Munjiza (2004)). The most advanced and often used method for continuum problems are the Finite element Method (FEM). This method is based on the discretisation of a domain into finite sub-domains, also called finite elements. These elements share nodes, edges and surfaces. Balancing principles are then imposed into the method in averaged form. For instance based on the equilibrium of nodal forces, the governing partial differential equation can be effectively replaced with a system of simultaneous algebraic equations.

The discontinuous nature of problems can be taken care by either Discontinuous Deformation Analysis (DDA) or Discrete Element Method (DEM). These methods are designed to handle contact situations for a large number of irregular particles. DDA is more suitable for static problems, while DEM is more suitable for problems involving transient dynamics until the state of rest or steady state is achieved.

Discrete Element Methods (DEM) is a computational simulation, which is initiated by locating all particles in a certain domain, followed by giving them initial conditions (e.g.: velocity, force). Then the forces which act on each particle are computed from the initial data and the relevant contact laws. All these forces are added up to find the total force acting on each particle

A time integration method is then employed to compute the change in the position and the velocity of each particle during a certain time step from Newton's law of motion.

After that, the new positions are used to compute the forces during the next step, and this loop is repeated until the simulation ends (Munijza (2004)).

Due to the discontinuous nature that agglomerate involves, different authors developed some DEM based numerical models to simulate the behavior of wetted particulate in vibrated bed [Y. Tatemoto et al (2005), S. S. Hsiau et al (2003), S.C. Yang at al (2001)].

1.4 Problem encounter in Wet agglomerate DEM simulation.

In a DEM analysis, the equilibrium equation governs the linear/nonlinear response of a system is expressed as:

$$m\ddot{U}+c\dot{U}+kU=F \qquad (1.1)$$

where m, c and k are the mass, damping and stiffness matrices; U, $\dot{U}$ and $\ddot{U}$ are the displacement, velocity and acceleration vectors; and F is the vector of total loadings. $m\ddot{U}$, $c\dot{U}$, kU are the inertia forces, damping forces and restoring forces, respectively, and all of them are time-dependent. Therefore, the principle of dynamic analysis is to carry out a time-history analysis to seek for the response of the system within a time period.

Direct integration methods utilize the finite difference approximation to replace the time derivatives that appear in the equation (1.1), i.e. the accelerations and velocities are represented by the differences of displacement at various time instances (Cook R. D. et al (1989)). The accuracy of these time integration schemes is based on the size of the time step, the finer time step size is used, the higher accuracy can be obtain. However, the degree accuracy is compensated by a great computational demand and simulation time. As a result, time steps size for DEM simulation is always chosen to be as large as possible with the maximum value of time step size Δt available for time integration, which is called critical time step

$$\Delta t_{cr} = \frac{l}{c}$$

where $c \approx \sqrt{\frac{E}{\rho}}$, is the wave speed; in which E is the Young's modulus; ρ is the density; and l is the effective length of the smallest element used in the analysis; and If $\Delta t > \Delta t_{cr}$, the solution will grow unboundedly and causes erroneous time-history solutions. As a result, this method could be computationally expensive due to this restriction. However, providing that the stability criterion is satisfied, a satisfactory accuracy is usually obtained.

In order to simulation the wet agglomerate, it is necessary to understand the theories involved in different stages of the 'load-deform-unload' system. This system involves the solid to solid contact, squeezing a liquid bridge and stretching a liquid bridge, and the theories for each of these components are discussed in later chapters. Whereas a detail investigation of the system is carried out, a relatively small time step size is needed for wet agglomerate DEM simulations.

However, for wet agglomerate, when two particles touch each other, the time integration leads to an unstable simulation results because an infinite liquid bridge repulsive force is predicted from a theoretical equation. In order to solve this numerical problem of DEM simulations and obtain a more realistic model for simulation, some relevant theoretical and experimental results of the behavior of liquid bridge are reviewed in this project. In addition, different numerical methods, FEM and DEM, are used to tackle the 'load-deform-unload' problem. Eventually, a combination of theoretical theories, relevant experimental results and numerical analysis results is carried out, so as to propose an integrated interaction law for the load-deform-unload system.

Although the above mentioned theories and experimental results are based on the investigations of the behavior of liquid bridge on sphere particles in three dimensional cases, for simplicity, a two dimensional modeling is used in this work instead of three dimensional modeling. For this reason, several assumptions have made.

A simply application of this proposed interaction law of moist particles is carried out by implementing the law and simulating a moist agglomerate undergoing a free falling test.

1.5 Presentation Order

In Chapter 2, the theory of Hertz (K.L. Johnson 1985) for elastic deformation of spheres and the theory of K. L. Johnson et al (1971) (JKR-model) and a brief explanation of B. V. Derjaguin et al (1975) (DMT-model) are presented.

Chapter 3 includes a review of the previous research work on a pendular liquid bridge, which includes the method of resolving liquid bridge profiles and methods of evaluating the static liquid bridge forces. Theories behind the dynamic liquid bridge viscous forces are also presented.

Chapter 4 presents some relevant experimental results from the literature on the behavior of a liquid bridge at a small separation distance between two particles and the investigation of suitability of numerical method FEM to tackle the 'load-deform-unload' system by using an FEM program 'Elfen'. Eventually, a method is proposed in this project. The concept of behind this proposed method is based on the combination of those theoretical, experimental and numerical results, which is present in this chapter as well.

Chapter 5 presents the assumptions for two dimensional modeling and the structure of a DEM code, (DEMC) developed during this project. Moreover, the results of moist agglomerate free-falling test will be presented in chapter 6.

Finally, chapter 7 provides some concluding remarks concerned with criteria for using the proposed equations and some recommendations for further research.

References:

F. Podczeck (1998), Particle-particle adhesion in pharmaceutical powder handling, 1st edition, Imperial college Press.

C.E. Capes, K. Darkovich (1984), A survey of oil agglomeration in wet fine coal processing, Powder Technol. 40 , pp. 43-52.

R. Petela, B. Ignasiak, W. Pawlak (1995), Selective agglomeration of coal: analysis of laboratory batch test result, Fuel 74(8): 1200-1210.

Z. Sadowsky (1995), Selective spherical agglomeration of fine salt-type mineral particles in aqueous solution, Colloid Surf. 96: 277-285.

C. I. House, C. J. Veal (1992), Spherical agglomeration in minerals processing in: R. A. Williams (Ed.), Colloid and Surface Engineering: Application in the Process Industries, Oxford, Boston, pp. 189-212.

H. C. Hamaker (1937), The London-van der Waals attraction between spherical particles, Physica, 4:1058-1072.

K. L. Johnson, K. Kendall and A. D. Robert (1971), Surface energy and the contact of elastc solids, Proc. R. Soc. Lond., A324: 301-13.

B. V. Derjaguin, V. M. Muller and Y. P. Toporob (1975), Effect of contact deformations on the adhesion of particles, J. Colloid Interface Sci., 53:314-26.

D. Tabor (1977), Surface forces and surface interactions, J. Colloid Interface Sci., 58:2-3.

V. M. Muller, V. S. Yushchenko and B. V. Derjaguin (1980), On the influence of molecular forces on the deformation of an elastic sphere and its sticking to a rigid plane, J. Colloid Interface Sci., 77: 91-101.

D. Maugis (1992), Adhesion of spheres: the JKR-DMT transition using a Dugdale model, J. Colloid Interface Sci., 150:243-69.

S. C. Yang, S. S. Hsiau (2001), The simulation of powders with liquid bridges in a 2D vibrated bed, Chemical Eng. Sci., 56: 6837-6849.

Y. Tatemoto, Y. Mawatari, K. Noda (2005), Numerical simulation of cohesive particle motion in vibrated fluidized bed, Chem. Eng. Sci., 60:5010-5021.

S. S. Hsiau, S. C. Yang (2003), Numerical simulation of self-diffusion and mixing in a vibrated granular bed with the cohesive effect of liquid bridges, Chem. Eng. Sci, 58:339-351.

S. H. Liu, D. A. Sun, Yisen Wang (2003), Numerical study of soil collapse behaviour by discrete element modeling, Computer and Geotechnics, 30:399-408.

S. H. Liu and D. A. Sun (2002), Simulating the collapse of unsaturated soil by DEM, Int. J. Numer. And Meth. Geomech, 26: 633-646.

M. J. Jiang, S. Leroueil, J.M. Konrad (2004), Insight into shear strength function of unstarated granulates by DEM analyses, Computer and Geotechnics, 31: 473-489.

G. Lian, C.thornton and M. J. Adams (1993), A theoretical study of the liquid bridge forces between two rigid spherical bodies, J. of Colloid and interface Sci. 161:138-147.

S. Vafaei and M.X. Podowski (2005), Analysis of the relationship between liquid droplet size and contact angle, Advance in Colliods and interface Sci., 113:133-146.

J. Meseguer, J. L. Espino, J. M. Perales, A. Laveron-Simavilla (2003), On the breaking of log, axisymmetric liquid bridges between unequal supporting disks at minimum volume stability limit., European Journal of Mechanics B/Fluids, 22 355-368.

T. Weigert, S. Ripperger (1999), Calculation of the Liquid bridge volume and Bulk Saturation from the half-filling Angle, Part. Syst. Charact., 13: 238-242.

M. H. Meurisse and M. Querry (2006), Squeeze effects in a flat liquid bridge between parallel solid surfaces, J. of Tribology, 123, 575-584.

F. Podczeck (1998), Particle-Particle adhesion in Pharmaceutical Powder Handling, World scientific publishing Co. Ltd, Imperial College Press,

S. Antonyuk, M. Khanal, J. Tomas, S. Heinrich and L. Morl (2006), Impact breakage of spherical granules: Experimental study and DEM simulation., Chemical Engineering and Processing, 45, 838-856.

J. Fu, M. J. Adams, G. K. Renolds, A.D.Salman & M.J. Hounslow (2004), Impact deformation and rebounds of wet granules, Powder Technology,140: 248-257.

A. Munijza, (2004), The combined Finite-Discrete element Method, John Wiley & Sons, Ltd

Chapter 2

Contact Mechanics

2.1 Background

When two solid bodies are brought into contact, even under a very small loading, there will be a deformation in the vicinity of their contact point. Even so, these two bodies touch over an area which is considered to be comparably small to the dimensions of the two bodies. The theory of contact mechanics is necessary to establish the shape of the area of contact and eventually the deformation and stresses in both bodies in the vicinity of the contact region.

The Hertz theory (H. Hertz, 1896) provides the first satisfactory analysis of the stresses at the contact of two elastic particles. It simplifies each body as an elastic half-space loaded over a small elliptical region of its plane surface, and highly concentrated contact stresses are treated separately from the general distribution of the stress in the two bodies which arises from their shapes and the way in which they are supported.

However in reality, for solid particles in contact, not only the elastic interaction force occurs inside the contact region, but also the Van der Waals attraction at the place out of contact region. In the transition region from this attraction force to repulsive force, a short range molecular attraction force arises, namely adhesion force. Therefore theories are developed to consider the reciprocal influence between the contact deformation and surface adhesion of elastic spheres. For example, the Johnson-Kendall-Roberts Model (JKR) extended the Hertz theory to adhering elastic spheres by saying that the contact

force is not simply the sum of the applied load and the adhesion force. K.L. Johnson et al (1975) derived an expression for the out of balance applied load in relation to the adhesion force through an energy balance approach. Later on, Deryaguin et al (1975) criticised the JKR-theory and developed another theory to describe the deformation of surface during adhesion, which is known as the "Deryaguin-Muller-Toporov-theory (DMT)".

Later on, Tabor (F. Podczeck (1998)) introduced an indicator ϕ, which is a measure of the magnitude of elastic deformation compared with the range of surface forces, to distinguish the above mentioned two models. Muller et al (1980) derived a similar criterion μ, which gives more distinctive limiting values for the two theories. Besides, Muller et al (1980) also stated that the JKR-theory is more suitable for low surface free energy materials, while DMT-theory should be considered for materials comprising a high surface free energy. This is agreed with the conclusion drawn by (Derjaguin et al 1978), which concluded that the JKR-theory applies mainly for very soft materials and the DMT-theory appears to be more suitable for rather rigid materials.

As mentioned previously, the main objective of this project is to propose an interaction law for the 'load-deform-unload' system solution. In order to minimise the influence of solid-solid contact on the squeezed liquid bridge behaviour, it is reasonable to choice a softer, lower young modulus, solid for this project. The JKR-theory is used in this project.

In this chapter, the Hertz theory for elastic deformation of spheres, the JKR-theory and DMT-theory are presented.

2.2 Hertz Theory

The Hertz theory provides the first satisfactory analysis of the stresses at the contact of two elastic particles, which is based on a few assumptions as listed below (K.L. Johnson 1985):

i) Each solid is elastic.
ii) Hooke's law holds.
iii) The material of the contacting bodies is homogeneous.
iv) The surfaces are frictionless.
v) The dimension of contact area must be small compared with the dimension of each body and with the relative radii of curvature of the surface.

These assumptions ensure that the stresses field is not seriously influenced by the proximity of its boundaries to the highly stressed region; the strains in the contact region are sufficiently small to lie within the scope of the linear theory of elasticity and in view of the idealisation of each body as a half-space with a plane surface.

Further, the frictionless assumption leads to the fact that there is only the normal pressure transmitted between the surfaces. The normal tractions are taken to act parallel to the common normal of the two surfaces at the point of contact and the tangential tractions, which act in the x-y plane, are ignored.

2.2.1 Geometry of Hertz Theory

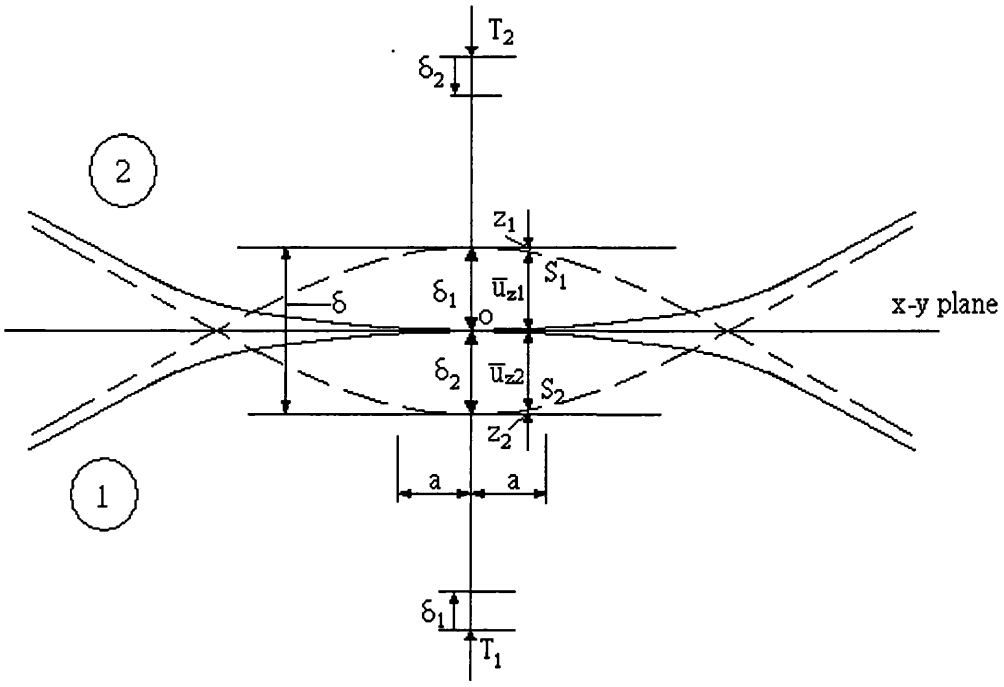

Figure 2. 1: Hertz Theory Illustration

The surfaces of the elastic solids in contact are considered to be topographically smooth at both micro and macro scales. This means that the microscopic surface irregularities, which would lead to discontinuous contact or high local contact pressure, are ignored and the macroscopic profile of the surfaces is continuous up to the second derivative in the contact region (Johnson (1985)). Thus, the profile of each surface close to the point of contact can be approximated by an expression of the form (higher order terms in x and y are neglected):

$$z = Ax^2 + By^2 + Cxy + ... \qquad (2.1)$$

By choosing the appropriate orientation of the x and y axes so that the term xy disappears, the expression can be written as

$$z_1 = \frac{1}{2R_1'} x_1^2 + \frac{1}{2R_1''} y_1^2;$$
$$z_2 = -\left(\frac{1}{2R_2'} x_2^2 + \frac{1}{2R_2''} y_2^2 \right); \quad (2.2)$$

where $R'_{1,2}$ and $R''_{1,2}$ are the minimum and maximum principal radii of curvature of the surface at the point of contact for surface 1 and 2 respectively. The separation between the two surfaces is then given by $h = z1 - z2$. With the expression of equations (2.1) and (2.2), it can be written as

$$h = z1 - z2 = Ax^2 + By^2$$
$$h = \frac{1}{2R'} x^2 + \frac{1}{2R''} y^2 \quad (2.3)$$

where A and B are positive constants and R' and R'' are the principal relative radii of curvature.

For the contact between solids of revolution, the minimum and maximum principal radii of curvature are the same (i.e. $R'_{1,2} = R''_{1,2} = R_{1,2}$), and the contact area between the two surfaces upon loading are circular. For the contact between two cylinders with their axes parallel, $R'_{1,2} = R_{1,2}$ and $R''_{1,2} = \infty$, and the contact area extents from a line to a narrow strip parallel to their axes upon loading.

2.2.2 Geometry of Deformation

When a normal load P is applied to two curve-shaped solids, the deformation at the contact is illustrated in Figure 2.1.

During compression, two distant points T1 and T2 move towards O, parallel to the Z-axis, by displacements of δ_1 and δ_2 respectively. This causes an overlap between the undeformed solids where the profiles are shown by the dotted lines. However, due to the contact pressure, the solid surfaces are displaced parallel to the z-axis by an amount of

$\bar{u}_{z1}$ and $\bar{u}_{z2}$ respectively into the bodies. The surface points S1 and S2 are given by equation (2.3), and will coincide within the contact surface after deformation when

$$\bar{u}_{z1} + \bar{u}_{z2} + h = \delta_1 + \delta_2 = \delta \tag{2.4}$$

Making use of the expression in equation (2.3) , this can be written as

$$\bar{u}_{z1} + \bar{u}_{z2} = \delta - Ax^2 - By^2 \tag{2.5}$$

If the surface points S1 and S2 lie outside the contact area after deformation, it follows that

$$\bar{u}_{z1} + \bar{u}_{z2} > \delta - Ax^2 - By^2 \tag{2.6}$$

Therefore, when solving for normal elastic displacements on the solid surfaces, equations 2.5 and 2.6, formulated by Hertz, need to be satisfied within and outside the contact area (K.L. Johnson (1985)).

2.2.3 Elastic contact between solid of Revolutions

The geometry of a solid of revolution is generated by revolving a plane object about an axis, namely the z-axis, and is axially symmetric. It is normally expressed by a cylindrical coordinate system with axes of r, θ and z. If the geometry, support conditions, loading and material properties are independent of θ, the displacements and stresses are also independent of θ, and the circumferential displacement u_θ is zero. There will only have radial displacement u_r, axial displacement u_z and non-zero stresses $\sigma_z, \sigma_r, \sigma_\theta$ and τ_{zr} (K.L. Johnson (1985)).

For the case of solids of revolution, the minimum and maximum principal radii of curvature of the solids are equal, i.e. $R'_{1,2} = R''_{1,2} = R_{1,2}$. When brought into contact by an applied normal load at the point O, a circular contact area is formed with radius a.

Therefore, it can be seen from equation (2.3) that A=B=$\frac{1}{2}\left(\frac{1}{R_1}+\frac{1}{R_2}\right)$. For the condition with the contact region to be satisfied, the expression in equation (2.5) can be written as

$$\bar{u}_{z1}+\bar{u}_{z2}=\delta-\frac{1}{2}\left(\frac{1}{R_1}+\frac{1}{R_2}\right)r^2 \tag{2.7}$$

where $\frac{1}{R}=\left(\frac{1}{R_1}+\frac{1}{R_2}\right)$ is the relative radius of curvature.

The pressure exerted between two contacting frictionless elastic solids of revolution is given by Hertz as

$$p(r)=p_o(1-r^2/a^2)^{1/2} \tag{2.8}$$

where p_o is the maximum pressure and induces normal displacements:

$$\bar{u}_z=\frac{1-\nu^2}{E}\frac{\pi p_o}{4a}\left(2a^2-r^2\right) \qquad r<<a \tag{2.9}$$

The pressure acting on the second body is the same as the pressure acting on the first body. The effective modulus for the two bodies can be written as

$$\frac{1}{E^*}=\frac{1-\nu_1^{\,2}}{E_1}+\frac{1-\nu_2^{\,2}}{E_2} \tag{2.10}$$

Substituting the expressions of $\bar{u}_{z1}$ and $\bar{u}_{z2}$ into equation (2.7), the following expression is obtained

$$\frac{\pi p_o}{4aE^*}\left(2a^2 - r^2\right) = \delta - \frac{1}{2}\left(\frac{1}{R_1} + \frac{1}{R_2}\right)r^2 \tag{2.11}$$

By considering the centre, r=0, of the contact point in equation (2.11), the total overlap between the two bodies is given by

$$\delta = \frac{\pi p_o a}{2E^*} \tag{2.12}$$

With the expression of $\delta = \frac{a^2}{R}$ the contact radius can be written as:

$$a = \frac{\pi p_o R}{2E^*} \tag{2.13}$$

In a practical problem, the total load is usually specified, so it is convenient to establish the relationship between the total load (P) with the radius of the contact circle (a) and mutual approach (δ) by integrating the pressure over contact area:

$$P = \int_0^a p(r) 2\pi r dr = \frac{2}{3} p_o \pi a^2 \tag{2.14}$$

Therefore, the contact force P, mutual and contact radius a can also be expressed in terms of the total force as

$$a = \left(\frac{3PR}{4E^*}\right)^{1/3} \tag{2.15}$$

$$\delta = \frac{a^2}{R} = \left(\frac{9P^2}{16RE^{*2}}\right)^{1/3} \tag{2.16}$$

$$p_o = \frac{3P}{2\pi a^2} = \left(\frac{6PE^{*2}}{\pi^3 R^2}\right)^{1/3} \qquad (2.17)$$

Equations 2.15- 2.17 provide a relationship of the total applied load with the contact width, the overlap/approach and the maximum pressure respectively, provided that the radii and material properties of the two solid bodies are known.

2.3 The Johnson-Kendall-Roberts Model (JKR)

Now if the two bodies are considered as adhesive, an additional attractive force will apparently act between the two contact bodies. K. L. Johnson et al (1975) argues that because of the additional attractive adhesion force, the equilibrium contact area between the two bodies would increase and it could be regarded as corresponding to an equivalent hertzian force P_1. They tried to model such contact deformations under the assumption that two perfectly elastic spheres, whose surfaces are smooth, are in contact.

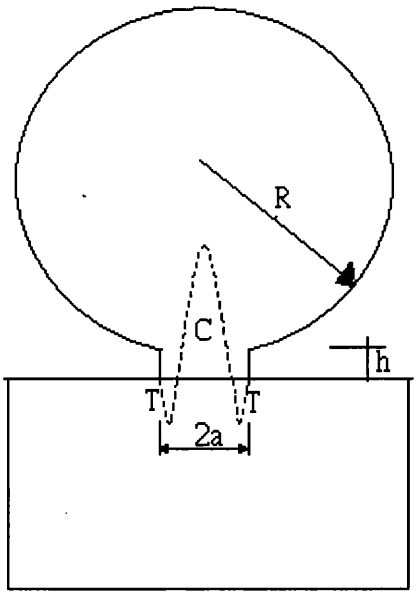

Figure 2. 2: Stress distribution and formation of a neck during the contact of an elastic sphere with a half-space.

The Hertz theory assumes that the contact stress is compressive over the whole area of contact. However, the JKR theory is based on the assumption that compressive stress occurs only in the centre of the contact point, while the tensile stress occur at the outer circle of the contact area. Figure 2.2 illustrates for a sphere of radius R adhering to a half-space. It is important to note that the adhesion forces operate only within the deformed area of contact, (F. Podczeck (1998)).

In order to take the adhesive force into consideration, an extra term is superimposed into the pressure distribution equation, which yields

$$p(r) = p_o\left(1-r^2/a^2\right)^{1/2} + p_o'\left(1-r^2/a^2\right)^{-1/2} \qquad (2.18)$$

Integrating the second term in equation (2.18) to obtain a normal displacement (Johnson (1985)), for the 'adhesive term':

$$\bar{u}_z = \frac{\pi p_o' a}{E^*} \qquad (2.19)$$

Substituting (2.19) into (2.11) to get the mutual approach (δ), with r=0, to attain the mutual approach of the second term in equation (2.18)

$$\delta = \frac{\pi p_o' a}{E^*} \qquad (2.20)$$

The total δ will be the summation of equations (2.12) and (2.20)

$$\delta = \frac{\pi p_o a}{2E^*} + \frac{\pi p_o' a}{E^*} = \frac{\pi a}{2E^*}\left(p_o + 2p_o'\right) \qquad (2.21)$$

In order to estimate p_o', K. L. Johnson et al (1971) considered the total surface energy (U_T), which is a sum of elastic strain energy stored (U_E) in the two bodies by the compressive pressure (2.18) and surface energy by the adhesive force (U_S).

$$U_E = \frac{\pi^2 a^3}{E^*}\left(\frac{2p_o^2}{15} + \frac{2p_o p_o'}{3} + p_o'^2\right) \tag{2.22}$$

$$U_S = -2\gamma\pi a^2 \tag{2.23}$$

The total free energy of the system now is:

$$U_T = U_E + U_S \tag{2.24}$$

Consider the variation in the total energy with contact radius (a) and keeping the overall relative displacement of the two bodies (δ) constant:

$$\frac{\partial U_T}{\partial a} = \frac{\partial U_E}{\partial a} + \frac{\partial U_S}{\partial a}$$

$$\frac{\partial U_T}{\partial a} = \frac{\pi^2 a^2}{E^*} p_o' - 4\gamma\pi a$$

For equilibrium $\frac{\partial U_T}{\partial a} = 0$ gives

$$\frac{\pi^2 a^2}{E^*} p_o'^2 = 4\gamma\pi a$$

$$p_o' = \sqrt{\frac{4E^*\gamma}{\pi a}} \tag{2.25}$$

Eventually, the net contact force becomes:

$$P = \int_{o}^{a} 2\pi r p(r) dr$$

$$P = \left(\frac{2}{3} p_o + 2p_o{}' \right) \pi a^2 \qquad (2.26)$$

From equation (2.17), the maximum pressure p_o:

$$p_o = \frac{2aE}{\pi R}$$

Substitute into 2.26 to obtain a function of the total net contact force (P), in terms of the contact width (a)

$$P = \left(\frac{4aE^*}{3\pi R} + 2\sqrt{\frac{4E^*\gamma}{\pi a}} \right) \pi a^2$$

$$P = \frac{4a^3 E^*}{3R} + \sqrt{16E^*\gamma\pi a^3} \qquad (2.27)$$

Equation 2.27 shows the relationship of the total net contact force, with the elastic stress, the adhesive force, and the contact width (a), and also provides an explicit expression for the applied out-of-balance force for the adhering spheres in terms of the radius of the contact area and the surface energy.

B. V. Derjaguin et al (1975) criticized the JKR-theory and developed another theory to describe the deformation of surfaces during adhesion, which is known as the 'Derjaguin-Muller-Toporov theory (DMT)', which is discussed briefly in the following section.

2.4 The Derjaguin-Muller-Toporov model (DMT)

B. V. Derjaguin et al (1975) made an alternative attempt to take into account the effect of contact deformation on the adhesion force of spherical particles. They consider the energy of molecular attractions in the ring-shaped zone of the adhesion contact.

In the DMT-theory, the shape of the deformed surface of the sphere in the contact zone has been assumed to follow the Hertz theory and to be unaffected by the surface force. Van der Waals forces are able to increase the area of elastic contact, and consequently surface forces outside the contact region will exist. These are the model using the surface free energy approach.

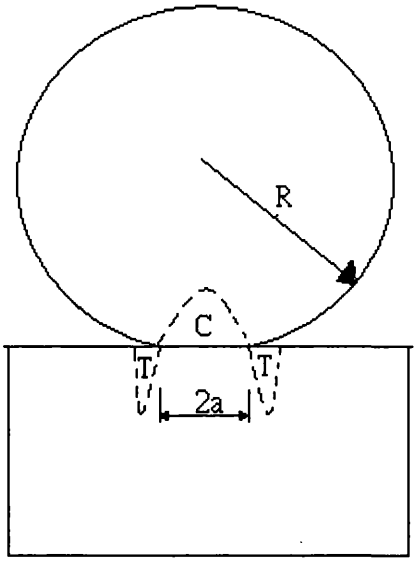

Figure 2. 3: Stress distribution at the interface of a sphere in contact with a half-space according to the original DMT-theory

The resulting stress distribution is of a compressive nature inside the contact area and of a tensile nature outside the contact area.

Comparing the JKR theory and DMT theory, the JKR theory applies mainly for very soft materials while DMT theory is considered to be more suitable for rather rigid material (V. M. Muller et al 1980). Besides material stiffness, the magnitude of loading is also an essential issue to affect the validity of both theories.

At sufficiently high loads, the elastic deformation of the surfaces caused by the adhesion force can be neglected, and the Hertz theory (H. Hertz al (1896)) appears a reasonable modeling of an adhesion contact, independent of the deformability or stiffness of the materials. For a low loading of rigid contacting bodies, the elastic deformation will be small compared to the range of the surface force, and the DMT theory could be applied, while in cases where the elastic deformation caused by the adhesion force is large, the JKR theory appears valid.

As a conclusion, in order to minimize the effect of solid-solid phase contact on the liquid bridge behavior, a softer, lower young modulus material will be used in this project. Hence, the more appropriate model, the JKR model, is chosen, as it is commented to be more suitable for softer materials and low loadings.

References:

H. Hertz, Eds. Jones and Schott (1896), On the contact of elastic solids, London: Macmillan, 90, 243.

K. L. Johnson, K. Kendall and A. D. Roberts (1971), Surface energy and the contact of elastic solids, Proc. R. Soc, Lond. A., 324, 301-313.

B. V. Derjaguin, V. M. Muller and Y. P. Toporov (1975), Effect of contact deformations on the adhesion of particles, Journal of collid and interface science, 53, 314-326

V. M. Muller, V.S. Yushchenko and B.V. Derjaguin (1980), On the influence of molecular forces on the deformation of an elastic sphere and its sticking to a rigid plane., Journal of Colloid and interface science, 77, 91-107.

K. L. Johnson (1985), Contact Mechanics, 1st edition, Cambridge University Press.

Chapter 3

Static and Dynamic Liquid Bridge Force

3.1 Introduction

As mentioned in Chapter 1 that besides the adhesive force of particles, the liquid bridge force is another major force that affects the strength of bonding in agglomeration. When a small amount of liquid is added in between two contact areas, a meniscus shaped liquid bridge is formed by the influence of capillary action. Depending on the ratio of the liquid volume to the void volume, degree of saturation (S), of the system, the liquid bridge can be classified into: pendular, funicular and capillary bridges, as illustrated as below:

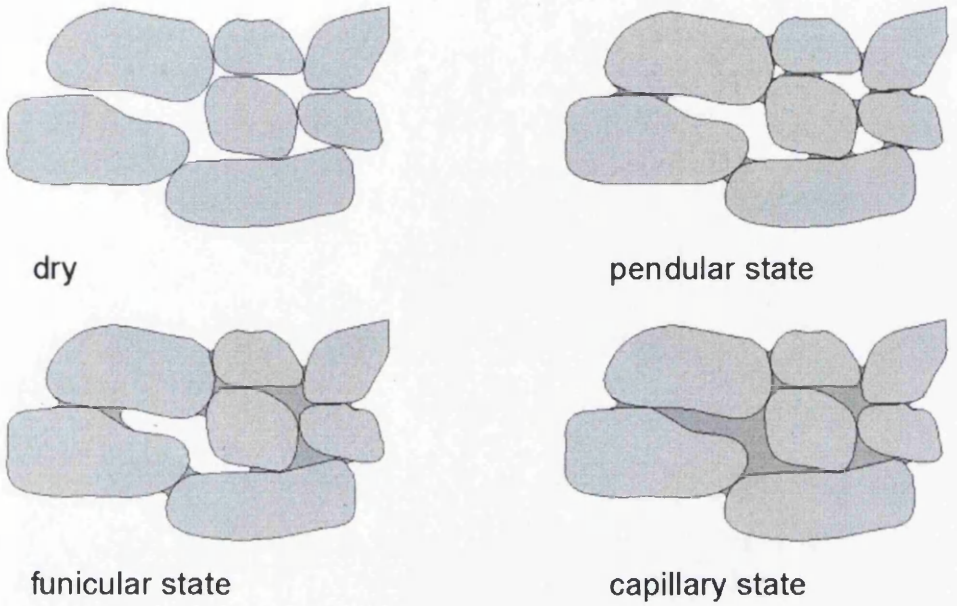

Figure 3. 1: Different stage of liquid bridge

Pendular state is defined as a stage where liquid bridges exist individually between two particles. By increasing the degree of saturation to $S \approx 0.3$ (Weigert and Ripperger 1999), pendular stage starts to transform into funicular stage, in which the group of particles contains some pores filled with excessive liquid. Further increase in volume of liquid leads to the capillary stage, where all pores of a group of particles are completely filled with liquid, S=1.

Liquid bridge force varies with different degrees of saturation in a static system, as this force is induced by pressure deficiency and surface tension in a meniscus shape of liquid-gas surface, which is a function of volume of water, liquid surface tension, wetting angle and particle roughness (T. Groger et.al. 2003). Some researchers, such as G. Lian et al 1993, concerned with the liquid bridge in pendular stage and Urso et al 1999 investigated on the liquid bridge for those three stages. Moreover, liquid bridge viscosity increases in importance when relative movement exist between spheres, due to more vigorous bubble behaviour and more likeness of slug-like behaviour (Wright, Raper 1998). In another word, liquid bridge force can be considered as a combination of forces induced by the

hydrostatic pressure, surface tension and also viscous force, where the summation of first two factors is called the static liquid bridge force and the last one is called the dynamic liquid bridge force.

The static liquid bridge force is depending on the shape of the liquid-air meniscus interface, which is induced by the pressure deficiency across and surface tension along the interface. This interface is governed by the Laplace-young equation which relates the mean curvature of the geometry to the pressure deficiency of the liquid. However, this nonlinear differential equation cannot be solved analytically except for the case of zero gravity or buoyant liquid, or in the case of a narrow capillary tube, or with zero contact angle (C. Ligoure 2000). In order to solve this equation, it is common to assume that the volume of liquid is small to a certain extend that the influence of gravity can be neglect. After that Fisher (Fisher 1926) proposed a simpler and one of the most recognized approaches to estimating the liquid bridge force, by approximating the meridional profile of the liquid-gas interface as an arc of a circle, named as the toroidal approximation.

With the help of the toroidal approximation, the static liquid bridge force can be found by two different methods, namely "gorge method" and "mixed method". They are distinguished by the location, along the liquid bridge, being used to compute the two components of static liquid bridge force. G. Lian et al (1993) conclude that for the toroidal approximation, the best estimation of the static liquid bridge force is obtained using the gorge method, which underestimates the numerical values by less than 10% corresponding to a large separation distance between the two particles, while the mixed method severely underestimates the liquid bridge force at a large separation distance.

This chapter presents the deviation of the Laplace equation for pendular liquid bridge, numerical solutions to the toroidal approximation (Fisher 1926) and the methods of evaluating static liquid bridge force.

3.2 The Laplace Equation

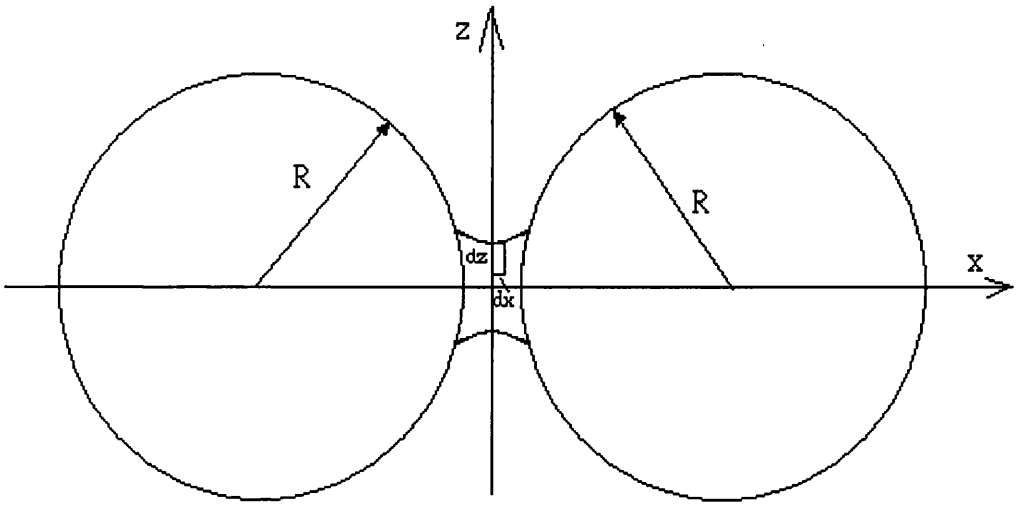

Figure 3. 2: A symmetric liquid bridge between two equal sized spheres

Consider a small deviates of liquid bridge between two equal sized spheres, as shown in Figure 3.1. The equilibrium state of the system corresponds to a minimum of thermodynamic potential, Gibbs free energy Ω (Kralchevsky & Nagayama 2001, G. Lian et al 1993), where Ω is the sum of internal energy and product of it's volume and pressure minimum.

$$\Omega = \int_{V_1} P_1 dV + \int_{V_2} P_2 - \gamma A \tag{3. 1}$$

where A is the area of the interface; P_1 and P_2 is the pressure constant for two phases; γ is the surface tension of liquid, as shown in Figure 3.2.

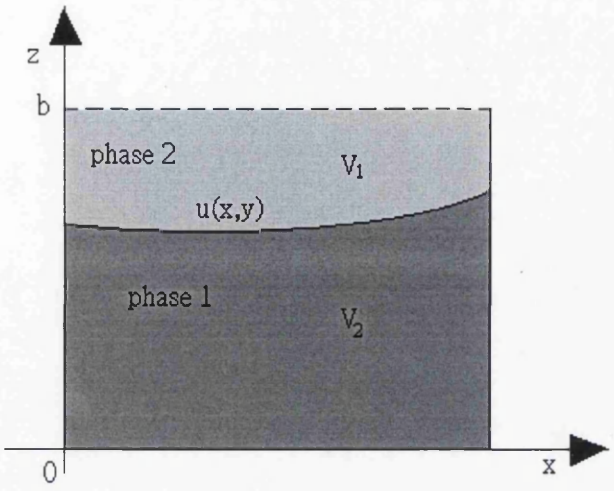

Figure 3. 3: Sketch of a two-phase system composed of phases 1 and 2, which occupy volumes V1 and V2, repectively; z=u(x,y) is the equation of the phase boundary

Let z=u(x,y) to be the equation describing the shape of the interface and the area of the interface is

$$A = \int_{A_0} dxdy\sqrt{1+u_x^2+u_y^2} \tag{3. 2}$$

$u_x = \partial u / \partial x$; $u_y = \partial u / \partial y$

A is the projection of the interface on the coordinate plane xy

$$\int_{V_a} P_1 dV = \int_{A_0} dxdy \int_0^{u(x,y)} P_1 dz \; ; \quad \int_{V_2} P_2 dV = \int_{A_0} dxdy \int_{u(x,y)}^{a} P_2 dz \tag{3. 3}$$

Substitute equations (3.2) and (3.3) into (3.1)

$$\Omega = \int_{A_o} dxdy \int_0^{u(x,y)} P_1 dz + \int_{A_o} dxdy \int_{u(x,y)}^{a} P_2 dz - \gamma \int_{A_0} dxdy\sqrt{1+u_x^2+u_y^2}$$

$$\Omega = \int_{A_o} dxdy \left(\int_0^{u(x,y)} P_1 dz + \int_{u(x,y)}^{a} P_2 dz - \gamma\sqrt{1+u_x^2+u_y^2} \right) \tag{3.4}$$

$$\text{Let } W(u(x,y),u_x(x,y),u_y(x,y)) = \left(\int_0^{u(x,y)} P_1 dz + \int_{u(x,y)}^{a} P_2 dz - \gamma\sqrt{1+u_x^2+u_y^2} \right) \tag{3.5}$$

Equations (3.4) and (3.5) show that the free energy depends on the interfacial shape u(x,y). Then the minimum of Ω is given by the well-known Euler equation (Kralchevsky & Nagayama 2001, G. Lian et al 1993)

$$\frac{\partial W}{\partial u} - \frac{\partial}{\partial x}\frac{\partial W}{\partial u_x} - \frac{\partial}{\partial y}\frac{\partial W}{\partial u_y} = 0 \tag{3.6}$$

Differentiating the first term of equation (3.5) yields

$$\frac{\partial W}{\partial u} = -P_1(u) + P_2(u) \tag{3.7}$$

Differentiating the remaining terms of equation (3.5) gives

$$\frac{\partial}{\partial x}\frac{\partial W}{\partial u_x} + \frac{\partial}{\partial y}\frac{\partial W}{\partial u_y} = 2H\gamma \tag{3.8}$$

where H defined by equation (3.8) is a basic quantity in differential geometry, which is termed the mean curvature of the surface. This means that curvature can be expressed through the two principle radii of curvature of the surface, R1 and R2, as

$$\text{H} = -\frac{1}{2}\left(\frac{1}{R_1} + \frac{1}{R_2}\right) \tag{3.9}$$

Combining Equations (3.7-3.9) with (3.6) yields

$$2H\gamma = -(P_1(u) - P_2(u)) \tag{3.10}$$

$$\gamma\left(\frac{1}{R_1}+\frac{1}{R_2}\right) = P_1(u) - P_2(u) \tag{3.11}$$

where $P_1(u) - P_2(u)$ is termed as the capillary pressure $P_c = P_1(u) - P_2(u)$.

The general differential form of equation (3.8) can be expressed in the Cartesian coordinates:

$$\frac{\left(1+u_y^2\right)u_{xx} - 2u_{xy}u_z u_y + \left(1+u_x^2\right)u_{yy}}{\left(1+u_x^2+u_y^2\right)^{3/2}} = \left[P_2(u) - P_1(u)\right]/\gamma \tag{3.12}$$

where u_{xx}, u_{xy} and u_{yy} denote the second derivates of u (x,y).

If the curved interface has rotational symmetry around the z-axis, it is convenient to express the equation of interface in the form of z=u(Y) and substitute it into equation (3.8) to obtain:

$$\frac{1}{Y}\frac{d}{dY}\left[\frac{Yu_Y}{\left(1+u_Y^2\right)^{1/2}}\right] = \left(P_2 - P_1\right)/\gamma \tag{3.13}$$

where u_Y =du/dY. Equation (3.13) can be transformed in an equivalent form by inversing the function of z=u(Y), that is Y=Y(z) (Kralchevsky & Nagayama 2001):

$$-\frac{Y_{zz}}{\left(1+Y_z^2\right)^{3/2}} + \frac{1}{Y\left(1+Y_z^2\right)^{1/2}} = \frac{P_2 - P_1}{\gamma} \tag{3.14}$$

where $Y_z = \frac{dY}{dz}$; $Y_{zz} = \frac{d^2Y}{dz^2}$

As shown in the above equations (3.10-3.14), the mean curvature of the surface (H) is a second order partial differential equation, which makes the analytical solution too complicated to be found. As a result, solving equation (3.14) numerically and also by approximation provide different ways to find the meridional profile of liquid bridge.

3.3 Liquid bridge profile establishment method

3.3.1 Mathematical evaluation of liquid bridge meridional profile

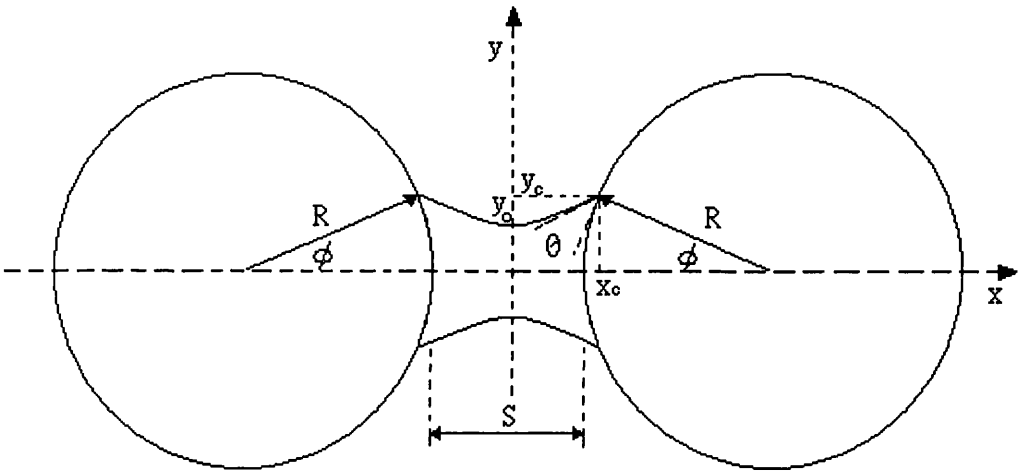

Figure 3. 4: A symmetric liquid bridge for Numerical Analysis

In the absence of gravitational force, the pressure deficiency across the liquid-gas interface of the liquid bridge is expressed by a second order non-linear partial differential equation (3.14). The numerical solution of equation may be approximated by a truncated Taylor series:

$$Y_{i+1} \cong Y_i + (X_{i+1} - X_i)\dot{Y}_i + \frac{1}{2}(X_{i+1} - X_i)^2 \ddot{Y}_i \quad i=0,1,2,..... \qquad (3.15)$$

where $\dot{Y}_i = \frac{dY_i}{dx}; \ddot{Y}_i = \frac{d^2Y_i}{dx^2}$

In order to solve equation (3.15), it is necessary to obtain the expressions for $\dot{Y}_i, \ddot{Y}_i$, and two boundary conditions are applied (G. Lian et al 1993, Soulie et al 2006): 1) at the neck of the liquid bridge, X=0, the shape of the bridge corresponds to the apex of the profile where $\dot{Y}_i(0)=0$;2) the value of Y(0) should be determined.

Substituting $T=\dot{Y}^2+1$ and integrate equation (3.14) with respect to T (G. Lian et al 1993, soulie et al 2006) :

$$T = \frac{4Y^2(x)}{\left(2C - \left(\frac{P_2 - P_1}{\gamma}\right)Y^2(x)\right)^2} \tag{3.16}$$

Then

$$\frac{Y(x)}{\sqrt{1+\dot{Y}^2(x)}} + \frac{1}{2}\left(\frac{P_2 - P_1}{\gamma}\right)Y^2(x) = C \tag{3.17}$$

where C is an integration constant, which is determined from the boundary condition, $x=x_c$, and $Y(x_c)=R_1\sin\delta$ and $\dot{Y}(xc) = 1/\tan(\theta+\delta)$; which yields :

$$C= R_1\sin\delta\,\sin(\delta+\theta)+\frac{1}{2}\left(\frac{P_2 - P_1}{\gamma}\right)R_1^2\sin^2\delta \tag{3.18}$$

Since the liquid bridge is symmetrical about the Y axis, the condition $\dot{Y}(0) = 0$ yields the neck radius Y_0:

$$Y_0=C \qquad \text{if } \left(\frac{P_2-P_1}{\gamma}\right)=0$$

$$Y_0=\frac{-1+\sqrt{1+2\left(\frac{P_2-P_1}{\sigma}\right)C}}{\left(\frac{P_2-P_1}{\sigma}\right)} \qquad \text{if } \left(\frac{P_2-P_1}{\gamma}\right)\neq 0 \qquad (3.19)$$

Rearrange (3.14) and (3.17) to obtain $\dot{Y}_i$ and $\ddot{Y}_i$ as

$$\dot{Y}_i=\sqrt{\left(\frac{Y_i}{C-\left(\frac{P_2-P_1}{\gamma}\right)Y_i^2}\right)^2-1} \qquad (3.20)$$

$$\ddot{Y}_i=\frac{1+\dot{Y}_i^2}{Y_i}+2\left(\frac{P_2-P_1}{\gamma}\right)\left(1+\dot{Y}_i^2\right)^{3/2} \qquad (3.21)$$

Eventually, the Laplace-Young equation (3.15) can be evaluated by combining equations (3.19-3.21) in the interval from X=0 to X=Xc.

The static liquid bridge force is calculated by multiplying the circumference and projected area of liquid contact to the surface tension acting at the three-phase contact line and hydrostatic pressure respectively.

Besides solving the profile numerically, approximating the shape of this meridional profile by an arc of a circle, namely the torodial approximation, enhanced and simplified the calculation of static liquid bridge force.

3.3.2 Toroidal Approximation

Fisher (Fisher 1926) proposed a much simpler approach to estimate the liquid bridge profile, by approximating the meridional profile of the liquid-gas interface as an arc of a circle with zero contact angle. Two different methods have been developed from the toroidal approximation to calculate liquid bridge force, the neck or gorge method (Hotta et al 1974), which estimates the force at the neck of the bridge, and the mixed method that computes the force at the liquid bridge solid contact region. G. Lian et al 1993 states that the best estimation of the total liquid bridge force is obtained by using the gorge method with maximum 10 % underestimation of the force, and this accuracy does not change much when the separation distance increases.

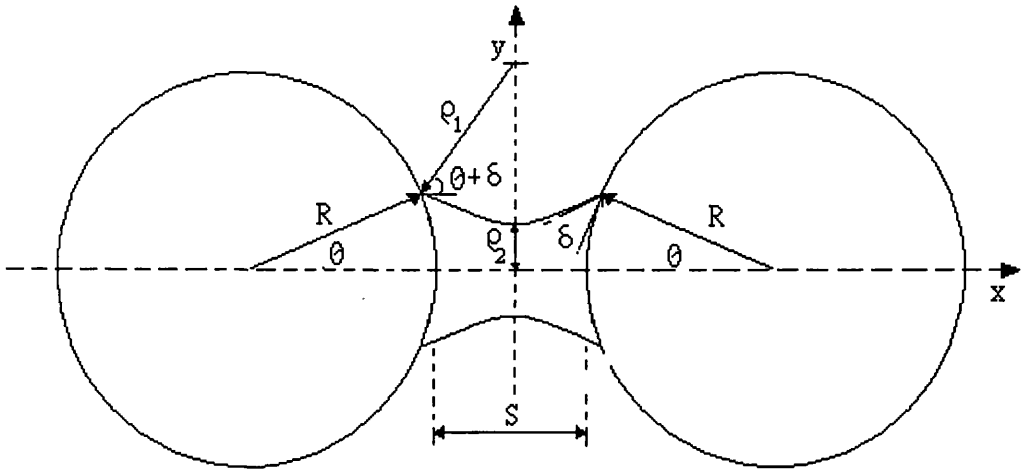

Figure 3. 5: Concave toroidal geometry of pendular liquid bridge

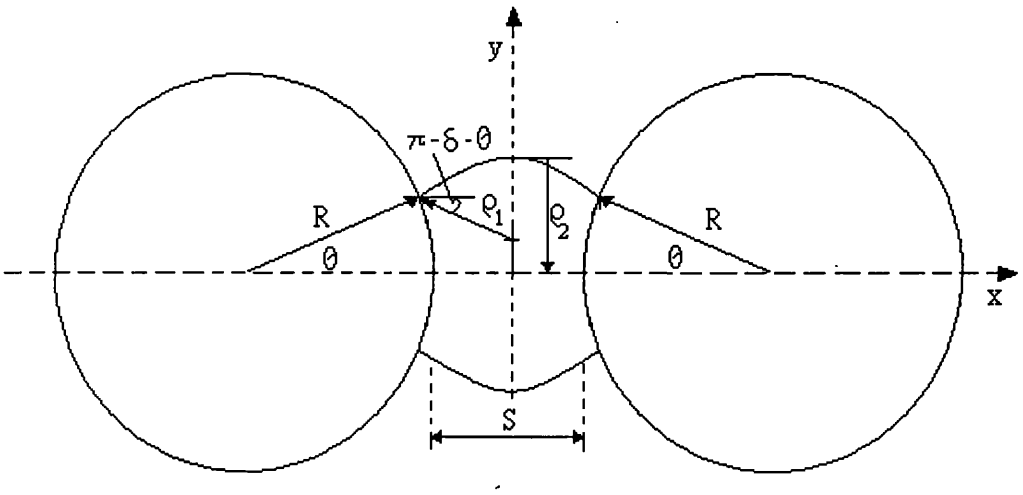

Figure 3. 6: Schematic of convex toroidal geometry

The configurations of the toroidal approximation for a concave and convex liquid bridge are shown in Figures 3.4 and 3.5. Two mono-sized spheres are separated by a distance S. The liquid bridge is approximated by a principal radius of curvature ρ_1 in the plane of the page and the other principal radius of curvature ρ_2 perpendicular to the page at the narrowest point of the liquid bridge. θ and δ are the filling angle and contact angle respectively.

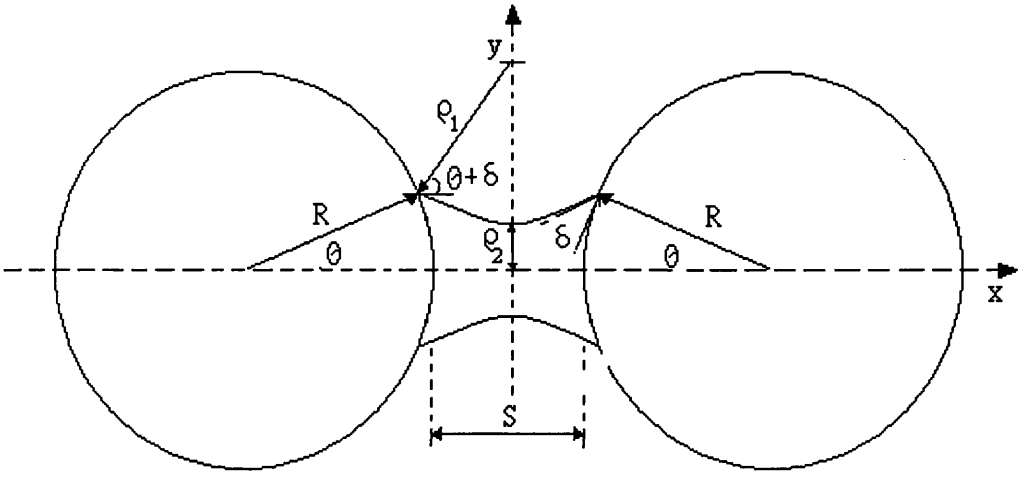

Figure 3. 7: Concave torodial geometry of a liquid bridge

Two principal radii of curvature for concave liquid bridge can be obtained geometrically as follows, refer to Figure 3.6

$$\rho_1 = \frac{s + r_i(1-\cos\theta_i)}{(\cos\theta_i + \delta)} \tag{3.22}$$

$$\rho_2 = r_i \sin\theta_i - \rho_1[1-\sin(\theta_i + \delta)] \tag{3.23}$$

where s is the half separation distance, $s = S/2$; r and θ are the radius and filling angle of particle I respectively, and δ is the contact angle in radians.

The principal radii of curvature for the convex case yield two similar equations:

$$\rho_1 = -\frac{s + r_i(1-\cos\theta_i)}{(\cos\theta_i - \delta)} \tag{3.24}$$

$$\rho_2 = r_i \sin\theta_i + \rho_1[1-\sin(\theta_i - \delta)] \tag{3.25}$$

The above two equations establish the maximum and minimum of the principal radii of curvature, which are assumed to define the shape of liquid bridge as an arc of a circle and are used to calculate liquid bridge force later in this chapter.

3.4 Static Liquid Bridge Force

Liquid bridge force acting between two spheres is the combination of two components: a) the axial component of the surface tension at the three phase contact line and b) the hydrostatic pressure acting on the axially projected area of the liquid bridge on each sphere.

Depending on the location along the liquid bridge that is used to compute the two components of the static liquid bridge force, two different methods are reported in literature. Namely, the gorge method, which compute the static liquid bridge force based purely on the cross-section area and circumference of the neck of a liquid bridge; and the Mixed Method, which evaluates the static liquid bridge force by a combination of the cross-section area of the neck and circumference of the liquid solid contact line. Those two methods are discussed next.

3.4.1 Gorge's method

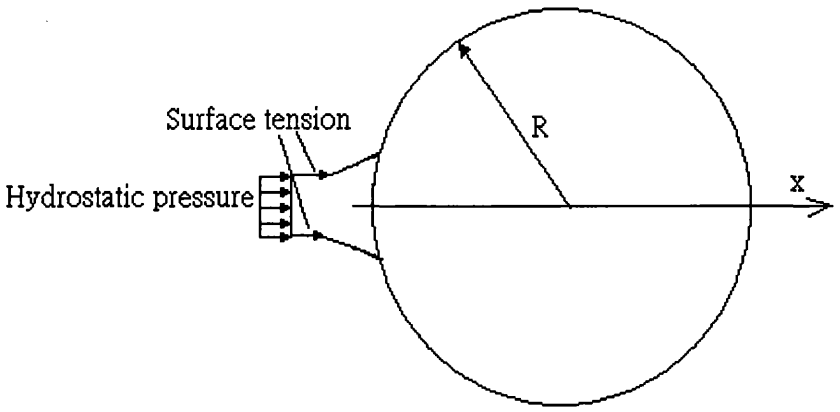

Figure 3. 8 : Gorge method illustration

The Gorge method (Hotta et al 1974) involves using the area at the neck to obtain the force generated from the hydrostatic pressure deficiency and the tangent, or circumference, of the neck to obtain the surface tension component of the static liquid bridge force. Hence, the governing equation for gorge method is as follow:

$$F = r_i^2 \pi Pc + 2\pi r_i \gamma \tag{3.26}$$

where Pc is capillary pressure, and hence the hydrostatic pressure different across the liquid-gas interface can be expressed as; $P_c = P_1 - P_2$; r_i is the radius of the neck of liquid bridge which is approximated by the minimum of the principal radii of curvature, ρ_2, and γ is a surface tension of liquid.

Combining equation (3.11) with (3.26) yields:

$$F = r_i^2 \pi\gamma\left(\frac{1}{\rho_1} - \frac{1}{\rho_2}\right) + 2\pi\rho_2\gamma \tag{3.27}$$

where ρ_1 and ρ_2 are the two radii of curvature of the liquid bridge surface from equations (3.24) and (3.25).

3.4.2 Mixed method

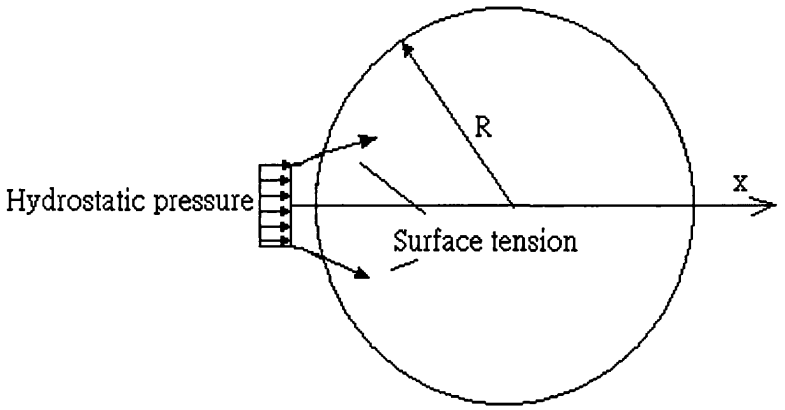

Figure 3. 9: Mixed method illustration

The mixed method involves the consideration of not only the effect of hydrostatic pressure from the neck of the liquid bridge, but also the surface tension at the three phase contact line. Thus, the governing equation for the method is slightly different from the Gorge method as follow:

$$F = 2\pi\gamma_{lv} r \sin\phi \sin(\phi + \theta) + \pi r^2 Pc \sin^2\phi \qquad (3.28)$$

where the first term represents the contribution of surface tension and the second term is the force arises from the hydrostatic pressure.

Although the consideration of this method is physically more correct than gorge method, Comparison of two methods with numerical analysis has been made and concluded in(G. Lian et al 1993), that the best estimation of static liquid bridge force is obtained by using the gorge method with maximum underestimation by 10 % to the greatest volume considered and with the largest separation distance, while the mixed method severely underestimates the static liquid bridge force at large separation distances.

3.5 Dynamic liquid bridge force

As mentioned earlier in this Chapter that liquid bridge force is a combination of forces induced by the "hydrostatic pressure and surface tension" and liquid viscous force; those are called the static liquid bridge force and the dynamic liquid bridge force respectively.

The dynamic liquid bridge force occurs when the spheres are subjected to relative movement in normal direction. Recently studies have been made by Adams and Perchard (1985), Mazzone et al (1987), Matthewson (1988) and Ennis et al (1990). They considered the Reynolds' lubrication equation for the case of a sphere moving normal to a flat surface or another sphere at a small separation distance.

Adams and Perchard (1985), based on lubrication theory, established an expression for the viscous force of the dynamic liquid bridge in the case of two spheres with a separation distance S, which is an inversely proportional function of S.

The basic Reynolds lubrication theory and the brief discuss of equation for the viscous force of the dynamic liquid bridge force from lubrication theory will be reported as below.

3.5.1 Reynolds lubrication theory

Nearly all mechanical designs fall into the consideration of wearing and friction, The most common way to prevent wearing is through lubrication. The idea of lubrication is to maintain a liquid or grease layer between moving solid surfaces. The standard theory to find out the stress in this liquid layer is first developed by Osborne Reynolds in 1886, named Reynolds lubrication theory. (J. Kestin (1955))

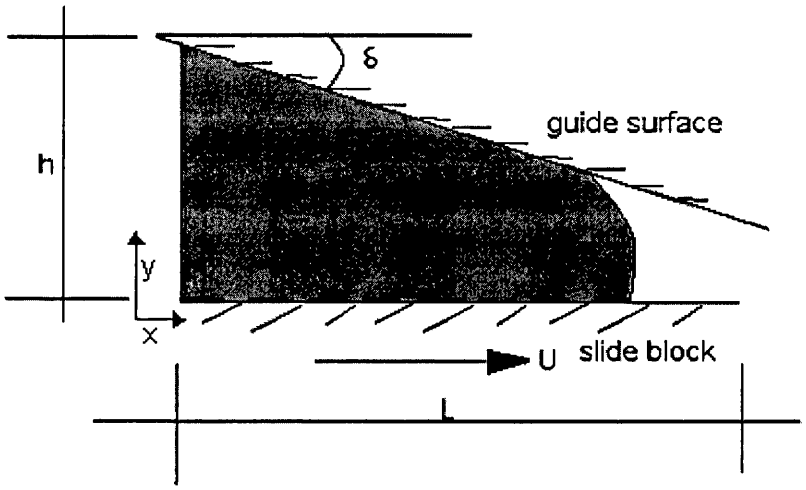

Figure 3. 10: Lubrication in a bearing: Flow in wedge between slide block and plane guide surface

The standard model used to describe lubrication theory is the slider bearing shown in Figure 3.10, where the upper surface is assumed to be stationary and smooth, while the lower surface moves to right with speed U. It is important that these two surfaces are inclined at a small angle δ to each other, and it is assumed that the sliding surfaces are very large in a transverse direction with respect to the motion, so that the problem is two dimensional.

As a result, the acceleration caused by the cross-section area variation and experienced by a fluid particle will be relatively small. It turns out that the fluid acceleration and the forces required to cause it can be neglected. This leads to the main approximation of Reynolds lubrication theory, which is the restriction to flows having negligible inertial forces.

Based on the assumption that inertial force is negligible, or in another words, the viscous force is dominate in the Reynolds number, and thus, the Reynolds number becomes very small. An approximate solution of the Navier-stroke equation is obtained by neglecting the inertia terms in ordinary Navier-stroke equation, which is shown as follow:

$$\begin{aligned}\rho\frac{Du}{Dt} &= X-\frac{\partial p}{\partial x}+\frac{\partial}{\partial x}\left[\mu\left(2\frac{\partial u}{\partial x}-\frac{2}{3}divW\right)\right]+\frac{\partial}{\partial y}\left[\mu\left(\frac{\partial u}{\partial y}-\frac{\partial v}{\partial x}\right)\right]\\ \rho\frac{Dv}{Dt} &= Y-\frac{\partial p}{\partial y}+\frac{\partial}{\partial y}\left[\mu\left(2\frac{\partial v}{\partial y}-\frac{2}{3}divW\right)\right]+\frac{\partial}{\partial x}\left[\mu\left(\frac{\partial u}{\partial y}-\frac{\partial v}{\partial x}\right)\right]\end{aligned} \tag{3.29}$$

where $\frac{Du}{Dt}$ and $\frac{Dv}{Dt}$ are the substantive accelerations, which consist of the local contribution $\frac{\partial u}{\partial t}$ and $\frac{\partial v}{\partial t}$, and the convective contribution $\frac{du}{dt}, \frac{dv}{dt}$ in the x and y directions respectively; W is the velocity vector, $W = iu + jv$; u and v are the velocities in the x and y directions respectively; p is the fluid pressure involved in the Navier-stroke equation deviation; X and Y are the body forces in the x and y direction respectively and ρ, μ are the density and viscosity of fluid.

Besides ignoring the inertial force term, the liquid is assumed to be incompressible, which leads to $divW = 0$, i.e. $\frac{\partial u}{\partial x}+\frac{\partial v}{\partial y}=0$, thus:

$$\begin{aligned}0 &= -\frac{\partial p}{\partial x}+\mu\left(\frac{\partial^2 u}{\partial x^2}+\frac{\partial^2 u}{\partial y^2}\right)\\ 0 &= -\frac{\partial p}{\partial y}+\mu\left(\frac{\partial^2 v}{\partial x^2}+\frac{\partial^2 v}{\partial y^2}\right)\\ \frac{\partial u}{\partial x}+\frac{\partial v}{\partial y} &= 0\end{aligned} \tag{3.30}$$

Equation (3.30) can be further simplified for the case of lubrication. The equation for the y-direction can be omitted altogether (H. Ping et al (1999)), because the component v is very small with respect to u. Further, in the equation for the x direction $\frac{\partial^2 u}{\partial x^2}$ can be neglected with respect to $\frac{\partial^2 u}{\partial y^2}$, because the former is smaller than the latter by a factor of the order $\left(\frac{h}{L}\right)^2$. The pressure distribution must satisfy the condition that $p = p_o$ at both ends of the slippers. Compared with the case of flow between the parallel sliding walls, the pressure gradient in the direction of motion, $\frac{\partial p}{\partial x}$, is no longer constant, but a very small pressure gradient in the y-direction can be neglected, $\frac{\partial p}{\partial y} = 0$. With these simplifications the original equation (3.29) reduces to:

$$\frac{\partial p}{\partial x} = \mu \frac{\partial^2 u}{\partial y^2} \tag{3.31}$$

The boundary conditions of velocity in equation (3.31) are as follows.

$$(u)_{y=0} = U; (u)_{y=h} = 0 \tag{3.32}$$

According to the above simplifications, $\frac{\partial p}{\partial y} = 0$, i.e. the pressure is only a function of x. Therefore, to integrate u in equation (3.4) over y and to substitute equation (3.32), the velocity can be written as follows:

$$u = \frac{1}{2\mu}\frac{dp}{dx}\left(y^2 - hy\right) + \frac{u_o}{h}(h - y) \tag{3.33}$$

Because $(v)_{y=0}$ and $(u)_{y=h}$ are equal to zero, integrate u and v in equation (3.30), $\frac{\partial u}{\partial x}+\frac{\partial v}{\partial y}=0$, over y from 0 to h and substitute into the above equation, yield

$$\frac{d}{dx}\left(\frac{h^3 dp}{6\mu dx}\right)=U\frac{dh}{dx} \tag{3.34}$$

Equation (3.34) is the famous Reynolds equation, which is used to solve pressure in classical lubrication theory. In order to obtain the pressure distribution, different boundary conditions are used for different lubrication performances.

3.5.2 Lubrication theory for Liquid Bridge.

As illustrated in Figure 4.2, let consider two identical elastic and spherical particles with radius R and mass m being immersed in a viscous fluid and approaching each other. For the initial condition at time=0, the spheres start with a gap h_o between their undeformed surfaces at r=0 and with a relative approaching velocity v_o. The minimum surface distance that can be approached is denoted as h_{min}. Only head-on collisions and no rotational movements are considered in this theory.

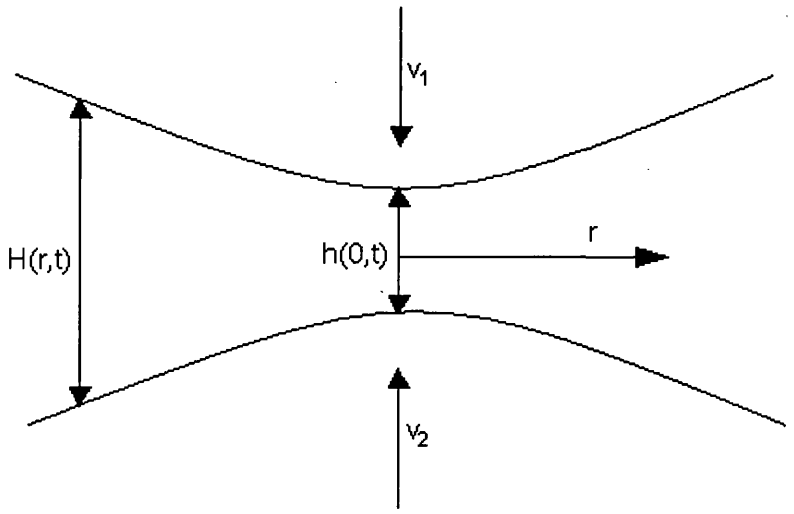

Figure 3. 11: illustration of two approaching elastic and rigid spheres in a viscous fluid

This theory is originally established based on liquid-solid systems, in which the following assumptions are made:

1) The initial gap size h_o , from which lubrication effect is considered to be significant, is assumed to be much smaller than particle radius (R.H. Davis (1986)).
2) The upper limit of integration of pressure for lubrication force is extened from particle radius to infinity;
3) Paraboloid approximation of undeformed surface is applied in order to get the simplified gap profile.

$$H(r,t)=h(0,t)+\frac{r^2}{R} \tag{3.35}$$

4) The fluid is treated as continuum no matter how close the two surface approach.

According to the lubrication theory (R.H. Davis (1986)), analytical expressions for interstitial pressure distribution and lubrication force can be derived as:

$$\frac{\partial p}{\partial r}=-\frac{6\mu r v}{H^3} \tag{3.36}$$

$$p(r,t) = \frac{3\mu R v}{2\left(h + \frac{r^2}{R}\right)^2} \tag{3.37}$$

$$F_{L,\infty} = \int_0^\infty 2\pi p(r,t)dr = \frac{6\pi\mu R^2 v}{h} \tag{3.38}$$

Adams and Perchard (1985) reported a similar expression as equation (3.38), which is believed to be valid to compute the viscous force of a dynamic bridge between two equal sized particles.

The above analysis only considers the relative movement of rigid solid spheres. The more general case is the viscous resistance of an elastic sphere moving towards another elastic sphere or a plane surface, under the condition that the two solid surfaces are separated by a thin infinite fluid layer or a finite liquid bridge. The problem of elasto-hydrodynamic (EHL) collisions of particles has been studied by Davis (1987) and others (Davis et al (1986); Serayssol and Davis (1986); Barnocky and Davis (1988)). In their studies, the pressure profile of the Reynolds lubrication equation (4.6) is obtained numerically by considering the dynamic deformation of the solid spheres. However, this is a more complicated case for which analytical expressions are not possible. For most cases, we may assume that the spheres are rigid enough that the deformations of the surfaces are small and hence negligible in relation to the sphere displacement.

References:

T. Weigert, S. Ripperger (1999), Calculation of the liquid bridge Volume and Bulk saturation from the Hal-filling Anlge, Part. Part. Syst. Charat., 16, 238-242.

T. Groger, U. Tuzin and D. M. Heyes (2003), Modelling and measuring of cohesion in wet granular materials, Powder Technology, 133, 203-215.

G. Lain, C. Thornoton and M. J. Adams, (1993), A Theoretical study of the liquid bridge forces between two rigid spherical bodies, Journal of collid and interface scinec , 161, 138-147.

C. Ligoure (1999), Unusual interfacial phase behaviour of two nonmiscible liquids in a cylindrical test tube: equilibrium shapes and stability of axismmetric liquid bridges under gravity, Journal of collid and interface science, 223, 190-196.

Maria Elena D, Urso, Chris J. Lawrence and Michael J. Adams, (1999), Pendular, Funicular, and capillary bridges: Result for Two dimension., Journal of colloid and interface science, 220, 42-56.

P.C. Wright and J.A. Raper (1998), Role of liquid bridge forces in cohesive fluidization, Tans IChemE, 76 part A, 753-759.

R. A. Fisher (1926), On the capillary forces in an ideal soil; correction of formulae given by W.B. Haines., Journal of Agricultural Science, 16, 492-505.

P. A. Kralchevsky and K. Nagayama (2001), Particle at fluid interface and membranes, Elsevier, Amsterdam.

F. Soulie, F.Cherblanc, M. S. EI Youssoufi and C. Saix (2006), Influence of liquid bridges on the mechanical behaviour of polydisperse granular materials.

K. Hotta, K. Takeda and K. Linoya (1974), The capillary force of a liquid bridge. Powder Technology, 10 , 231-242.

J. Kestin (1955), Boundary layer theory, 1st edition, London: Pergamon Press Ltd.

H. Ping, L. Jianbin and W. Shizhu (1999), Theoretical study on the lubrication failure for the lubricant with a limiting shear stress, Tribology international, 32,421-426.

R. H. Davis, J. Serayssol, E. J. Hinch (1986), The elastohydrodynamic collision of two spheres, J. Fluid Mech., 163,479.

M. J. Adams and V. Perchard (1985), The cohesive forces between particles with interstitial liquid., In l. Chem. E. symposium Series, 91, 147-160.

M. J. Matthewson (1988), Adhesion of spheres by thin Liquid film., Philosophical Magazine !, 57, 207-261.

D. N. Mazzone, G. I. Tardos, R. Pfeffer (1987), The behavior of liquid bridges between two relatively moving particle. Powder Technology, 51, 71-83.

B. J. Ennis, G. I. Tardos and R. Pfeefer (1991), A microlevel-based characterization of granulation phenomena, Powder Technology, 65, 257-272.

R. H. Davis, J. M. Serayssol and E. J. Hinch (1986), The elastohydrodynamic collision of two spheres, J. Fluid Mech. , 163, 479-497.

J. M. Serayssol and R. H. Davis (1986), The influence of surface interactions on the elastohydrodynamic collision of two spheres, Journal of colloid and interface science, 114, 54-66.

Chapter 4

A Proposed Integrated Interaction Law for Wet Agglomerate

4.1 Introduction

The integration of solid phase and liquid phase happens in many places, such as partially saturated soil, agglomeration or granulation ...etc, although many theories have been derived to govern the behavior of either solid or liquid phase, there are, to the best of the author's knowledge that, no interaction laws for a system which integrate the behavior of two phases together.

This interaction law intends to describe the whole loading and unloading process of a system with two solid particles sandwiching an interstitial liquid bridge. The two solid particles first approach toward each other with a relative motion and hence, the liquid bridge is being squeezed until they contact, then deform slightly and eventually rebound from each other. This process is shown in Figure 4.1.

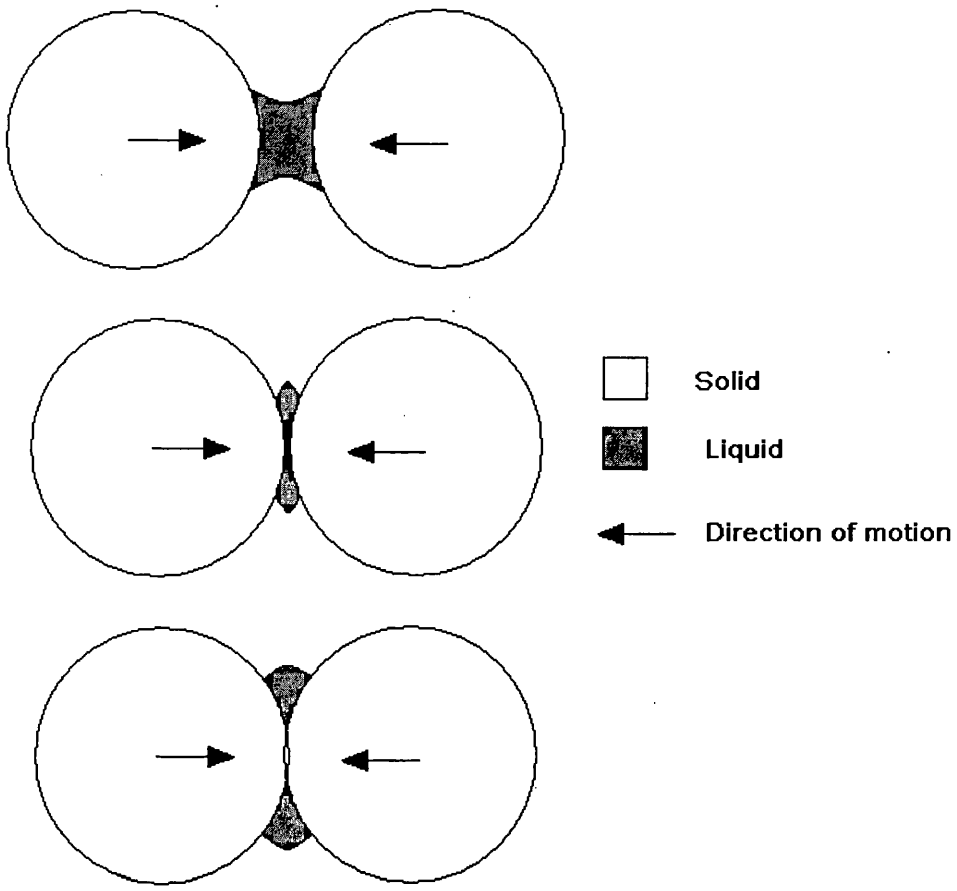

Figure 4. 1: Illustration of Load-deform-unload process

Main reasons for no such interaction law available are, believed by the author, because of the complexities and cost of experiments for this process. The complexities are due to be the following factors:

1) The precision of sample preparation: in order to obtain a series of comparable experiment results, it is necessary to prepare the profile of liquid bridge as identical as possible among different sets of experiment. However, it is very difficult to achieve an identical symmetric layout for different sets of experiment, as shown in the top sketch in Figure 4.1, on two curve particle surface.
2) Experimental methodology: as a liquid bridge force is relatively small when comparing with the force of solid contact. As a result, very sensitive force measuring devices are needed for measuring this force. However, in order to avoid this measuring device from being damage due to excessive reading from

solid contact, they have to be withdraw at the time, when two surface is just contact.

3) Unpredictable and permanent deformation of two solids surface may occur due to inhomogeneous of materials.

Due to these difficulties on the experiments, a numerical analysis is used to investigate the behavior of this 'load-deform-unload' process.

In this chapter, the behavior of this 'load-deform-unload' system has been investigated by using a finite element method (FEM) based commercial program, Elfen. The ultimate object for using FEM is to obtain the inter-particle force through out the process, hence, find out the interaction law for the system. However, as will be shown, certain unpreventable numerical instabilities have been encountered in the FEM analysis and terminated the analysis before the two solid surfaces are in contact.

Although the FEM analysis does not serve its ultimate purpose, the results showed a similar pattern as the result from theoretical equations. This is convinced that the FEM models are correct and the reasons of simulation termination provided some hints for the proposed interaction laws. Apart from that, some experimental results for the loading case of the 'load-deform-unload' system have been reported by Meurisse and Querry (2006). These results provide another information for the proposed interaction laws, which is going to be discussed in this chapter

4.2 FEM analysis

A commercial finite element software Elfen is first used in this project to tackle the above mentioned problem. In order to simplify the FEM model and to reduce the computational costs, an assumption of axial symmetric has been made. The contact forces for the whole loading and unloading process are recorded and examined, thus, an interaction law can be obtained by a empirical equation fitting.

The model consists of two a quarter of solid particles with a radius R=0.1mm with the following properties:

- Density $\rho = 2400 \times 10^{-9}\ {kg}/{mm^3}$
- Young's Modulus $E = 10 \times 10^{3}\ {N}/{mm^3}$
- Poisson's ration $\nu = 0.35$

An interstitial liquid bridge is sandwiched between the two solid particles with an initial separation distance of 0.01mm; the profile of this liquid bridge is obtained by the numerical analysis method from equations (3.15)-(3.21) with volume of liquid $15\mu l$ and following properties:

- surface tension $\gamma_{lv} = 0.0725 \times 10^{-3}\ {N}/{mm}$
- solid-liquid contact angle $\theta = 0^{o}$
- filling angle $\phi = 10^{o}$

As illustrated in Figure 4.1 that both the liquid bridge and solid particles are fixed in the y direction due to the axial symmetric assumption and the x-direction of the right hand-side particle is fixed. An applied velocity, with 0.01 mm/s, is added on the left hand-side particle. This applied velocity drives the left particle to approach the fixed particle.

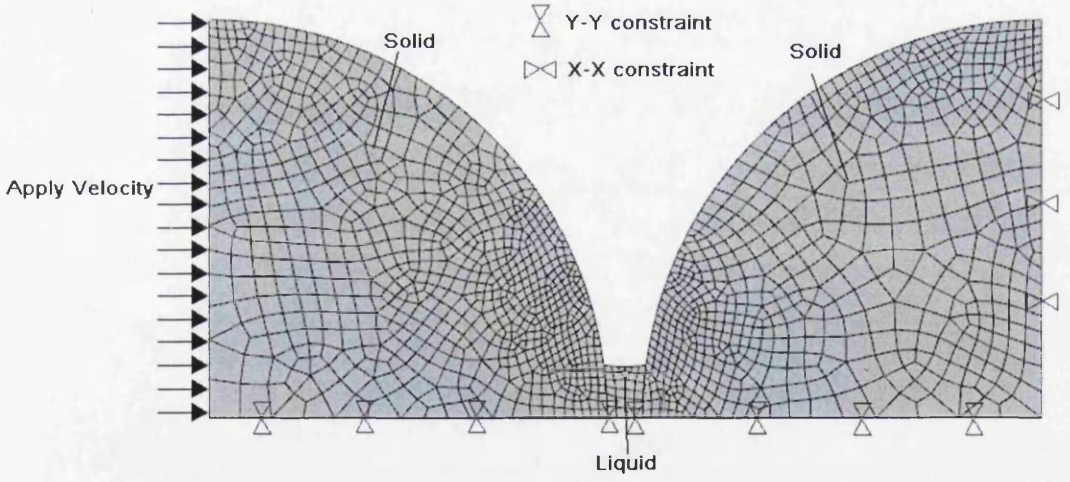

Figure 4. 2: Initial layout of FEM model

Variables such as reaction forces and contact pressure are recorded throughout the process, as shown below:

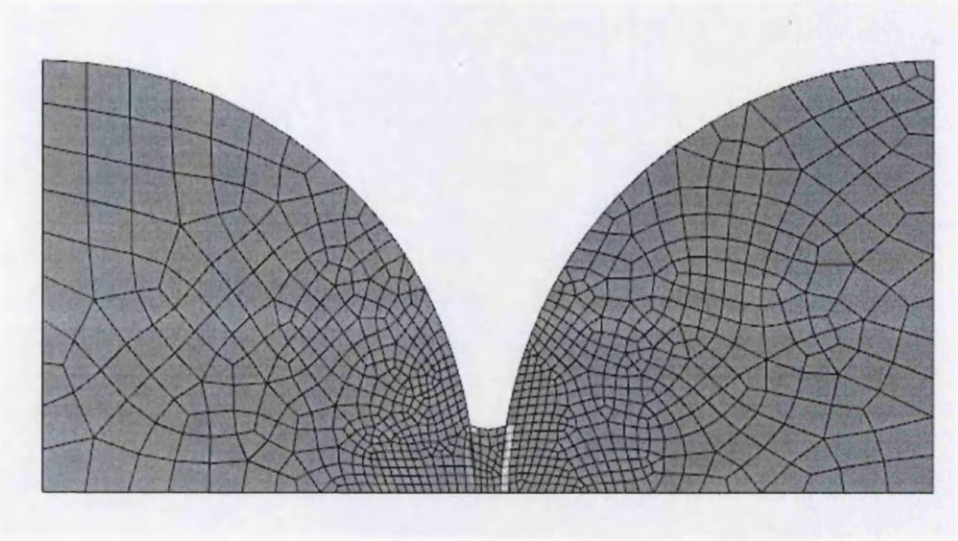

Figure 4. 3: Plotting of time =0.4 s

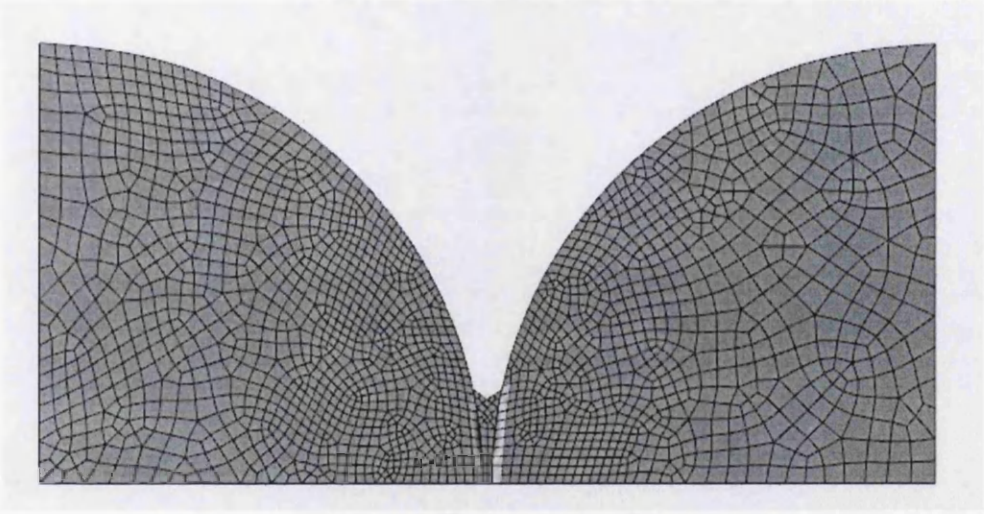

Figure 4. 4: Plotting of time = 0.8 s

Also note that mesh adaptivity is also employed in the simulation. Start form the simulation time 0.8 s (Figure 4.4) the mesh size around the liquid bridge area become finer and finer. The results show that the contact pressure at the place where the two solid surfaces are about to touch become very high, hence it is believed that liquid bridge at time larger than 0.9 become very stiff. This behavior is because of the constraint in the y direction of liquid bridge.

4.2.1 Examination of the failure in FEM numerical analysis

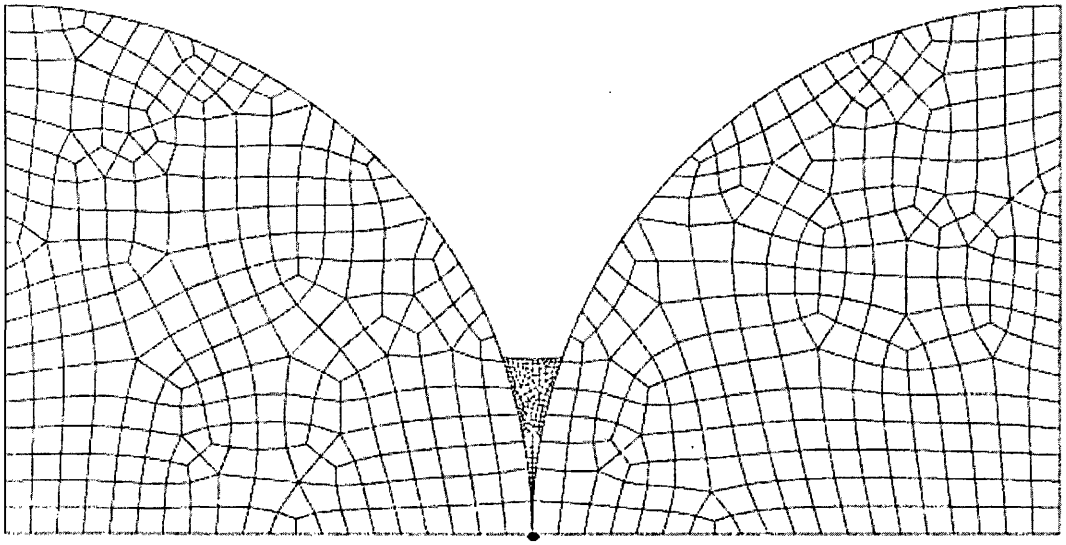

Figure 4. 5: Mesh layout at time = 0.988 s

The FEM program terminates due to a large deformation of mesh of the liquid bridge, at the place shows with a black dot in Figure 4.5. This numerical problem cannot be solve even with an extremely small mesh size. This is because of the same reason that would eventually encounter before two solid surfaces are actually in contact. In another words, this model does not service its purpose, unless the problem of large deformation of the liquid bridge mesh is solved.

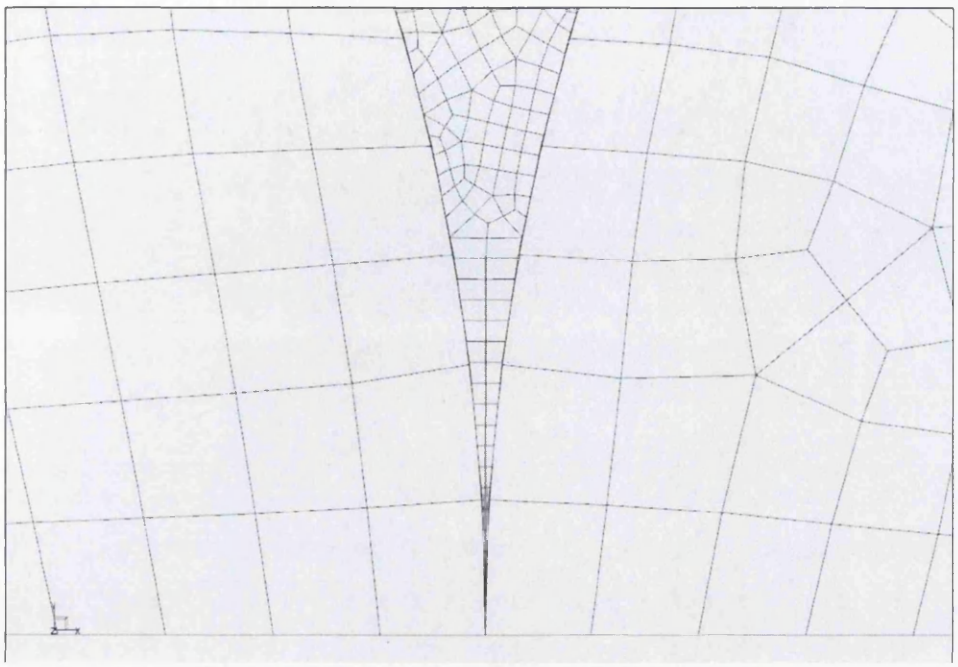

Figure 4. 6: Enlarge view of large mesh deformation

In order to solve the problem of large deformation of liquid bridge mesh, a relaxation of the y-direction constraint on liquid bridge has been applied. This relaxation is assumed to take place once the simulation time reaches 0.9 s and an upward velocity is applied to the bottom of the liquid bridge, with a magnitude obtained by trail and error, to push the liquid upwards and leave a small room for solid-solid contact, which is demonstrated in Figure 4.7.

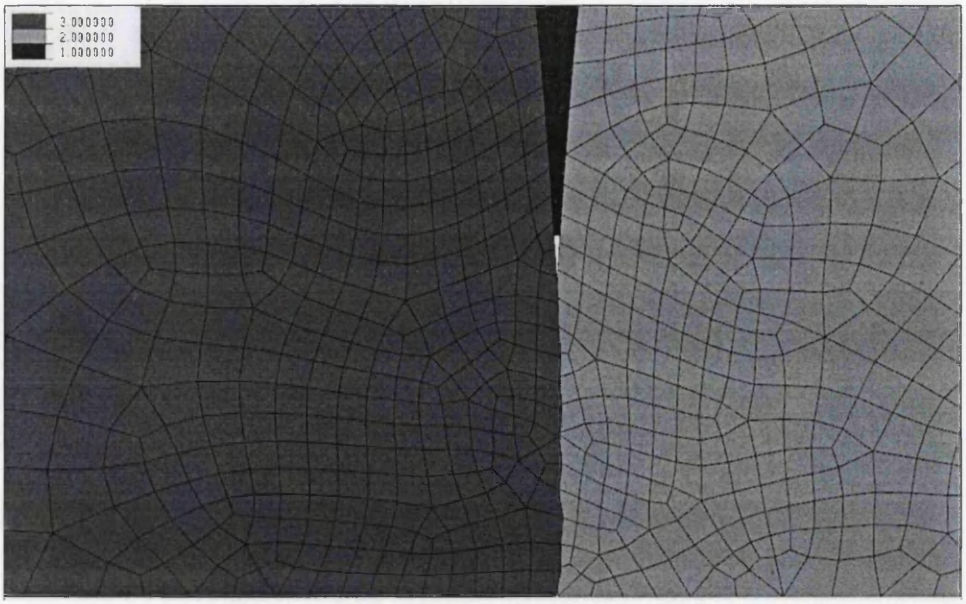

Figure 4. 7: Result of FEM model with relaxation

Although the large deformation problem of the FEM model has been solved and solid to solid contact becomes possible, the meshes of three elements start to penetrate with each other, as shown in Figure 4.8. There is neither contact pressure nor reaction force detected from the FEM model, once the meshes penetrate with each other.

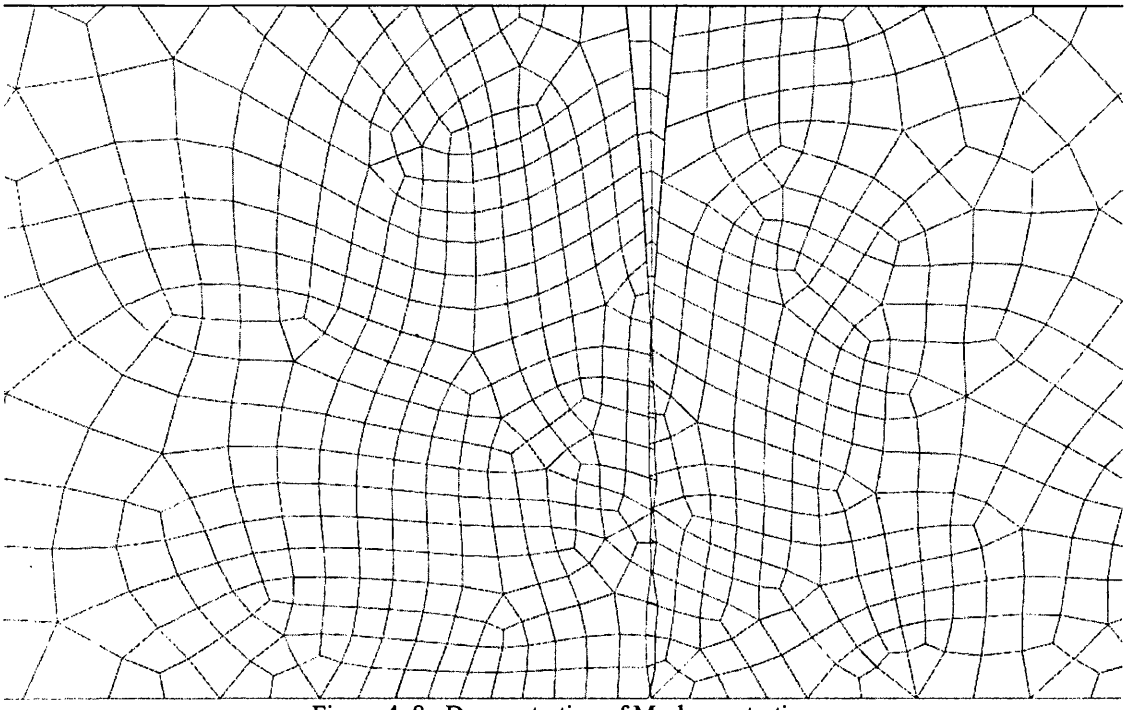

Figure 4. 8 : Demonstration of Mesh penetration

This problem, to the best of the author knowledge, is mainly due to the unbalance of the penalty coefficient that is used in Elfen. This coefficient serves as a stiffness coefficient to resist two contacting surfaces from penetrating with each other and is obtained empirically by trial and error.

In order to initiate the simulation, a penalty coefficient is assigned for the liquid-solid contact surface. However, the problem of penetration occurs when two solid surfaces are in contact. This is because the assigned coefficient being used in the simulation program is unsuitable for solid to solid contact surface properties. Conversely, a similar mesh penetration problem appears, for liquid-solid contact, when a penalty coefficient is assigned for solid-solid contact surface.

Although the FEM models seem not achieve its objective, the trend of the FEM simulation results is worthy to mention. The trend-line shown in Figure 4.9 represents the relationship of contact pressure, of squeezing a liquid bridge, and separation distance between two solid surfaces. This line shows a gradually decrement as the separation distance decrease, where the obligation of results are mainly due to the mesh refinement of the simulation program. This trend of contact force shows a similar result obtained from equation of static liquid bridge force from equation (3.27) in Figure 4.10. Thus, it is believed that the FEM models show the correct behavior of a liquid bridge.

However, as the viscosity of liquid bridge cannot be implemented into Elfen, the result for this FEM model can only serves as evidences that a main problem of getting the interaction law for the 'load-deform-unload' system at very small separation distances.

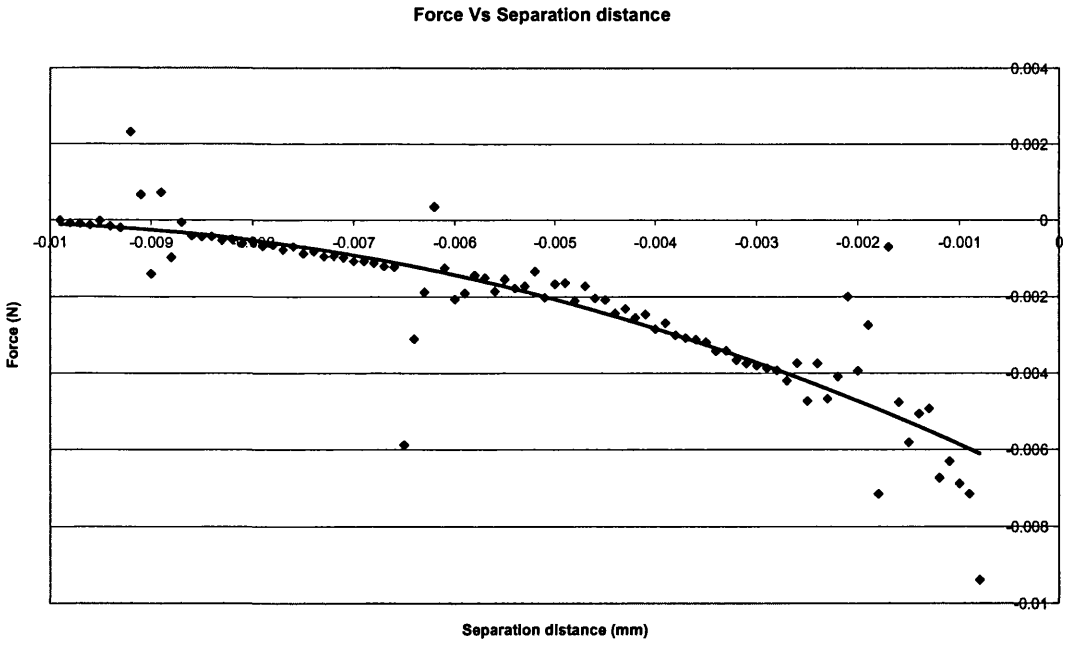

Figure 4. 9: FEM modeling result

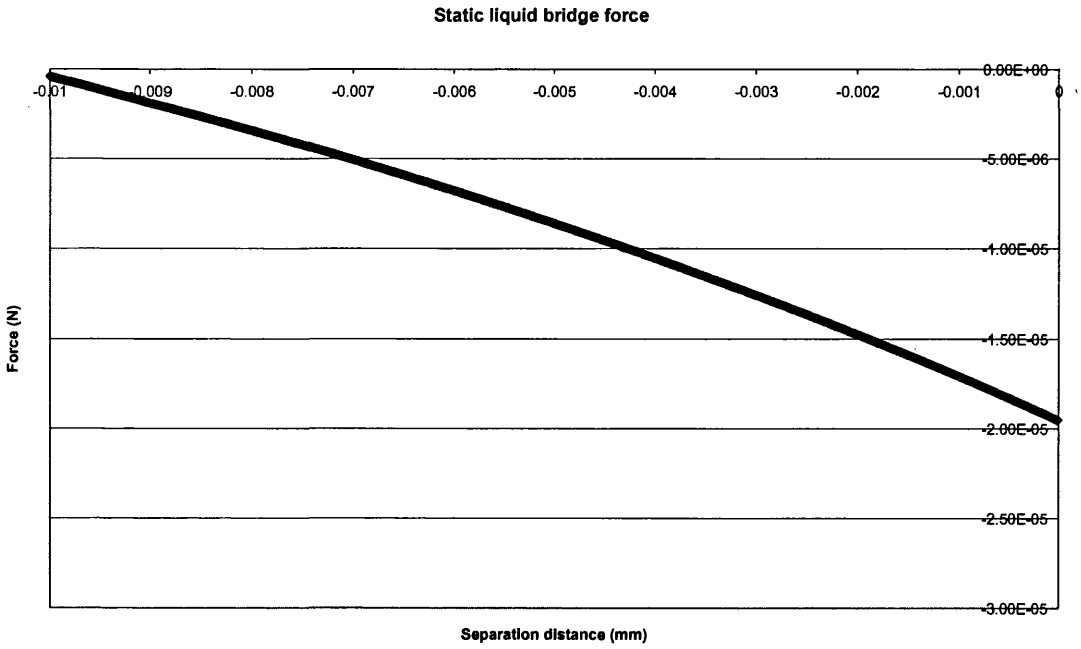

Figure 4. 10: Static Liquid bridge force

4.2.2 Experimental analysis

In order to take the viscous liquid bridge force into consideration, some experimental results reported in Meurisse and Querry (2006) are considered. The results state that the static liquid bridge force verse the gap between two surfaces is always attractive for concave liquid bridges, this is because the part of the static liquid bridge force due to the surface tension at the contact interface always dominates the part of static liquid bridge force due to hydrostatic pressure. This also explains the gradually decreased force obtained from the FEM analysis.

When squeezing a liquid bridge at constant speed, static liquid bridge force always dominates in the early stage of squeezing. Conversely, dynamic liquid bridge force is dominant in the asymptotic behavior for very small separation distance. This means that a normal force is always attractive at the beginning or the squeezing motion and becomes repulsive at small gaps,

as illustrated as below.

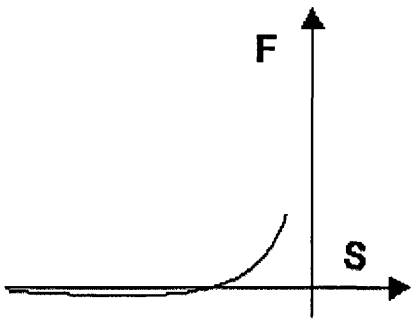

Figure 4. 11: Illustration of dramatic change in force of squeezing liquid bridge

In summary, FEM results provide some evidences which show the potential problem of using FEM numerical analysis to find out the interaction laws for 'load-deform-unload' system that happens when separation distance between two solid surfaces is small. Besides, the literature reports a phenomenon of squeezing a liquid bridge that an attractive force occurs at the early stage, or large separation distance, and this force changes from attractive to repulsive at a small separation distance due to the effect of viscous liquid bridge, which acts as a resistance to the squeezing motion of the particles. Hence, a repulsive viscous liquid bridge force occurs. However, both numerical and experimental analysis can only produce results up to a stage when two surfaces are about to touch.

4.3 Interaction Law for 'load-deform-unload' system

As both numerical and experiment results can only provide a limited information on the objective of this project, a study of the theories involve in the 'load-deform-unload' is carried to find out any potential difficulties of establishing the interaction law for the system from those theories. Different governing equations from the previous chapters are investigated next.

4.3.1 Solid-Solid interaction law

A well-known and experimental proven contact model, the JKR model, is used in this project for the loading and unloading process of solid to solid contact. The derivation this equation for two elastic adhesive solid particles can be found in Chapter 2. The JKR

model accounts for the influence of Van der Waals force within the contact zone, hence, an attraction arises which weakens the force of elastic repulsion (reaction force from each contact surface) and results in a negative force as shown in Figure 4.11.

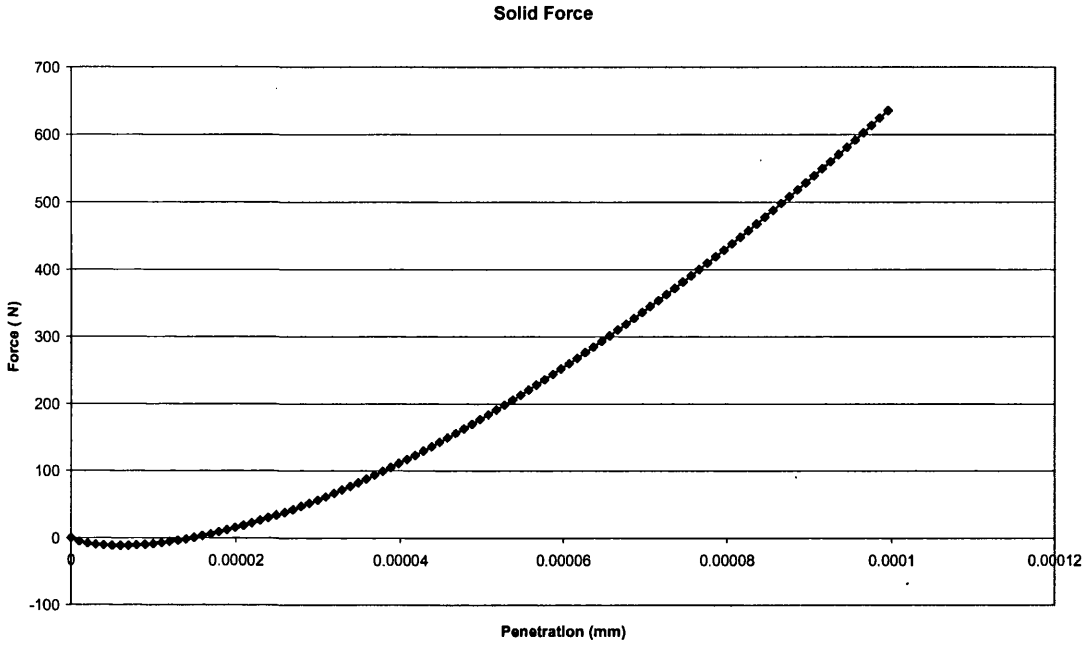

Figure 4. 12 : Force vs displacement (the JKR Model)

It can be seen that the contact force for pure solid-solid contact is zero at the instance when the two surfaces just contact.

4.3.2 Liquid bridge interaction law

The liquid bridge force can be distinguished into two components; the static and the dynamic liquid bridge force. Evaluation for both forces is discussed in Chapter 3 and the force verse displacement graphs are plotted separately for both static and liquid bridge forces. Attention is drawn at the forces when the separation distance, in the x axis, becomes zero.

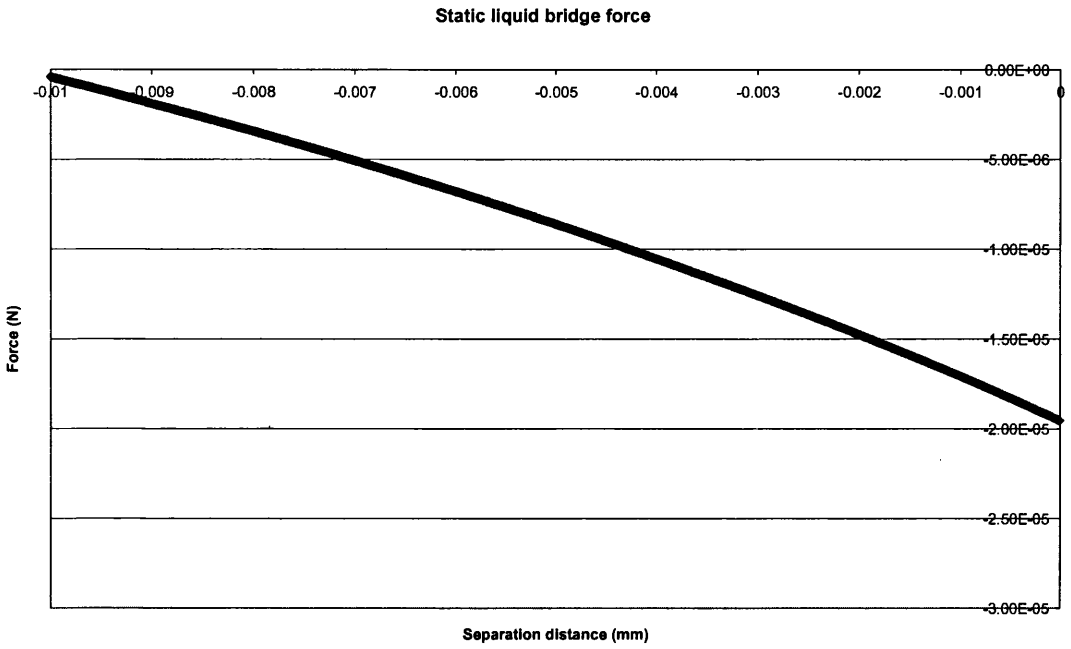

Figure 4. 13: Force Vs displacement (Static liquid bridge force)

The static liquid bridge force gives a certain value at separation distance equal to zero, which represents the situation of two solid surfaces close up. However, the dynamic liquid bridge force gives an infinite value of contact force as two solids surface contact, as demonstrates in Figure 4.14. This may causes a numerical instability in a simulation model, which uses equation (3.38) as the governing equation for dynamic liquid bridge force.

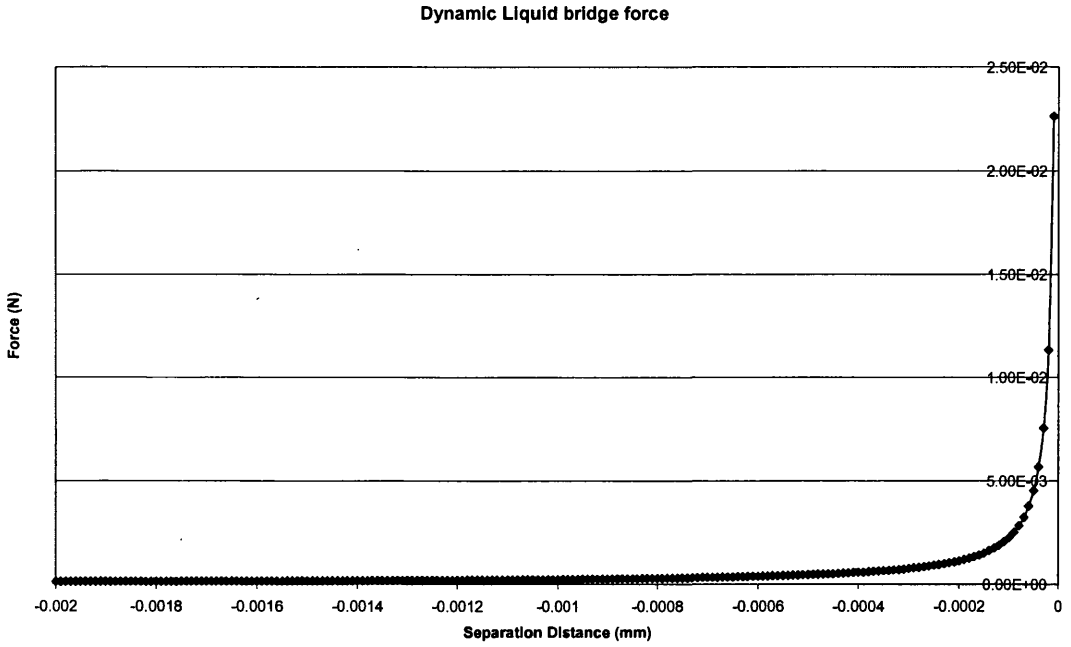

Figure 4. 14: Force Vs displacement (Dynamic Liquid bridge force)

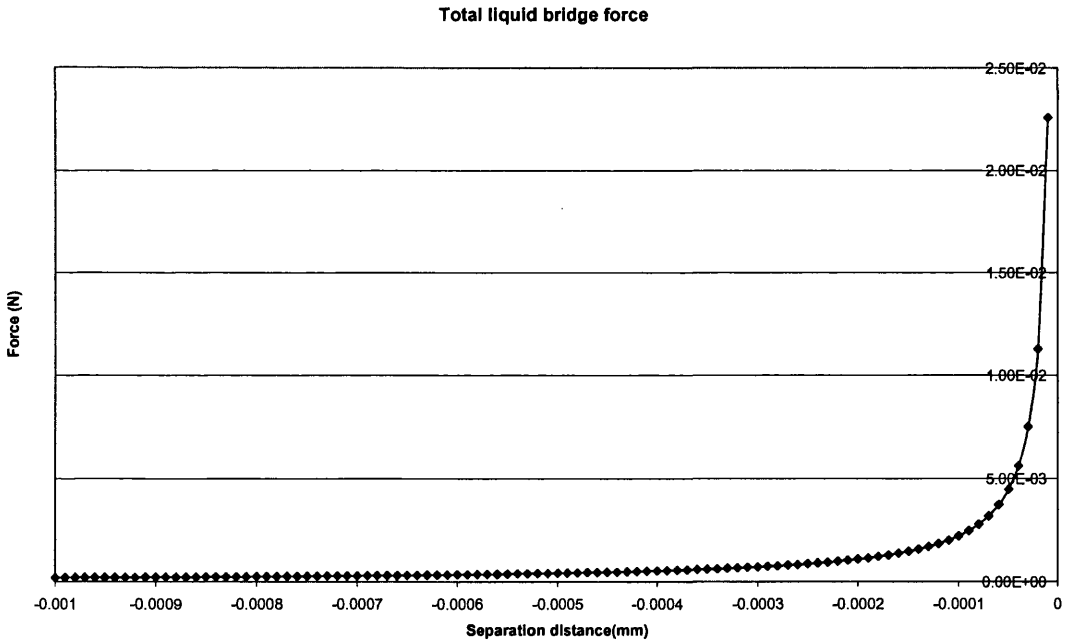

Figure 4. 15: Force Vs displacement (total liquid bridge force)

Figure 4.15 shows the total liquid bridge force as the separation distance approaches zero. It can be noticed that the force changes from a negative (attractive) force to a positive

(repulsive) force, as the separation distance decreases. This trend is similar to what has been reported in M.H. Meurisse and M.Querry (2006). As a result, it is believed that the theoretical equation provide a reasonably accurate predict of both liquid and solid phase as individual, and it is possible to form a set of equations to govern to behavior of the 'load-deform-unload' process.

4.3.3 Proposed integral interaction law

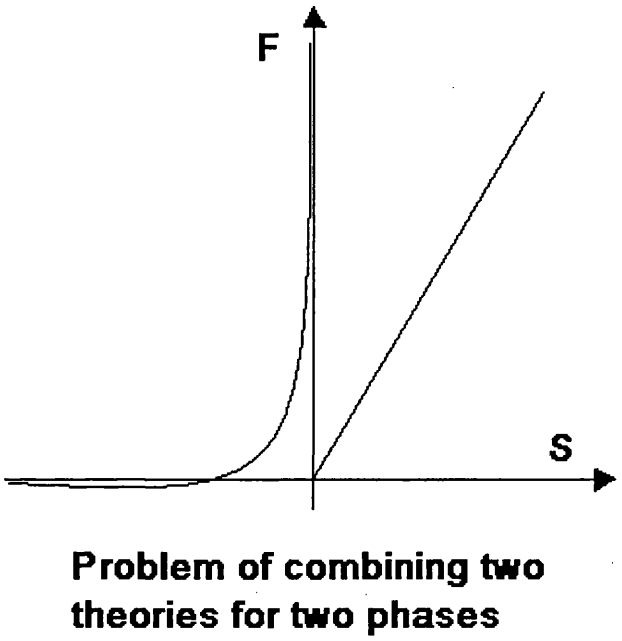

Figure 4. 16: Illustration of problem of combining two theories of solid and liquid phases

However, the problem of establishing this set of equations is the infinite value of force from the dynamic liquid bridge force when separation distance becomes zero. A simple combination of the theories is plotted in the above Figure. It shows a discontinuous of two expressions at separation distance (S) equals to zero. This infinite value of liquid bridge force is because of the theoretical model that uses for dynamic liquid bridge force derivation is based on the assumption that the spheres are rigid with prefect smooth surfaces. For real particles, however, the separation distance cannot reach zero due to many factors, for example:

1) The roughness of the surface (A. Dyson (1976); A. Cameron (1997)).
2) Elastic-plastic deformation of the spheres, when high viscous hydraulic pressure occurs.
3) Change in lubricant shear strength (Zhang and Wen (2001); Kannel and Bell (1971)) when heavy load, high rolling speeds and high lubricant temperature are encountered.

In fact, it will be too complicated to consider the full elasto-hydrodynamic lubrication (EHL) collision of particles with surface deformation and surface roughness. Therefore, several assumptions are made in this project. Firstly the spheres are assumed 'rigid' enough that the deformations of the surfaces are small and become negligible when comparing with the sphere displacement. Moreover, the third issues is believed to be invalid for this project, as the area of the contact is very small, the twisting resistance at the contact due to the relative spin about the line joining the centroids of the two spheres is ignored, and thus, the rotational movement particles are not considered. Finally, the change in lubricant shear strength is assumed to be negligible due to the absences of rotational motion.

In summary, for all these factors which avoid the separation distance from approaching zero, surface roughness is assumed to be the major issue among all the three factors. This is proposed in this project that the surface roughness is taken into account for establishing the interaction law for moist agglomerate by assigning a minimal separation distance as a cut-off distance. The viscous effect of the liquid bridge of any separation distances smaller than this minimum is modified in order to provide a smooth transition from liquid phase to solid contact phase, as illustrated in the Figure below.

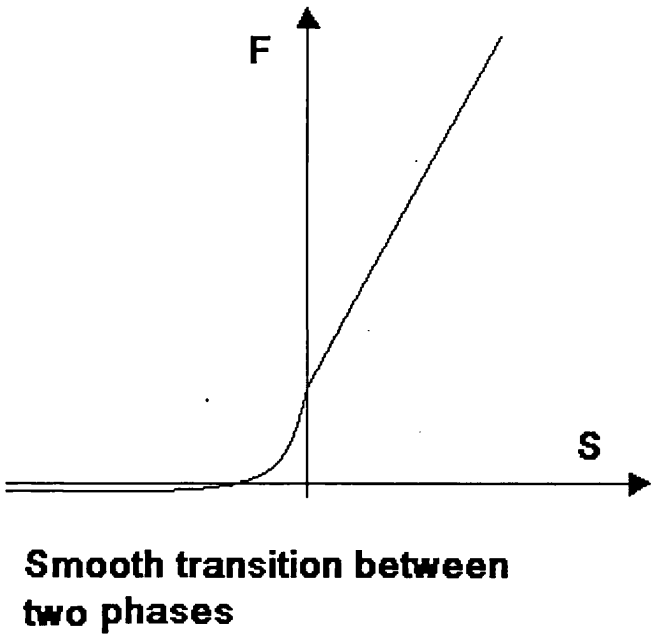

Figure 4. 17: Illustration of smooth transition

Surface roughness not only interacts with the hydrodynamics of the fluid film, but also leads to very high local contact pressures near the asperity tip regions where the fluid film is not thick enough to separate the contacting surfaces completely.

This phenomenon is responsible for causing the collapse of the fluid film, which leads to either failure of the lubrication system or change of lubrication from full film to mixed EHL. Both of these phenomena bring a larger portion of the contacting surfaces under direct contact.

Although different approximate profiles of surface roughness are reported in the literature, surface properties and roughness varies from particle to particle. Instead of going in depth to investigate the effect of each approximate profile of surface roughness, an alternative way is proposed in this project. It is to assign the value of surface roughness, S_r, to the interaction law. Any separation distance (S) smaller than S_r, lubrication theory is assumed to breakdown due to the collapse of fluid film. Moreover, the rate of change of viscous force to separation distance is assumed to remain constant

after lubrication breakdown and liquid bridge force is assumed to remain constant and effective throughout the solid-solid contact.

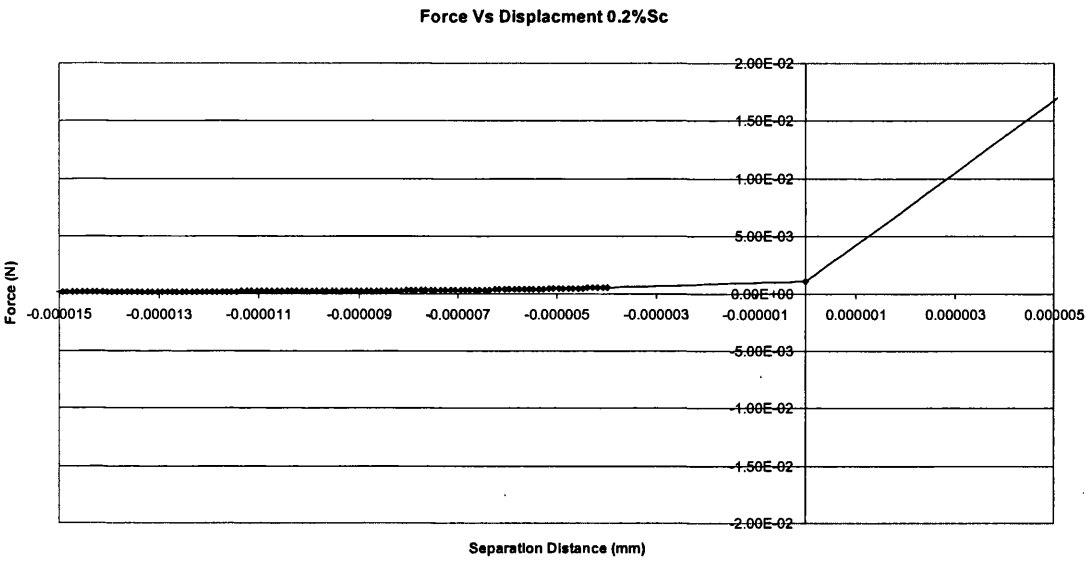

Figure 4. 18: Force verse separation distance for S_r=0.2%Sc

An example of force verse separation distance graph is shown in Figure 4.18, which illustrates the assumptions that have been made in this project, where negative value in x-axis represents a gap between two particles surface and positive value in the x-axis represents a contact of two particles. The separation distance, or displacement, can be separated into three cases, i.e. 1) before failure of lubrication theory; 2) after lubrication theory breakdown and before solids contact happens and 3) solid contact takes place.

Case 1:

$S_c < S < S_r$

This part of the graph is explained by M.H. Meurisse and M.Querry (2006) for the liquid bridge being squeezed before it fails due to surface roughness, $S < S_r$. They report that the static liquid bridge force verse the gap between two surfaces is always attractive for concave liquid bridge, this is because the part of the static liquid bridge force due to surface tension at the contact interface always dominates the parts of static liquid bridge force due to hydrostatic pressure. When squeezing a liquid bridge at a constant speed, static liquid bridge force always dominates in the early stage of squeezing. Conversely,

dynamic liquid bridge force is dominant in the asymptotic behavior for very small separation distances. This means that a normal force is always attractive at the beginning or the squeezing motion and becomes repulsive at small gaps. This explains why the force does change from negative to positive.

Case 2:

$S_r < S < 0$

For $S_r < S$, the lubrication theory is assumed to fail due to the effect of surface roughness of the solid particles, hence, collapse of the fluid film (P. Kumar et al (2001)).

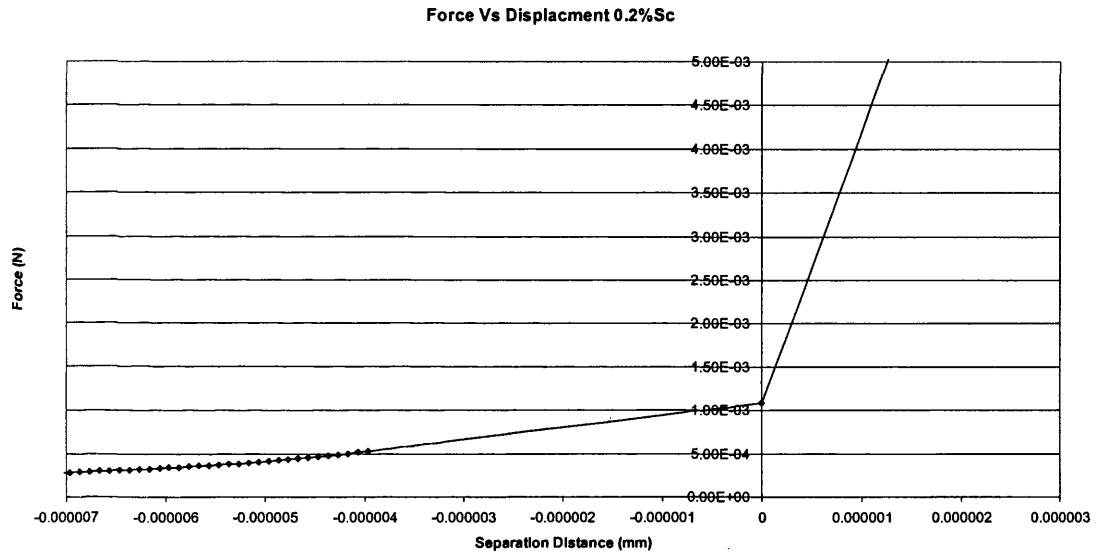

Figure 4. 19: Constant rate of Change after S_r ~-0.000004mm

However, the repulsive force of the fluid films between those asperity regions are assumed to remain effective after lubrication theory breaks down. The contribution of these fluid films is assumed to be represented by a constant rate of change of the liquid bridge force against the displacement until the two surfaces are actually in contact. As illustrated in Figure 4.5, the parabolic curve stops at the breakdown distance, S_r, and then a linear line is used to represent the repulsive force of the remaining fluid films between the asperity regions.

Case 3:

$S \geq 0$

Finally, the liquid bridge force is assumed to be constant through out the solid-solid contact, with a magnitude just before two particles are in contact. As a result, a smooth curve for the loading case is obtained and it is demonstrated in Figure 4.20.

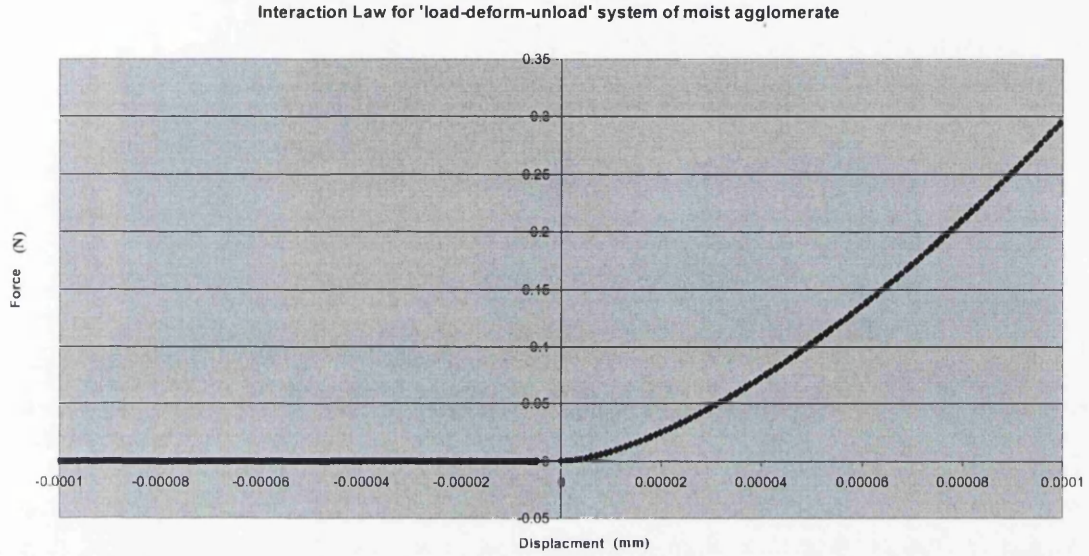

Figure 4. 20: illustration of proposed interaction law (Sr=0.25% Sc)

Unloading case

As the solid phase is assumed to be elastic and no energy loss throughout the whole loading and unloading process, the unloading case for solid contact is assumed to reverse the process of loading case. However, as the viscous liquid bridge force is always against the direction of motion, the effect of liquid bridge change from repulsive to attractive at the loading case to unloading case respectively, which is illustrated below:

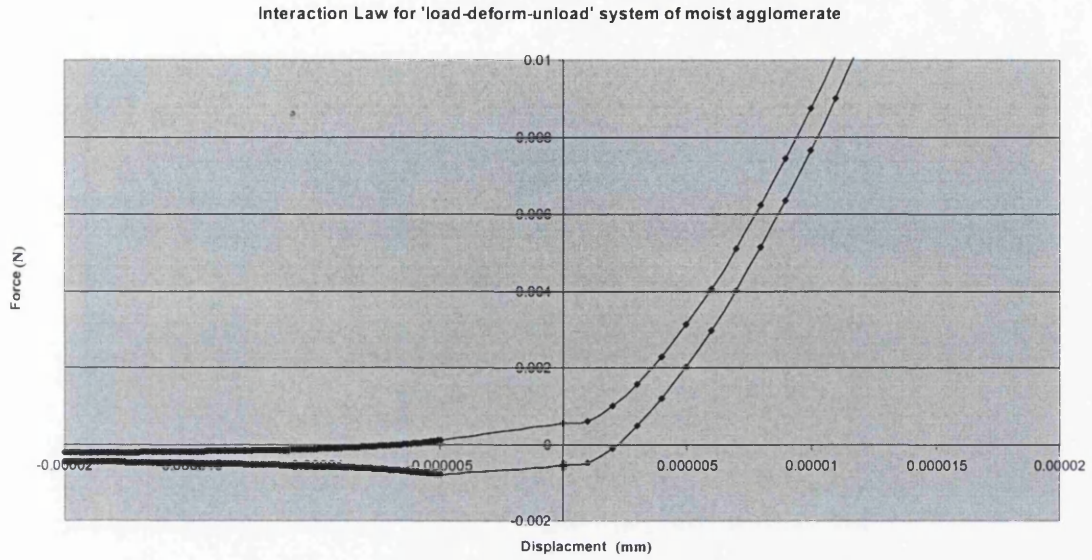

Figure4. 21:Interaction Law for 'load-deform-unload' system of moist agglomerate

The interception of the x-axis in unloading curve is assumed to be the viscous effect and adhesive effect from the liquid bridge and solid particles respectively. A neck of solid plus liquid bridge is assumed to happen just before two elastic particles detach.

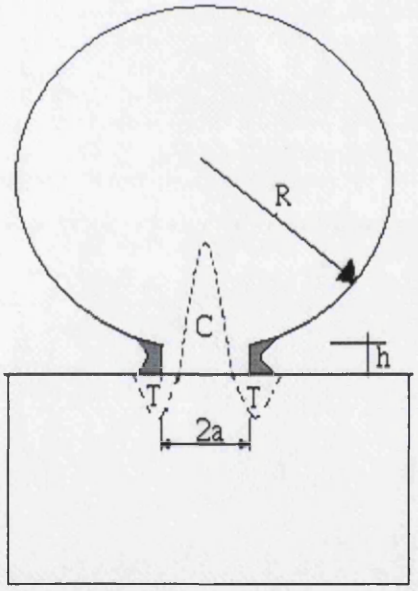

Figure 4. 212: Illustration of modified 'neck' for the 'load-deform-unload' system

Different values of breakdown distance, S_r, due to surface roughness are assigned and be implemented in a DEM code (DEMC) developed by the author. The investigation of the

effect of surface roughness and the interaction law to a group of particles in a free-falling simulation is presented in Chapter 6.

References:

A. Dyson (1976), Inst. Mech. Eng. Proc. 190, 52.

A. Cameron (1997), Some open questions in boundary lubrication, Tribology letter,3,13-18.

Y. Zhang and S. Wen (2001), A lubrication deviation from the classical EHL theory by the lubricant viscoplasticity: part I-film thickness dependence, trib. Trans., 44, 224-232.

J. W. Kannel and J. C. Bell, (1971), Interpretations of the thickness of lubricant films in rolling contact: part I- examination of measurements obtained by X-rays, ASME J. of lubri. Tech., 478-484.

J. Kestin (1955), Boundary layer theory, 1st edition, London: Pergamon Press Ltd.

H. Ping, L. Jianbin and W. Shizhu (1999), Theoretical study on the lubrication failure for the lubricant with a limiting shear stress, Tribology international, 32,421-426.

R. H. Davis, J. Serayssol, E. J. Hinch (1986), The elastohydrodynamic collision of two spheres, J. Fluid Mech., 163,479.

M. H. Meurisss, M. Querry ,(2006), Squeeze effects in a flat liquid bridge between parallel solid surfaces, Journal of Tribology, 128,575-584.

P. Kumar, S. C. Jain and S. Ray, (2001), Study of surface roughness effects in elastohydrodynamic lubrication of rollin line contacts using a deterministic model., Tribology International, 34, 713-722.

M. J. Adams and V. Perchard, (1985), The cohesive forces between particles with interstitial liquid. Int. Chem. E. Symposium Series, 91, 147-160.

M. J. Matthewson, (1988), Adhesion of spheres by thin Liquid film., Philosophical Magazine !, 57, 207-261.

D. N. Mazzone, G. I. Tardos, R. Pfeffer, (1987), The behavior of liquid bridges between two relatively moving particle., Powder Technology, 51, 71-83.

B. J. Ennis, G. I. Tardos and R. Pfeefer (1991), A microlevel-based characterization of granulation phenomena, Powder Technology, 65, 257-272.

R. H. Davis, (1987), Elastohydrodynamic collision of particles, Physicochemical Hydrodynamics, 9, 41-52.

R. H. Davis, J. M. Serayssol and E. J. Hinch (1986), The elastohydrodynamic collision of two spheres, J. Fluid Mech. , 163, 479-497.

J. M. Serayssol and R. H. Davis (1986), The influence of surface interactions on the elastohydrodynamic collision of two spheres, Journal of colloid and interface science, 114, 54-66.

G. Barnocky and R. H. Davis (1988), Elastohydrodynamic collision and rebound of spheres: Experiemental Verification., Phys. Fluids, 31, 1324-1329.

Chapter 5

Development of a Discrete Element Method Program

5.1 Introduction

A proportion of engineering studies do not take the discontinuous nature of the materials into account. This is because these engineering problems consider material in quantities large enough so that the microstructure of the material can be described by averaged material properties. These kind of engineering problems are classified as continuous. The continuous nature of such material properties is best governed by a set of partial differential equations or integral equations, which couple with external actions in the form of boundary and initial boundary value problem. The solution of a particular boundary value problem is sometimes expressed in analytical form.

However, some other engineering studies consider the discontinuous nature of materials. For example: in many manufacturing industries such as the chemical engineering, pharmaceutical and food sector, the production of granular materials play an essential parts (J. Fu et al (2004)). Their behavior under impact loading is important during granulation since an intense agitation of the feed materials causes the granules to interact with each other and the equipment walls with deformation. Consequently, an understanding of the behavior of granules is needed to optimize the design and quality control of such granulation process.

In order to achieve this, mathematical description of the examples ought to take into account the shape, size and mass of individual particles. Eventually, a set of governing equations for different particles are coupled thorough inter-particles interaction. The resulting global set of coupled governing equations describes the behavior of the particulate system as a whole.

As mentioned before the objective of this project is to obtain and investigate the effect of the proposed set of governing equations for the 'load-deform-unload' system, thus, the interaction law is implemented into a DEM model (DEMC), which simulates a moist agglomerate in free falling test.

In this chapter, the implementation of interaction laws for liquid-solid interaction and solid-solid interaction is discussed. Finally, the structure of the DEM code (DEMC) will also be presented in this chapter.

5.2 Implementation of various interaction laws

5.2.1 Solid contact forces

The interaction force between each pair of contacting spheres is computed in an incremental way. In the case of two spheres contact, because the area of the contact is very small, the twisting resistance at the contact due to the relative spin about the line joining the centroids of the two spheres is ignored and hence only normal and tangential contact force are considered. For simplicity, tangential movement at the contact point is also neglected in this project. As a result, the relative movement at the contact has only one component, which is the relative normal approach along the centre line of the two spheres.

For a pair of spheres in contact, if the linear velocities are denoted by v^A_i and v^B_i respectively, the relative normal displacement increment at the contact in a time step can be given by,

$$\Delta s = \left(v^B_i - v^A_i\right) n_i \Delta t \qquad (5.1)$$

where i= 1,2,3 (if you say "sphere", you need the index up to 3) indicate the two coordinate directions and n_i is the component of the unit vector normal to the contact plane and directed from sphere A to sphere B. The updated normal force at the contact point is given by,

$$F_n^{new} = F_n^{old} + \Delta F_n \tag{5.2}$$

where ΔF_n is the normal force increment which is obtained from (2.27) which applies to both adhesive and non-adhesive spheres. From the updated normal contact forces, the contribution to the out-of-balance force of each sphere is obtained as:

Sphere A: $F_i^A = F_n^{new} n_i$ (5.3)

Sphere B: $F_i^B = -F_n^{new} n_i$ (5.4)

5.2.2 Liquid bridge forces

Liquid bridge is introduced by specifying the liquid volume, surface tension, contact angles and viscosity of the liquid bridges. The same specification may also be used to remove the liquid bridge if those parameters are set to zero.

When values are assigned, rupture distance of each identical liquid bridge is calculated by a widely accepted equation from G. Lian et al (1993). For a liquid bridge between two equal sized spheres of radius R, the rupture distance S_c may be related to the liquid volume by,

$$S_c = \frac{1}{2}(1+0.5\theta)\sqrt[3]{V} \tag{5.5}$$

where V is the liquid volume and θ is the contact angle.

Liquid-solid contact is assumed to begin and end when the separation distance between two particles surface is equal or small than S_c and larger than S_c respectively. As a result, the contact search array varies when the parameters for liquid bridge is specified.

During the time integration calculations, instead of using the incremental method, both the static and dynamic liquid bridge force is calculated directly by using integral equations. The static liquid bridge forces are calculated according to Fisher's toroidal approximation using the 'gorge' method of equation (3.27). As it has been mentioned in chapter 3, the gorge method gives the best estimate of the total static force. In equation (3.27), the static force that a liquid bridge exerts on the spheres is given in terms of ρ_1 and ρ_2, which are expressed in terms of separation distances and filling angle. Since the filling angle varies with separation for a given liquid bridge volume, an approximate relationship between the filling angle and separation distance is used. This relationship is obtained by fitting the numerical results with a third order polynomial function (G. Lian 1994). It states that for a constant dimensionless liquid volume, the dependence of the filling angle ϕ on the relative separation distance $\frac{S}{S_c}$ can be fitted by a third order polynomial function given as

$$\phi = C_0 + C_1\frac{S}{S_c} + C_2\left(\frac{S}{S_c}\right)^2 + C_3\left(\frac{S}{S_c}\right)^3 \qquad (5.6)$$

where C_0, C_1, C_2 *and* C_3 are four fitting coefficients.

It has also been mentioned that the four fitting coefficients are only dependent on the dimensionless volume of liquid bridge and the ratio of the sphere radii. For different sets of dimensionless liquid volume, the four fitting coefficients obtained are given in the following table:

V/R^3	C_0	C_1	C_2	C_3
0.001	0.16702	-0.28582	0.37579	-0.1644
0.005	0.25947	-0.35601	0.43167	-0.17593
0.01	0.31461	-0.38911	0.45302	-0.17792
0.02	0.38246	-0.42474	0.47284	-0.17819
0.03	0.42938	-0.44723	0.4839	-0.17763

Table 5. 1: Fitting coefficients for the filling angle

In summary, the procedures for calculating the static force of liquid bridge are described as follows. As the liquid volume and radii of particles are the same, the fitting coefficient for each liquid bridge is interpolated from Table 5.1, thus, the filling angle could be obtained from the equation (5.6) for a given separation distance. Finally, the calculation of the principal radii, ρ_1 and ρ_2 of the toroidal curvature can be done and hence the force is straightforward using equation (3.22), (3.23) and (3.27).

In order to prevent numerical instability in the 'load-deform-unload' system, a method proposed in chapter 4, that the lubrication theory is assumed to breakdown at certain point, which is assumed to be small enough for the effect of surface roughness to occurs, i.e. 0.2%~5% of the rupture distance, S_c, (0.000004-0.0001mm). The rate of change of total liquid bridge force is assumed to remain unchanged after the lubrication theory fails; and stays effective during the solid-to-solid contact.

5.2.3 Assumptions for two dimensional modeling

As mentioned earlier that those theories and experimental results govern the behavior of liquid bridge are in three dimensional cases. Nevertheless, for simplicity reason, two dimensional modeling is used instead. In order to do so, several assumptions have been made.

Contact Force

- All contact forces are radical from or toward the centre of gravity of the particles.
- Only the maximum solid contact pressure is considered. In another words the radius of the contact circle (a) in equation 2.13 will be zero.

Solid particle

- All disks are uniform with radius R.

Liquid Bridge

- The effect of the hydrostatic pressure deficiency, surface tension and viscous effect of a liquid bridge mechanical behavior is assumed to be represented by a damping/frictional slider. Which acts directly to the center of gravity.

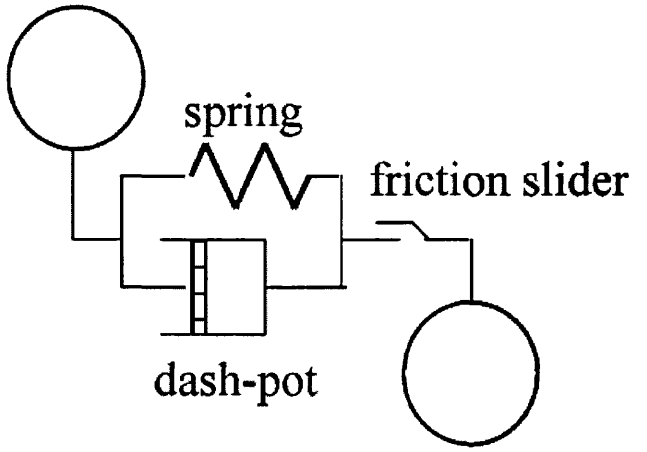

Figure 5. 1: Illustration of contact force model.

As a result, the contact model for solid and liquid bridge effect is illustrated as in Figure 5.1 and will be implemented into a DEM model.

5.3 General structure of DEMC code

5.3.1 Program structure

DEMC simulates the mechanical behavior of granular assemblies considering of spherical particles. In order to simulate a particulate assembly, time integration calculation is carried out, in DEM simulation, and compute the incremental contact forces and progressive movements of the spheres. For each calculation cycles, the translational accelerations of each of the constituent particles are given by Newton's second law of motion.

Numerical integration is then performed over small time-steps to give updated velocities and displacements of each sphere. The velocities of each particle are used to find the relative approach between contacting particles. The relative approach is in turn used to calculate the incremental contact force according to the interaction laws, which has been discussed earlier in this report. The contact forces are resolved to obtain the out-of-balance forces on each particle, from which new accelerations of each particle are then calculated at the next time step.

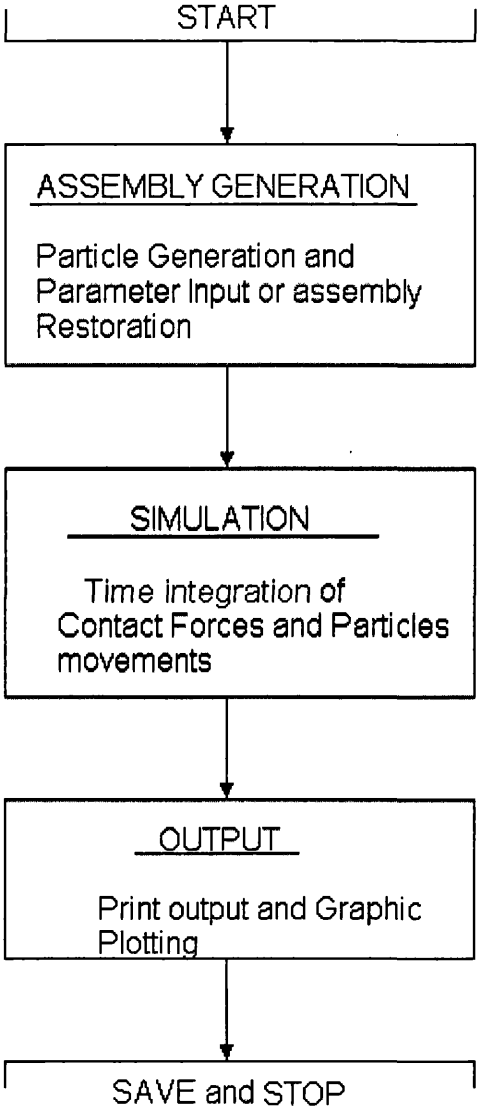

Figure 5. 2: The Program structure of DEMC.

The basic structure of DEMC is illustrated in Figure 5.1, which consists of three parts. The first part is the assembly generation module which is used to generate assemblies of the particles and to define particle properties. The main part of DEMC is the time integration module, with which the evolution of contact forces and particle movements are simulated. The third part of DEMC is the output module, which provides a graphic and print out to facilitate the interpretation of the simulated results.

5.3.2 Assembly generation

This stage includes the assignment of the size and the material properties of the solid particles, the volume and parameters for liquid bridge and the positions of the walls.

Then smooth and continuous elastic walls are introduced, and particles with specified dimension will be arranged in a prescribed pattern, as illustrated in Figure 5.2, for a free-falling simulation. The program stops when it reaches the final packing stage, i.e. total energy of the system equals to zero.

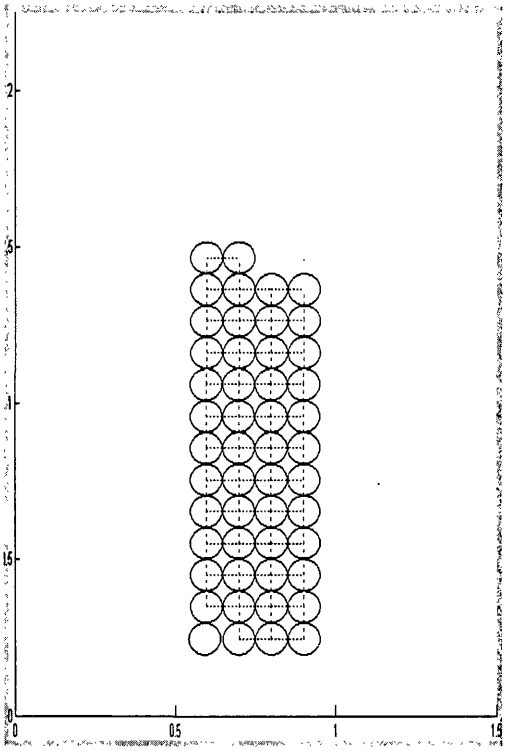

Figure 5. 3: Particule arrangement for 50 particules.

5.3.3 Simulation modules

In order to keep track the contact force of each particle in the systems, it is necessary to identify which pairs of particles are in contact. As a result the contact search algorithm is essential to be carried out first.

After that, the interaction forces of all contacting particles are calculated and coupled. The resulting forces are then used to obtain the new displacements and velocities of all the particles through time integration.

Kinetic and potential energies of each particles are updated by the new velocities and displacement of each particles respectively. These two energies are then summed to give the global kinetic energy and global potential energy for the whole system. Eventually, the total energy of the system can be obtained by adding the global kinetic and global potential energy together. This total energy is also be utilized as a criteria to terminate the simulation, by checking it with a prescribe value of total energy for a balanced system.

Contact search algorithm rescans for contact detection of particles with updated positions. Simulation module repeats until a desired terminate point, which can be specified either the maximum number time steps or simulation time.

Contact search

The contact search algorithm that has been used in this project is a direct checking contact detection algorithm, the simplest contact detection algorithm possible. This algorithm is implemented in two steps:

- A bounding object for each discrete element is defined.
- A simple intersection check for bounding objects is made, if bounding objects of any two discrete elements are found to be intersecting each other, it is assumed that the two discrete elements are in contact.

The bounding object for each equal sized particle in this project is assumed to be circles of constant diameter d= R+S_c, where R is the radius for each particle and S_c is the rupture distance for liquid bridge. By chosen in such a way, no point of any discrete element is outside the circle. A loop over all bounding circles is performed, and each bounding circle is checked against all other for intersection with the expression below:

$$(x_i - x_j)^2 + (y_i - y_j)^2 < d^2 \tag{5.7}$$

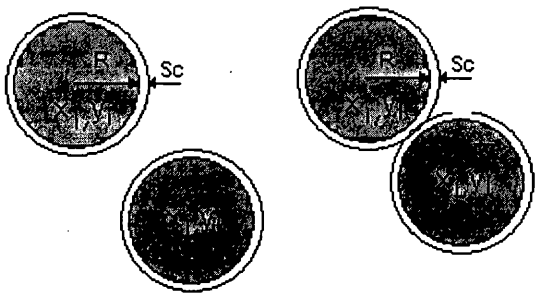

Figure 5.4: Identical bounding circle for 2D discrete element; No contact detected on left and possible contact detected on the right

where x and y denote the current coordinates of the centers of the bounding circles.

However, this simplest direct contact detection algorithm requires a large amount of computer memory and CPU time for a large number of particles. As a result, the number of particle used in moist agglomerate free falling test is limited to be 50.

Result output

In this version of DEMC, animation is also generated for the purpose of investigating the whole free falling process. It includes some visual functions, such as the contact forces are plotted by lines pass through the contact point. This provides information about the evolution of contacts, i.e. whether or not the contacts still exist, are deleted, or newly formed. Different colored and styled lines join the centers of spheres represent the contact

of different phases involved, where a solid black line represents a solid contact happening between two particles and a red dotted line represents liquid bridge force occurs verse the gap between two particles.

Beside, kinetic, potential and total energy versus time steps are plotted, as shown in Figure 5.5.

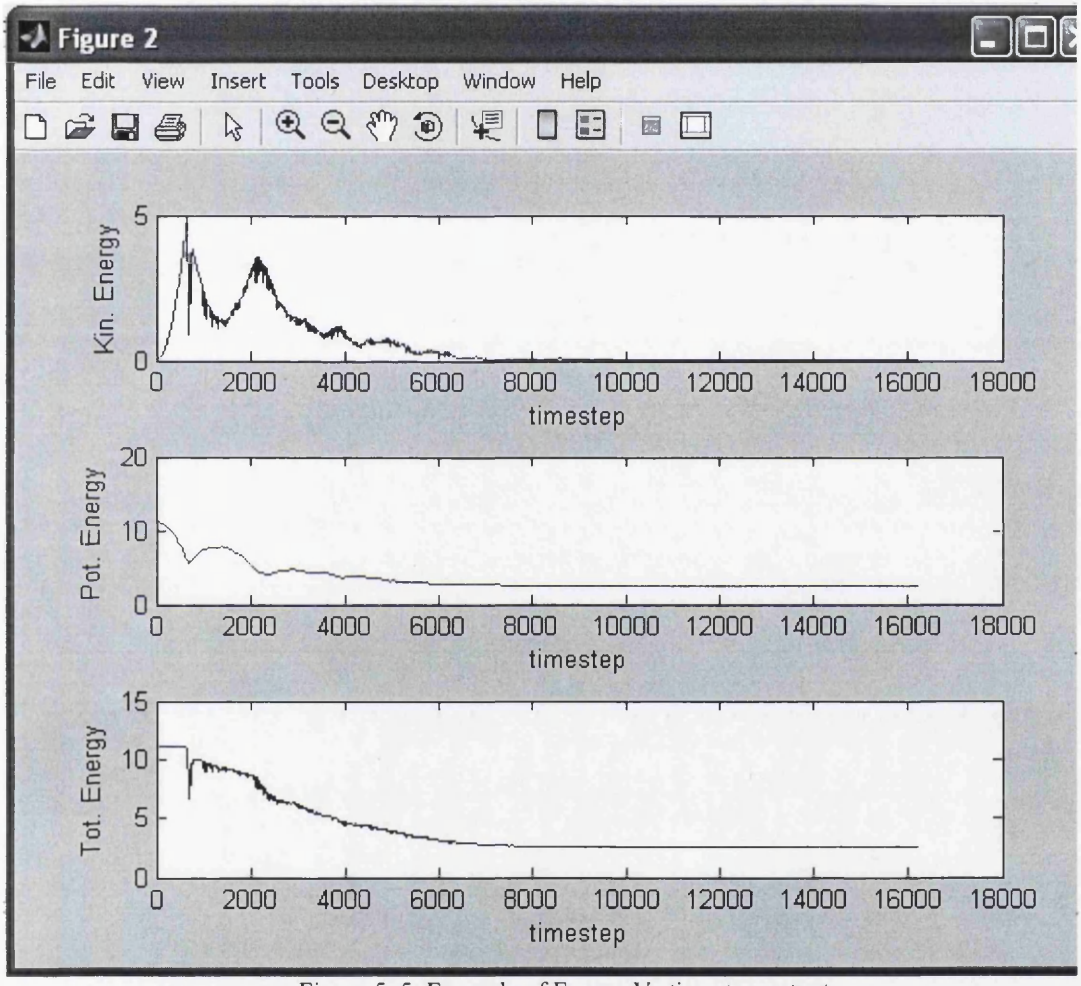

Figure 5. 5: Example of Energy Vs timestep output

References:

J. Fu, M. J. Adams, G. K. Renolds, A. D. Salman & M. J. Hounslow (2004), Impact deformation and rebounds of wet granules, Powder Technology,140, 248-257.

A. Munjiza (2004), The combined Finite-discrete Element Methods, John Wiley & son,Ltd.

R. D. Cook, D. S. Malkus and M. E. Plesha (1989), Concepts and applications of finite element analysis. 3rd edition, John Wiley & sons.

G. Lian (1994), Computer simulation of moist agglomerate collisions, PhD Thesis, The University of Aston in Birmingham.

Chapter 6

Computer simulation of moist agglomerate free falling test

6.1 Introduction

In this chapter, the effect of the proposed interaction law to a system of moist agglomerate is examined and presented. As the effect of the proposed interaction law depends on the breakdown distance, different values of the breakdown distance are assigned to the moist agglomerate, which are tested under free falling. Eventually, based on the results of the simulations, the range of the breakdown distance is recommended for the interaction law for a 'load-deform-unload' system.

6.2 Head on collision of two particles

Before applying the proposed interaction law into particle assemblies, the effect of the breakdown distance has been tested in a head-on collision between two particles. It is beneficial to point out some issues that help to explain the result for the head on collision. These issues are the assumptions that have been made in this project: 1) The viscous liquid bridge force remains effective throughout the whole 'contact process', which contains a loading and an unloading case; 2) The viscous force is always assumed to have a direction against the direction of relative motion of the particles; and 3) Any initial contact established in DEM simulations is assumed in the loading case.

Based on the first two assumptions, it can be understood that the magnitude of viscous force for the loading case is the same as the unloading case, but with the opposite direction. This is because the direction of relative motion of the particles changes from the loading case to the unloading case.

As a result, with the help of the third assumption, the viscous liquid bridge force for the loading case is the most critical force in the 'load-deform-unload' system.

Focus is drawn on the occurrence of repulsive viscous force when the value of (Sr) becomes small, as this is proven experimentally to be the correct physical behaviour of squeezed liquid bridge (M. H. Meurisss and M. Querry (2006)). For a convenient reason, the repulsive force, which is defined as the liquid bridge force at the separation distance equal to zero, will be called 'limit force', which is defined as the liquid bridge force at the separation distance equal to zero.

In order to investigate the effect of breakdown distance to Limit force on a 'head-on collision of two particles', different values of breakdown distance are assigned as shown in the table below.

Series	Different Breakdown Distance(S_r)
1	$5\% S_c$
2	$2\% S_c$
3	$1\% S_c$
4	$0.5\% S_c$
5	$0.2\% S_c$

Table 6. 1: Different Values of Sr in two particle head on collision test

Force versus displacement graphs for loading and unloading cases are generated and compared, as shown in Figures 6.1-6.5.

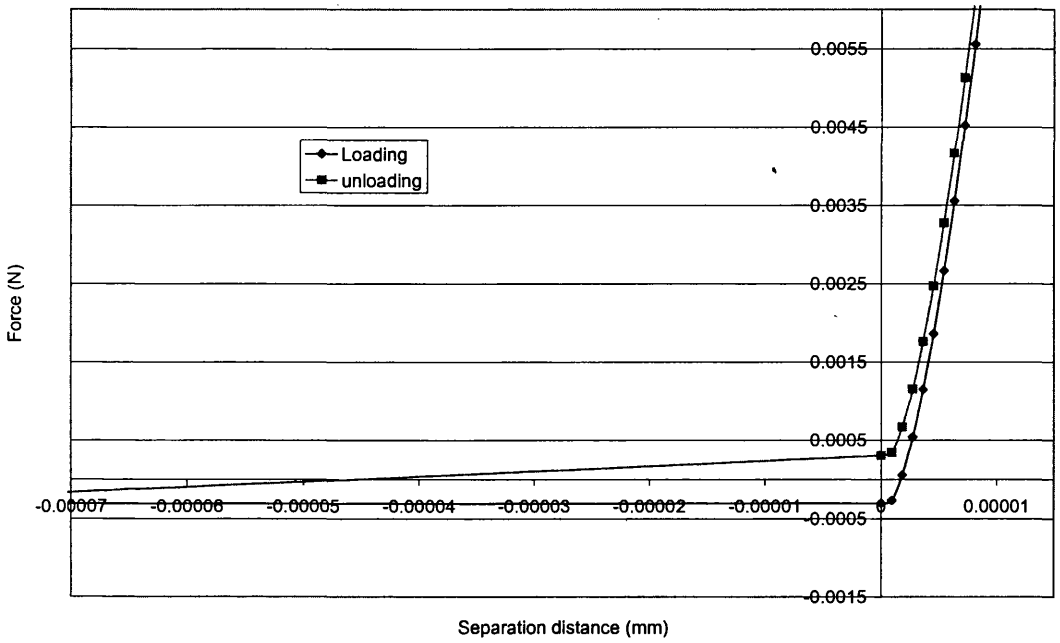

Figure 6. 1: Force Vs Displacement for Sr=5%Sc

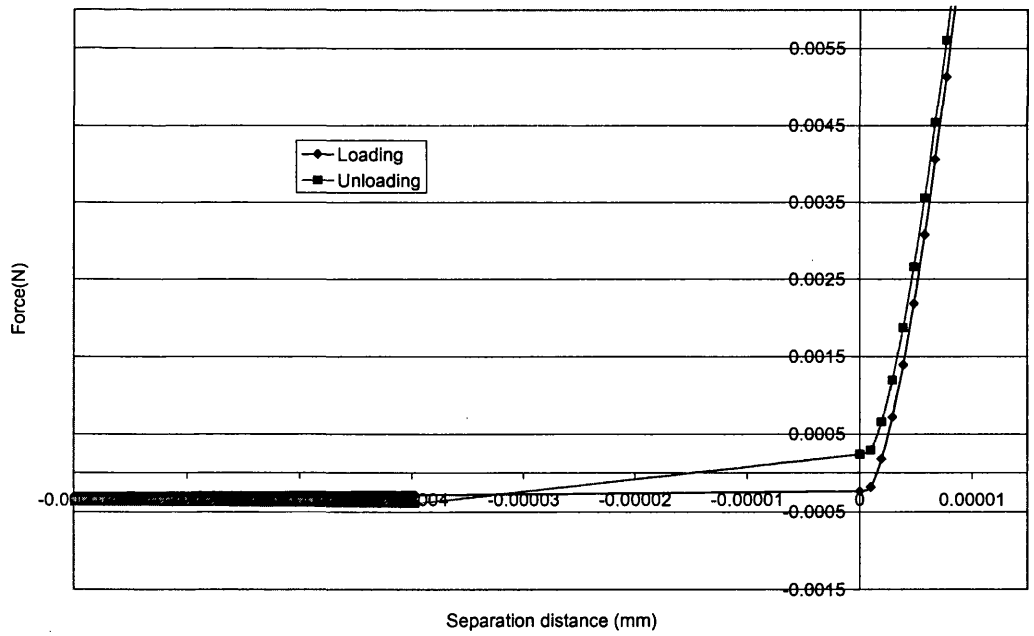

Figure 6. 2: Force Vs Displacement ,Sr=2%Sc

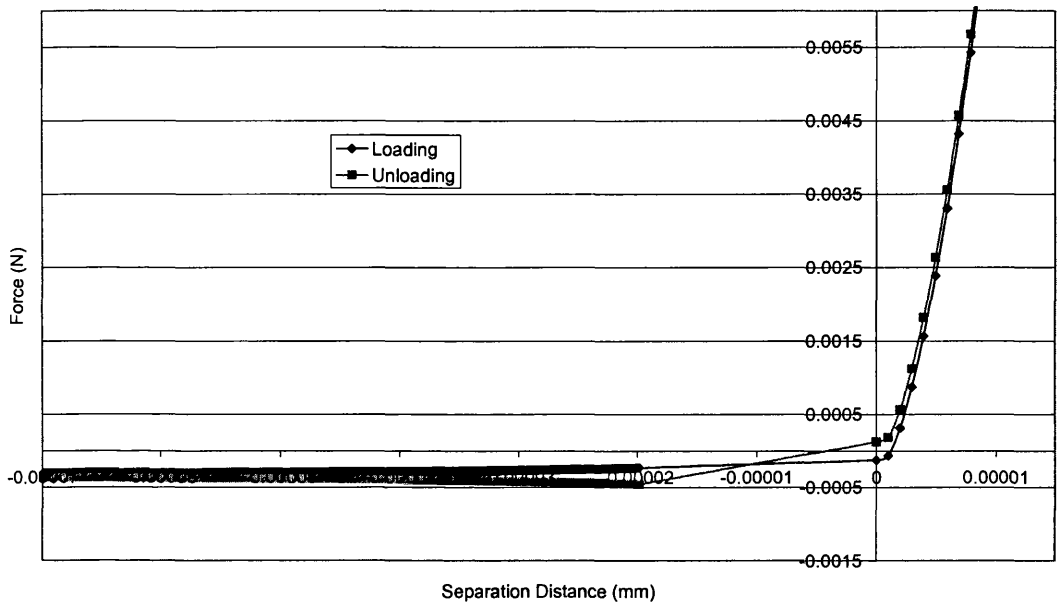

Figure 6. 3: Force Vs displacement for Sr=1%Sc

The Limit force, for loading cases, of any Sr(s) Larger than one percent of rupture distance gives an attractive force, a negative value. These results do not match with the experimental result (M. H. Meurisss and M. Querry, (2006)), because a repulsive liquid bridge force is expected rather than an attractive force.

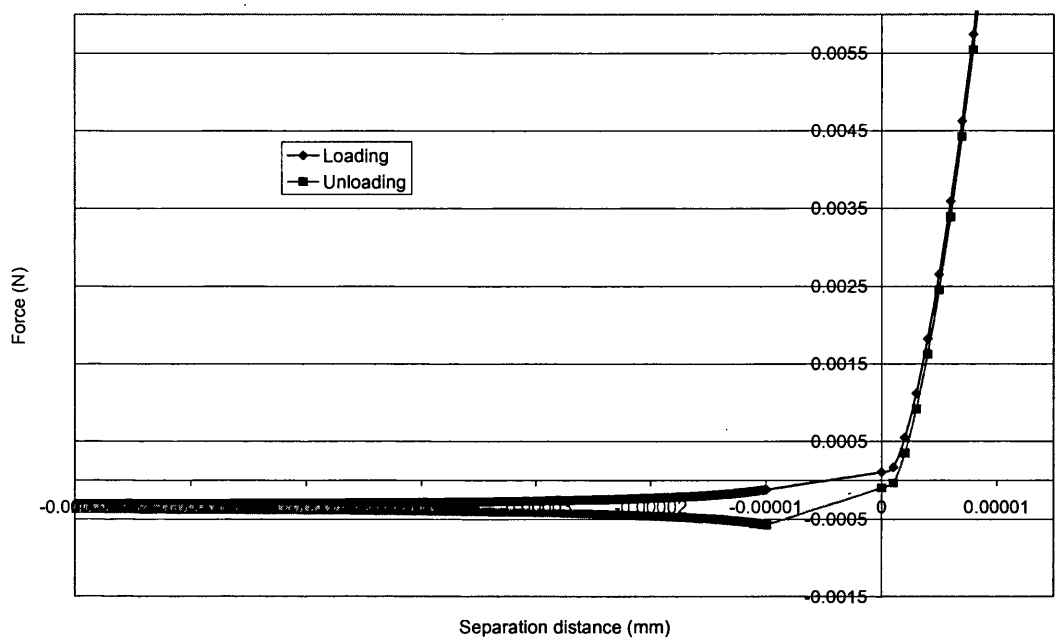

Figure 6. 4:Force Vs Displacement for Sr=0.5%Sc

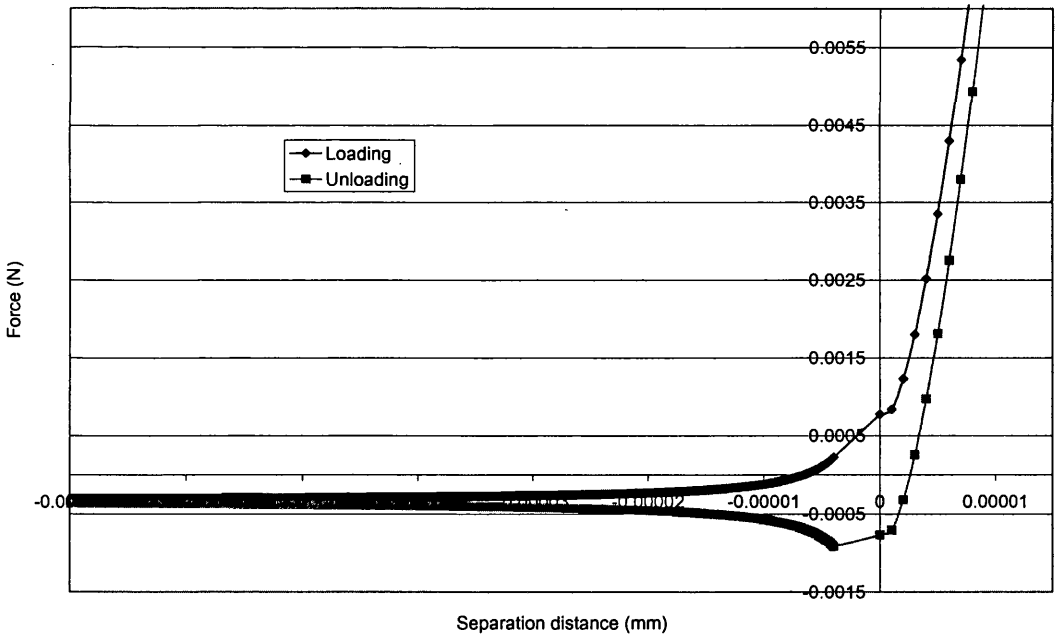

Figure 6. 5:Force Vs Displacement for Sr=0.2%Sc

The Limit force, for loading case, becomes repulsive, as the breakdown distance (Sr) decrease, as shown in Figures 6.4 and 6.5. . Those results are more likely to represent the physical behavior of the 'load-deform-unload' system.

6.2.1 Conclusion for two particles head on collision

In summary, the Limit force, for the loading case, remains attractive for breakdown distance (Sr) larger than 1 percent of rupture distance (Sc). This attractive force is, however, opposite to the experimental results from M. H. Meurisss and M. Querry (2006). This can be understood as the effect of the repulsive dynamic liquid bridge force has not be developed fully due to an early 'cut-off' by a large breakdown distance (Sr) and allows the attractive static liquid bridge force to dominate the behaviour of liquid bridge .

Conversely, the effect of repulsive dynamic liquid bridge force becomes more and more significant, when Sr is getting smaller and smaller. This is because of postponing the 'cut-off' allows dynamic liquid bridge force to develop. The Limit force for any Sr smaller than one percent becomes repulsive and agrees with the experiment behaviour of a squeezed liquid bridge.

Apart from that the effect of breakdown distance becomes more significant when Sr decreases, and the magnitude of the 'Limit force' increases exponentially as the Sr decreases, this idea can be illustrated in Figure 6.6.

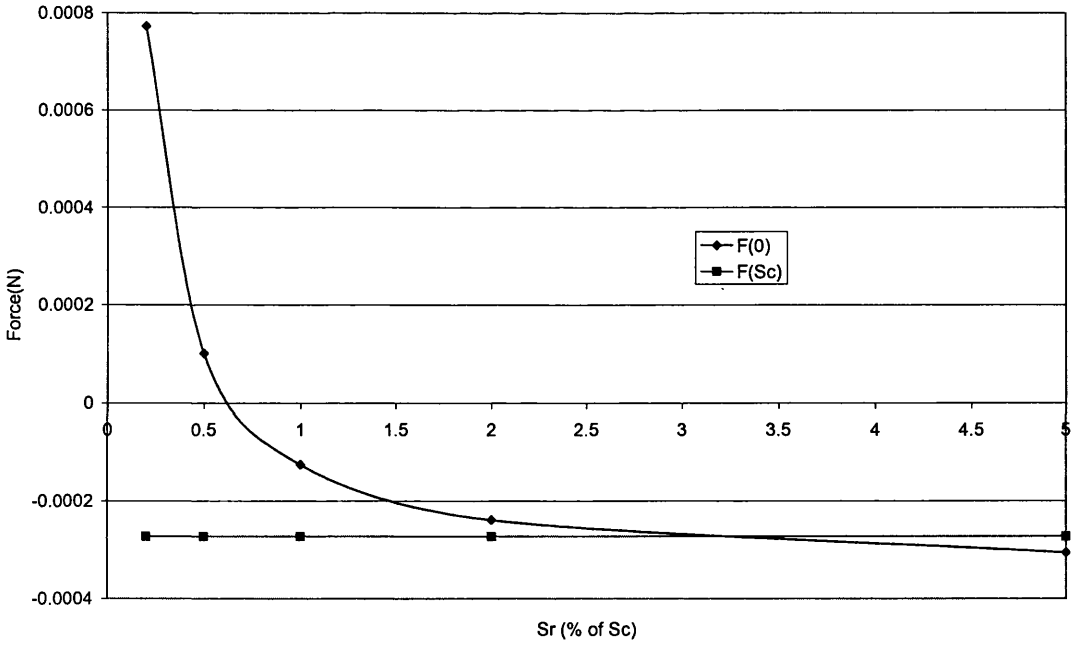

Figure 6. 6: Limit force and Attractive force at S= Sc for different breakdown distance

The blue line in the above figure represents the repulsive force when separation distance becomes zero and the red line represents the initial attractive force of the liquid bridge at the distance that liquid bridge just has formed.

It can be seen that the Limit force remains attractive for any Sr larger than 0.75 percent. However, the Limit force changes to repulsive and increases dramatically when Sr decreases. On the other hand the initial attractive force remains unchanged for a whole range of Sr. Thus, the difference between the repulsive force and the attractive force increases exponentially and the repulsive force becomes very significant for a small Sr.

For moist agglomerate DEM model with constant viscous of liquid and very small time step size, the selection of breakdown distance (Sr) becomes critical. If Sr is chosen randomly large, it may affect the effect of liquid bridge due to an early cut-off of the liquid bridge viscous effect. On the other hand, if Sr is chosen to be too small, as shown in Figure 6.9, a large Limit force would be obtained. An unrealistic DEM simulation result may be obtained. This may be due to an extra repulsive liquid force induced in each contact between particles.

Therefore, an extra care is needed on the selection of Sr. It has been shown earlier in this chapter that the behavior for any Sr larger than 1 percent is not physically correct.

However, it is convinced that liquid bridge does has a repulsive effect when it is being squeezed (M. H. Meurisss and M. Querry, (2006)). As a result, Sr is believed and recommended to be in the range smaller than 0.75% of rupture distance (Sc). This is because a repulsive Limit force is obtained for the loading case and it is agreed with this real behavior of liquid bridge.

In order to scrutinize the effects on different Sr on a 2D computer simulations of moist agglomerate, the proposed interaction law is implemented into the DEM program and the examination of the behavior from the DEM simulation has been carried out .

6.3 DEM simulation

Agglomerate properties, particularly strength and deformability, are clearly of relevance to granule coalescence, attrition and breakage. Although many different types of test have been described for assessing agglomerate strength and attrition tendency, the impact test is the most simple and direct method to quantify and measure the deformation and breakage of particulate solids. It is more closely related to the granulation, attrition and breakage processes, but, with real experiments, to the best knowledge of the author, it is primarily empirical. This is because of the difficulty to obtain internal parameters describing the packing structure of the agglomerates, such as particle shapes, sizes and inter-particle contact forces from real experiments.

Computer simulations in 2D and 3D dry agglomerate impact test are recently reported by Yin (1992), Thornton and Kafui (1992). These authors incorporated surface adhesion forces between particles into their model. It is clear from the computer result that the computer simulated agglomerate impact tests provide micro-level detail investigation of force propagation within the agglomerate during impaction. In this project, as the frictional contact force between particles or wall have not been considered, it is necessary to confine the particle within a region, otherwise, particles continue to slide along the bottom wall to infinite long. As a result, instead of using one horizontal wall beneath the agglomerate and letting the agglomerate to form slump, Figure 6.7, a container with 3 sides of walls has been used to enhance an initial packing of agglomerate, as shown in Figure 6.8.

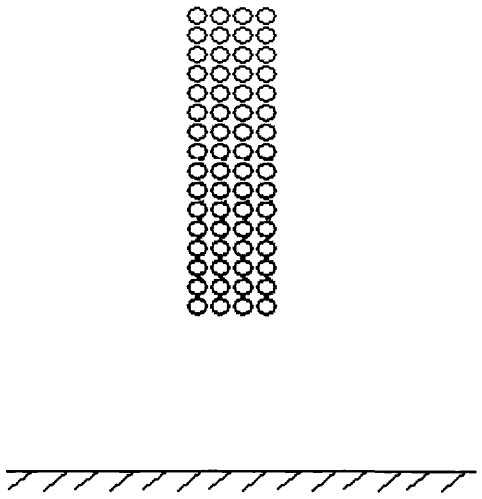

Figure 6. 7: Sketch of impact test setting

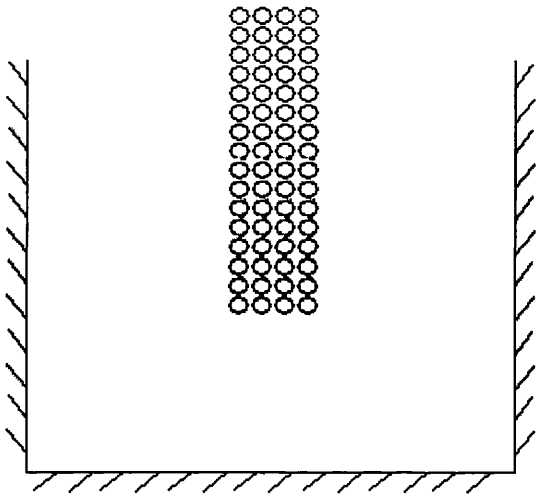

Figure 6. 8: Sketch of three sided container setting

A 2D simulated free-falling impact of a moist agglomerate consisting of 50 primary particles is reported. The mechanical behaviour of the moist inter-particle and agglomerate-wall collisions with different values of S_r has been examined.

6.4 Computer simulation procedures

6.4.1 Agglomerate preparation

For the computer simulated moist agglomerate impact free-fall into a container, 2D agglomerate is prepared. The particles of radius R=0.05mm have the following properties:

- Density $\rho = 2400 \times 10^{-9}\ kg/mm^3$
- Young's Modulus $E = 10 \times 10^3\ N/mm^3$
- Poisson's ratio $\nu = 0.35$

To prepare the agglomerate, particles are generated inside a rectangular region with width and height of $1.5mm \times 2.25mm$. The arrangement of the generated particles is in a grid mapping, as shown in Figure 5.3, with a rupture distance, S_c, separating each particle.

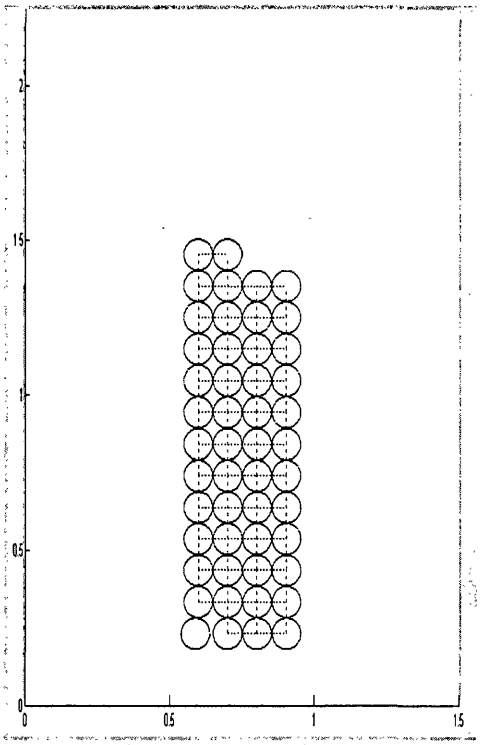

Figure 6. 9: Grid Mapping in agglomerate preparation.

Pendular liquid bridges are then specified for each gap between adjacent particles and the volume of liquid bridge is assigned to be 0.0001% of the particle volume. The liquid is modelled as pure water at about 25 °C with the following properties:

- surface tension $\gamma_{lv} = 0.0725 \times 10^{-3}\ {}^{N}/_{mm}$
- solid-liquid contact angle $\theta = 70^{o}$
- viscosity $\mu = 8.9 \times 10^{-4}$

As the model does not take frictional contact force into account, the columns of particle would only bounce up and down due to the transmission of contact force passing through all centroid of the particles in the same column in a straight line. For this reason, asymmetric setting is introduced by assigning to the particle at the bottom left corner, with a horizontal velocity $u = 5\ {}^{mm}/_{s}$ to the left at time $t = 0s$.

After the creation of the particles with liquid bridge, time integration calculations are performed to allow the agglomerate to reach a state of equilibrium. During the time integration calculations, water viscosity and damping effect with $\zeta = 2.5\%$ are used to dissipate the kinetic energy when the particles collide with each other. The system is assumed to be in equilibrium stage, when the global total energy of the system is less than $1 \times 10^{-4} Nmm$.

6.4.2 Testing procedures.

The bottom of the container is positioned at 5 times of the particles radii below the bottom row of the agglomerate. The properties of the walls are considered to be the same as the particles and thickness of the wall is simulated as a semi-infinite half-space. Each free falling test is performed by setting appropriate breakdown distance (S_r) to all the particles of the agglomerate and the walls are stationary. In total, 7 series of agglomerate free falling tests are performed with each series considering different breakdown distance, S_r, as shown in the table below.

Series	Different Breakdown Distance(S_r)
1	No liquid bridge involved
2	5% S_c
3	2% S_c
4	1% S_c
5	0.75% S_c
6	0.5% S_c
7	0.2% S_c

Table 6. 2: Different values of Sr used in moist agglomerate free falling tests

6.5 Results and discussions

6.5.1 Effectiveness of liquid bridge

Before analysing the effect of breakdown distance, it is necessary to confirm the significant of liquid bridge to the particle assemblies system. This is achieved by comparing the result from systems with and without the consideration of liquid bridge, namely moist agglomerate and dry agglomerate respectively.

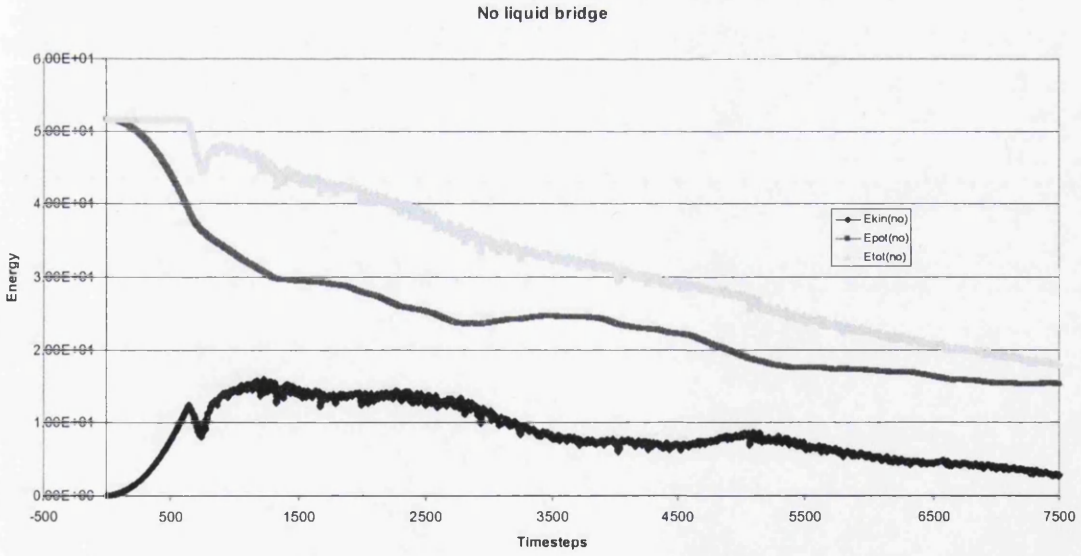

Figure 6. 10: Energy vs timestep (Dry agglomerate)

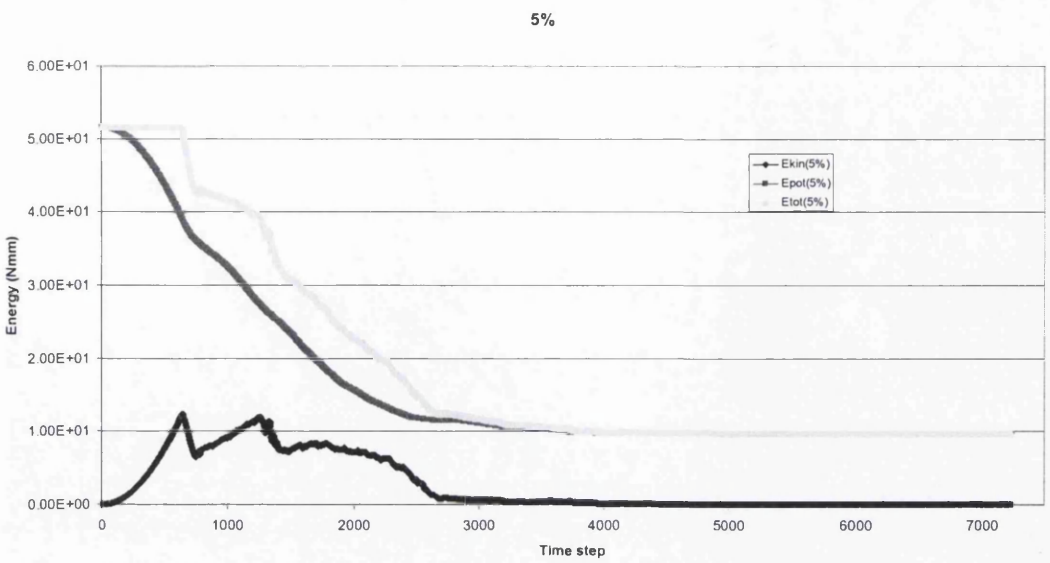

Figure 6. 11: Energy Vs timestep (Moist agglomerate, Sr=5% Sc)

As shown in Figures 6.10-11, the global potential energy of a moist agglomerate decreases continuously and gradually until all particles reach their finial packing position, while the global potential energy for a dry agglomerate also deceases gradually, yet with oscillations throughout the whole graph, this is caused by the rebound of particles after free falling and height recovery after each contact. This difference in potential energy graphs shows the influence of liquid bridge, which could be considered as an extended region of damping effect when two particles are in contact and this dissipates more energy in each contact, hence it takes least time to settle down.

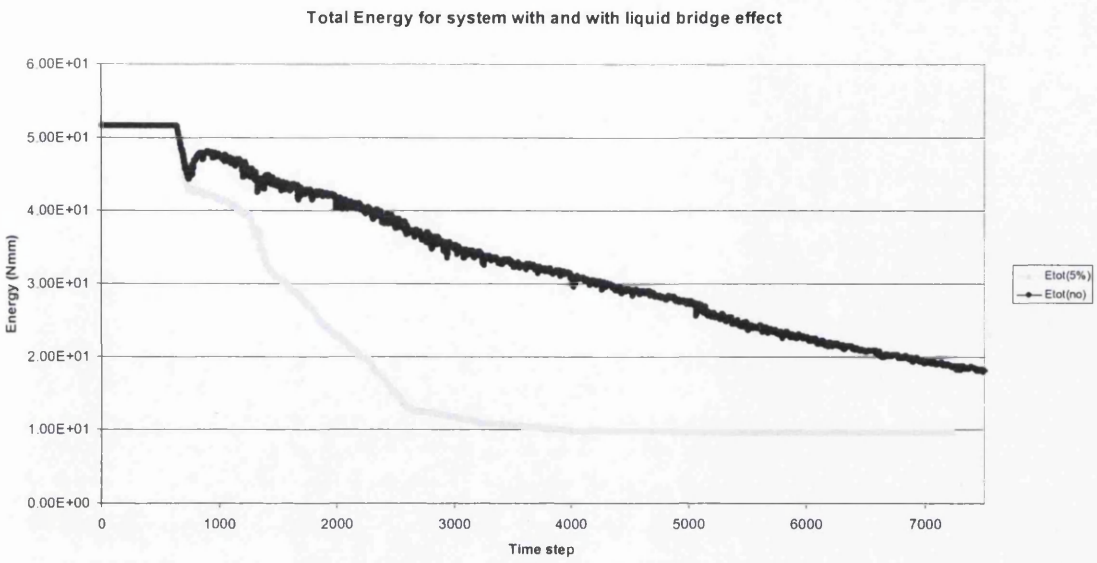

Figure 6. 12: Comparison of total energy for system with and without liquid bridge

The damping effect of liquid bridge becomes more obvious when comparing the total energy result of the two systems. It can be seen that the total energy for dry agglomerate with damping effect recovers part of its original energy, after the first rebound from the bottom wall, while the loss of energy is only due to the damping effect that happens in each contact. As the damping ratio is constant throughout the process, the total energy descends gradually with a constant rate of change.

Conversely, the total energy curve for moist agglomerate with damping effect shows no noticeable recovery of total energy after the first rebound from the bottom wall, follows by a continuous and relatively rapid reduction of total energy. Thus, by comparing the descending slope of both curves after the rebound, it is convincing that the liquid bridge occurs at all gaps between pairs of adjacent particles and contributes a significant damping effect in a moist agglomerate system.

After knowing the importance of liquid bridge on the damping effect in moist agglomerate system, the influence of the breakdown distance (Sr) on a moist agglomerate free-falling test is examined.

6.5.2 Effect of Breakdown distance (Sr) in free falling test

4 piles of particles lined up in the pattern with a height, 5 times of the radii of the particles, above the bottom boundary. The agglomerate is then released and allowed to free fall.

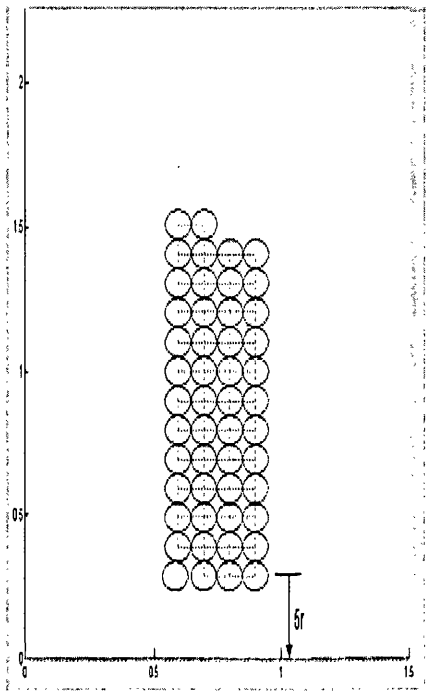

Figure 6. 13: Illustration of agglomerate initial arrangement.

The force propagation is evaluated by the different styles of lines shown between particles in contact and it has found that the reaction force from the bottom boundary wall started to propagate from the bottom to the top of the piles of particles, as shown in Figure 6.14, where the black line represents a solid contact between two adjacent particles.

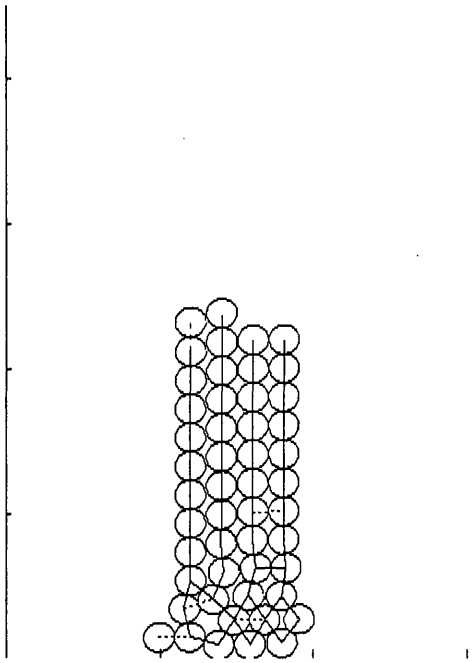

Figure 6. 14: Example of Reaction Force propagation (Sr=0.75%Sc)

It is valuable to mention that as the value of breakdown distance varies, the behaviour of the top row of particle change when the reaction force reaches the top row. This behaviour provides information for selecting the appropriate breakdown distance Sr.

For a dry agglomerate, as the reaction force propagates from the bottom and reachs the top row of particles, those particles detach and rise with a relatively large amount of vertical displacement, to certain height and then fall again due to the effect of gravity. This fall then turns into momentum to force the lower row particles to the both left and right boundaries of the container and caused a vigorous contact throughout the whole system. This vigorous contact can be seen in Figure 6.14 that most of the particles detach and bounce with each other.

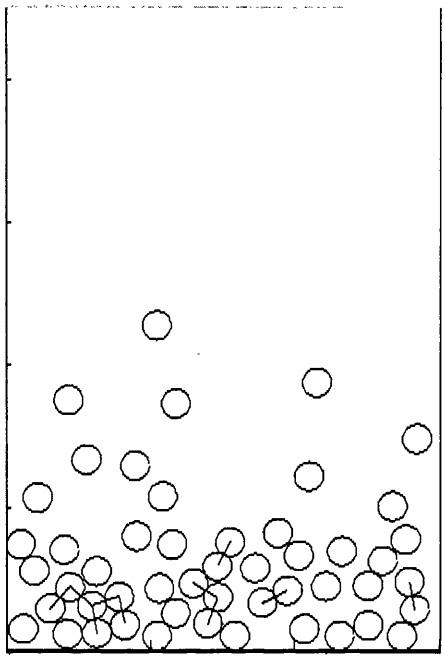

Figure 6. 15: Disintegrate of the dry agglomerate

While for the system of moist agglomerate, depending on the value of breakdown distance (Sr) for proposed interaction law, the top row of particles become least 'active' as the breakdown value changes. The particles behave more 'sticky' that particles tend to stick together without an observable detachment, for a small breakdown distance.

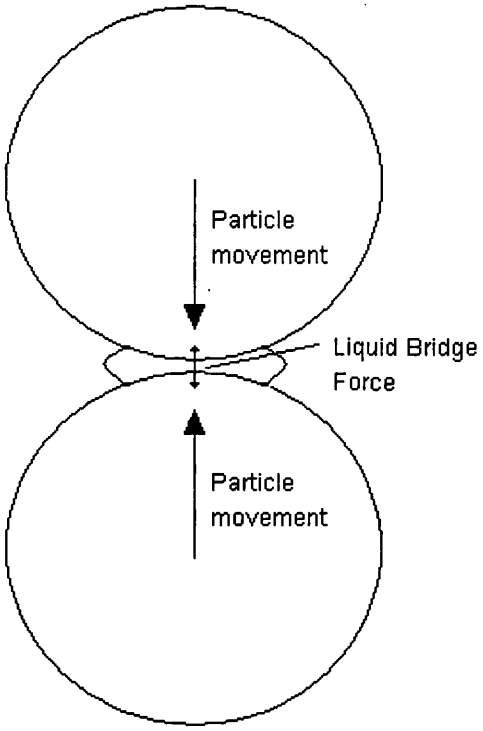

Figure 6. 16: Illustration of Cushion effect of liquid bridge for small breakdown distance

A repulsive liquid bridge force may occur between two particles in the loading case when the gap is small. Conversely, an attractive force occurs in unloading case. As illustrated in Fig. 6.16 this repulsive force can be considered as an extended range of damper and the attractive force can be regarded as an elongated spring between every adjacent pair of particles. Contact forces are reduced by this damping effect in each contact; this explained why the particles tend to stick together and less 'active' in moist agglomerate. As a result, when the reaction force propagates throughout the columns of particles the magnitudes of the reaction force that reach the top row of particle become less and no detachment of the top row of particle has been observed, when the breakdown distance smaller than 1% of rupture distance (Sc).

Vice versa, when the breakdown distance (Sr) increases to 2%, the detachment of the top row of particles begins to happen and becomes more and more obvious as Sr increases further. This means that the damping effect becomes relatively ineffective when the value of Sr is large, as expected.

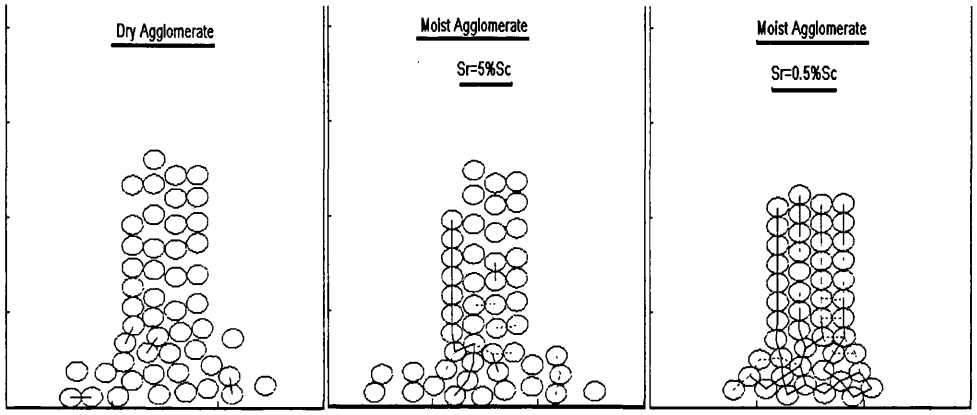

Figure 5. 2: Several snap shots of Dry agllomerate and Moist agglomerate

This idea is demonstrated in the Figures above. For the case of dry agglomerate, it can be noticed that less number of particles are in contact, which is represented by the solid line in black joining the two particle centres in contact. On the other hand, the percentage of particles in contact for the moist agglomerate system increase as the breakdown distance (Sr) decreases. Eventually, almost all the particles in the agglomerate stick together at Sr=0.5% Sc.

In a short summary, the damping effect of liquid bridge is influential in moist agglomerate. Because the repulsive and attractive liquid bridge force occur at a very small separation distance, those forces become an 'extended range of damper' in the loading case and 'elongated spring' in the unloading case between two particles in contact, and dissipate the kinetic energy out of the agglomerate. The magnitude of the viscous force increases with a decreasing breakdown distance (Sr); this shows the phenomena that particles become more 'attached' at agglomerate with lower Sr.

6.5.3 Limitation of breakdown distance (Sr)

After confirmation of the importance of liquid bridge and influence of breakdown distance to a moist agglomerate system, it is meaningful to investigate the limitation of the breakdown distance.

It is believed that the magnitude of viscous force increase exponentially as Sr decreases in the loading case and vice versa for the unloading case, as shown in Figure 6.6. Caution

is drawn to any numerically unstable effect arising from by the influence of this viscous liquid bridge force at a small Sr value.

The major effect of Sr takes place in viscous force from liquid bridge to particles about to contact. In order to check if there is any numerical instability for different values of Sr, the easiest way is to observe the total kinetic energy of each system. These results reveal the damping rate for different breakdown distances (Sr) in a dynamic contact system as shown in the Figure below:

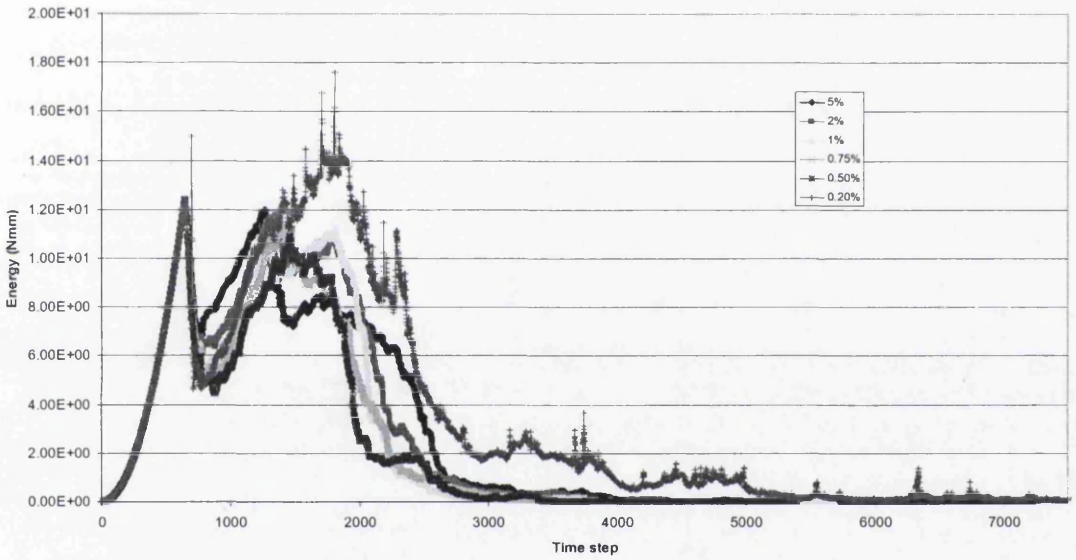

Figure 6. 17: Kinetic energy for different Sr values

It can be seen that the kinetic energy graphs for different Sr appear in a similar pattern. The amount of global kinetic energy gives the highest value in the case that the Sr is equal to 5% of Sc, which is about 7.5-8 Nmm, after the reaction force reaches the top row of particles; while this rebound energy continues to decrease as the Sr decreases. This is due to the greater repulsive liquid bridge force, hence, the greater damping effect involved in the particles contact for a smaller Sr value. This trend remains valid until Sr becomes smaller than 0.5% of Sc, as shown in Figure 6.17. Also the value of global kinetic energy of the case (Sr is equal to 0.2%), is higher than the case (Sr is equal to 0.5% of Sc).

This increase of kinetic energy for Sr equal to 0.2% of Sc would be understood by excessive repulsive forces happening between each pair of contacting particles. This excessive repulsive force not only shortens the time of contact, but also increases the stiffness of water to an unrealistic stage, hence, an extra imposition on energy into the agglomerate system and eventually causes the increase of rebound energy. Besides the instability happens at the first rebound from the bottom horizontal boundary, the particles contact more vigorously with each other for the agglomerate with Sr=0.2%Sc.

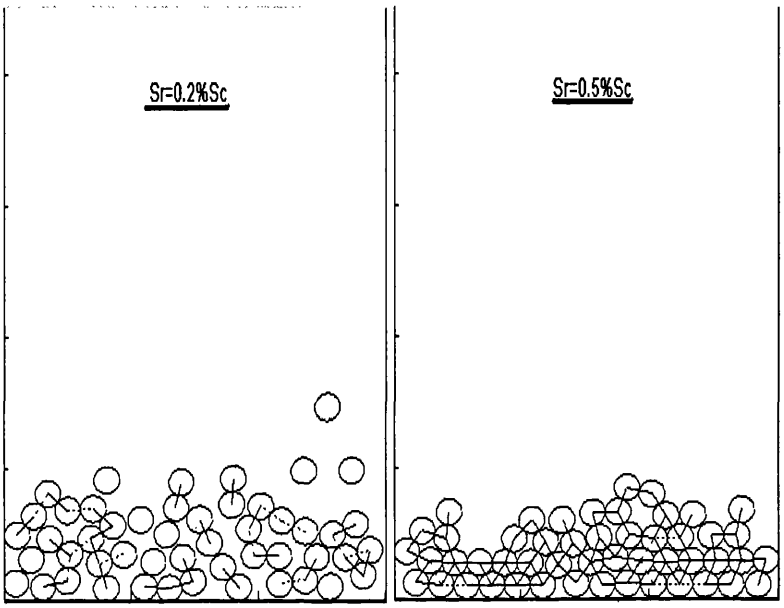

Figure 6. 18: Comparison of particle behavior for Sr=0.2%Sc and Sr=0.5%Sc

Particles in the system with Sr=0.2%Sc bounce more vigorously and more small clusters of particles appear, due to excessive repulsive force from liquid bridge to particles. In order to prevent this unnecessary excessive repulsive force from liquid bridge, Sr is then recommended to be a value smaller than or around 0.5% of Sc. Together with the recommendation from section 6.2.1 that the maximum limit for Sr is 0.75%, also the value of breakdown is recommended to be within a range of 0.5% to 0.75% of rupture distance.

Chapter 7

Conclusion and Future Work

7.1 Conclusion

Powder granulation with a liquid binder is heavily utilized in process industries. At the microscopic level, the fundamental mechanism of particle enlargement by granulation is based on competing interparticle forces. In the pendular stage, where the liquid is present as either absorbed immobile film or discrete liquid bridges, the cohesive force between particles mainly arise from two different mechanisms, the van der Waals intermolecular adhesive force and liquid bridge binding force. Approximate methods (the JKR and the DMT) for the van der Waals adhesive force between elastic particles have been reviewed and discussed.

For the liquid bridge, the interactive force between particles arises from the capillary pressure deficiency, surface tension and viscous resistance of the liquid. For static liquid bridge between two spherical rigid bodies of equal radii under conditions when the effects of gravity are negligible, the geometry is governed by the Laplace-young equation which relates the liquid bridge pressure deficiency to the mean curvature. Since the Laplace-Young equation cannot be solved analytically expect for a few special cases, a numerical scheme has been developed. A numerical solution has been obtained for a dimensionless liquid bridge between two spheres in close proximity.

For a liquid bridge between two spheres, R.A. Fisher (1926) proposed a much simpler approach for estimating the static liquid bridge forces. It is based on a toroidal approximation, which involves treating the meridional profile of the liquid-air interface as an arc of a circle, and leads to a range of values since this approximation results in a liquid bridge geometry of varying mean curvature which is inconsistent with the Laplace-Young equation. Consequently, there is no physically correct solution for the toroidal approximation, only one that leads to an optimal simple procedure in terms of the accuracy of calculating the forces. The uncertainty of the accuracy of the toroidal approximation has been checked against the numerical solution by G. Lain et al (1993). It has been found that the best estimate of the total static liquid bridge force is obtained using the 'gorge method' in which the area and mean curvature at the neck is used in the calculation of the force. For a wide range of liquid bridge volumes and all stable separation distance, this method of evaluation produces errors in the static liquid bridge force that are less than 10 % of those obtained using an exact numerical technique and the accuracy is independent of the contact angle.

Another component of the total liquid bridge force is the dynamic liquid bridge force which is induced by the viscous resistance to relative motion of two adjacent particles. Adams and Perchard (1985) established an expression for the viscous force in a dynamic liquid bridge force from the Lubrication Theory. This expression predicts an infinite viscous force as the separation distance between two particles becomes zero. Consequently, a method of solved this instability problem has been proposed in this project to obtain a set of governing equations. This is done by assigning a limiting separation distance, namely breakdown distance (Sr) which is a certain percentage of the liquid bridge rupture distance (Sc), to the governing equation. Lubrication theory is assumed to break down for any separation distance smaller than Sr and thus, a specific repulsive viscous force would be obtained as the separation distance become zero instead of going to infinity.

The effects of the proposed interaction law on two particles head on collision are examined. It has been found that repulsive force from the liquid bridge force occurs for

any breakdown distance smaller than 1 % of Sc and increases exponentially as Sr decreases.

This proposed interaction law is then implemented to a DEM computer program DEMC. The free falling test of and 2D agglomerate into a three sided container have been performed and the effects of the liquid bridge force haven been examined. The agglomerate consists of 50 mono-sized particles. It has been shown by the computer simulation that the damping rate is much greater for moist agglomerate than dry agglomerate. Hence, it is believed that the damping effect of liquid bridge is essential to moist agglomerate.

It has also shown that the particles in the systems, with a small value of Sr, tend to sticky together as an agglomerate. This is due to the effects of both the viscous repulsive force in the loading case and the viscous attractive force occurring at small separation distance in the unloading case. They reduce the momentum of each pair of particles that about to contact and during rebound.

During the investigation of the effect of different Sr to agglomerate behaviour, it has also found that an excessive repulsive force is imposed from the liquid bridge to the contacting particles when Sr is smaller than ~0.5% of Sc. This excessive repulsive force causes an unrealistic increase of kinetic energy on every particle contact. As a result, Sr is recommended to be within a range of 0.75% to 0.5% of the rupture distance to have an interaction law which involves the viscous effect of the liquid bridge in an appropriate magnitude.

7.2 Future work

It has been shown that the computer program DEMC using the Discrete Element Method is capable of modelling moist agglomerate collision. The advantage of the DEM simulation is that it provides detailed investigations of the micro-level mechanisms of agglomerate. The current DEMC simulates a moist agglomerate as an assembly of spherical particles held together by liquid bridge. For the interaction force between

particles, the force is exerted by particle deformation, surface adhesion and liquid bridge force.

In terms of future work, the present computer program DEMC has a few limitations and further improvements are recommended. Firstly, the tangential friction force of contact force is not considered, which causes the model to be less unrealistic. As a result, it is recommended that an implement of tangential force be needed. Secondly, the current research focuses on the modelling of moist agglomerate with immobile fluid which is present as pendular liquid bridge. Therefore, the dynamic effect of the liquid bridge profile, such as advancing contact angle for dynamic liquid bridge is recommended to be involved in future work. Thirdly, there is a need to develop new algorithms to model other stages of liquid bridge, which is funicular and capillary state liquid bridge. Finally, it is desirable to develop algorithms to model non-spherical particles and through computer simulations, to examine the effects of particle shape and size.

The DEM computer program has found a wide range of application in the simulation of particle systems. There are more potential applications and more powerful computer facilities are also required if the DEM is to be extended to simulate larger scale particle assemblies. The current version of DEMC is only capable of effectively simulating particles number up to few tens; this is because of the demanding direct contact detection algorithm has been used. As a result, more efficient algorithms are needed to be developed for the implementation of other interaction forces in the future.

References:

M. H. Meurisss and M. Querry (2006), Squeeze effects in a flat liquid bridge between parallel solid surfaces, Journal of Tribology, 128,575-584.

M. J. Adams and V. Perchard (1985), The cohesive forces between particles with interstitial liquid., In l. Chem. E. symposium Series, 91, 147-160.

Appendix

Main Program of DEMC

```
% function [xint,yint]=initialpack
%=========================================
% particles properties
%=========================================
clear all
clf
sigma=2.5/100;lqb=1;
r=0.05; %radius of particles in mm
E=1e4; %young modulus of particles.
pr=0.35; %poisson ratio of particles.
dens=2400*10e-9; % density of particles in kg/mm3
Vlp=0.2; e=0.7;
Vpp=4/3*pi*r^3;
EE=E^2/2/(E*(1-pr^2));rr=r^2/(2*r); %Relative E and radius.
m=Vpp*dens;% mass of particle
M=m/2;
k=4/3*EE*sqrt(rr);%stiffness coefficient
wn=sqrt(k*M);
c=2*sigma*wn;%damping ratio
%=========================================
%liquid properties
%=========================================
vis=8.9e-6; %vicousity of liquid kg/(mm*s).
Vlv=0.0725/1000; %liquid-solid surface energy per unit area (N/mm).
ca=70*pi/180;fa=10*pi/180; % contact angle and filling angle of liquid-solid
denl=1000*10e-9; % density of liquid in kg/mm3.
vol=15e-9; % volume of liquid in mm3.
bbp=0.35/100; % breakdown percentage.
cosfa=cos(fa);cosfaca=cos(fa+ca);sinfa=sin(fa);sinfaca=sin(fa+ca);
%=========================================
%intial packing
%=========================================
xmin=0;xmax=1.5;ymin=0;ymax=1.5*xmax; %boundarys
v=vol/r^3; %dimenionless radius and volume
Nop=50;
sc=(1+0.5*ca)*(v^(1/3))*rr; % critical distance for liquid bridge.
[xint,yint,Nop]=initialpack(lqb,r,xmin,xmax,ymin,ymax,sc,dens,e,Nop);
cor(1,:)=xint;cor(2,:)=yint;
% plot(cor(1,:),cor(2,:),'r*');
%=========================================
%drop the particles for random packing
%=========================================
n=1e7; % time intervals
dt=1/n; % time steps size
gravity=9.81*10e6; %gravity acceleration kgmm2/s2
F=zeros(Nop,2);
Z=zeros(Nop,2);
fid = fopen('0.35%.dat', 'wt');
```

```
T=1;
%=========================================================
%contact search for liquid bridge
%=========================================================
Term=10000;
Et=zeros(1,Term);
Ekin=zeros(1,Term);
Epot=zeros(1,Term);
for timestep=1:1:Term;
  [contl,Noc,Bcontl,Nob]=contactsearch(cor,r,sc,Nop,lqb,xmin,xmax,ymin,ymax,bbp);
  if timestep==1;Z=zeros(Nop,2);end
  %=======================================================
  %loop for contact force
  %=======================================================
  for i=1:1:Noc;
    obj(1)=contl(i,1);objx(1)=cor(1,obj(1));objy(1)=cor(2,obj(1));
    obj(2)=contl(i,2);objx(2)=cor(1,obj(2));objy(2)=cor(2,obj(2));
   [cosfa,cosfaca,sinfa,sinfaca]=newfil(ca,objx,objy,sc,v,r);
    if obj(1)<obj(2)

[Fx,Fy,Flt]=contactforce(bbp,r,cosfa,objx,objy,cosfaca,sinfa,sinfaca,Vlv,vis,Z(obj(1),1),Z(obj(1),
2),Z(obj(2),1),Z(obj(2),2),EE,rr,Vlp,sc,dt,c);
      F(obj(1),1)=F(obj(1),1)+Fx;F(obj(2),1)=F(obj(2),1)-Fx;
      F(obj(1),2)=F(obj(1),2)+Fy;F(obj(2),2)=F(obj(2),2)-Fy;
    end
  end
   if Bcontl~=0;
    for i=1:1:Nob;

[Fbx,Fby]=Boundaryforce(Bcontl(i,1),Bcontl(i,2),xmin,xmax,ymin,ymax,cor(1,Bcontl(i,1)),cor(2
,Bcontl(i,1)),E,pr,r,Vlp,c,Z(Bcontl(i,1),1),Z(Bcontl(i,1),2));
      F(Bcontl(i,1),1)=F(Bcontl(i,1),1)+Fbx;
      F(Bcontl(i,1),2)=F(Bcontl(i,1),2)+Fby;
    end
  end
  %=======================================================
  %loop for external force
  %=======================================================
  F(:,2)=F(:,2)-dens*Vpp*gravity;
  %=========================================
  % time integration
  %=========================================
  for i=1:1:Nop;
    [U,V,dx,dy]=timein(F(i,1),F(i,2),dt,Z(i,1),Z(i,2),m);
    Z(i,1)=U;Z(i,2)=V;
    if timestep==1
      if i==1;Z(i,1)=Z(i,1)-500;end;
      if i==2;Z(i,1)=Z(i,1)+00;end;
    end
    cor(1,i)=cor(1,i)+dx;
    cor(2,i)=cor(2,i)+dy;
```

```
    Ekin(timestep)=Ekin(timestep)+1/2*m*(Z(i,1)^2+Z(i,2)^2);
    Epot(timestep)=Epot(timestep)+m*gravity*cor(2,i);
  end
  Et(timestep)= Ekin(timestep)+Epot(timestep);
  fprintf(fid,'%10.3e %10.3e %10.3e\n',Ekin(timestep),Epot(timestep),Et(timestep));
  F=zeros(Nop,2);
  %=================================================
  %Animation generation
  %=================================================
      if timestep==T*10
        for i=1:1:Nop
          ccor=circor(cor(1,i),cor(2,i),r,180);
          axis([xmin xmax ymin ymax]);
          hold on;
          plot(ccor(1,:),ccor(2,:));
        end
        for i=1:1:Noc;
          obj(1)=contl(i,1);objx(1)=cor(1,obj(1));objy(1)=cor(2,obj(1));
          obj(2)=contl(i,2);objx(2)=cor(1,obj(2));objy(2)=cor(2,obj(2));
          if obj(1)<obj(2)
          if contl(i,3)==1& Vlv~=0;hold on;plot(objx,objy,'r:');end;
          if contl(i,3)==2& Vlv~=0;hold on;plot(objx,objy,'g-.');end;
          if contl(i,3)==3;hold on;plot(objx,objy,'k');end;
          end
        end
        frame(T)=getframe;
        T=T+1;
        clf;
      end
  %=================================================
  %=================================================
  if Ekin(timestep)<1e-4;
    break;end
end
j=1:1:timestep;
figure (2)
subplot(3,1,1); plot(j,Ekin(1:timestep));xlabel('timestep');ylabel('Kin. Energy');
subplot(3,1,2);plot(j,Epot(1:timestep));xlabel('timestep');ylabel('Pot. Energy');
subplot(3,1,3); plot(j,Et(1:timestep));xlabel('timestep');ylabel('Tot. Energy');
T=T-1;
%=====================================
% Animation Generation
%=====================================
movie2avi(frame,'035');
status = fclose(fid);
% movie (frame,1);
```

Subroutine : 'initialpacking'

For assembly the particles into a grid mapping pattern

```
function [xint,yint,Nop]=initialpack(lqb,r,xmin,xmax,ymin,ymax,sc,dens,e,Nop);
```

```
% void ratio of the control volume.
% N=e/(1+e); % porosity of the control volume.
% Vt=(xmax-xmin)*(ymax-xmin); %total volume of the control volume.
% Vv=N*Vt; % volume of void of the control volume.
% Vs=Vv/e; %volume of solid in the control volume.
% Vpp=4/3*pi*r^3; %volume of particle.
% Nop=round(Vs/Vpp); % number of particles.
%=========================================
%initial arragnement
%=========================================
% Nop=20;
j=1;k=1;xd=1;yd=5*r;
mid=(xmax-xmin)/2;
for i=1:1:Nop;
   if j==1; xint(i)=mid-1.5*sc*lqb*xd-3*r; yint(i)=yd+lqb*sc*(k-1)+2*r*(k-1);end
   if j==2; xint(i)=mid-lqb*sc/2*xd-r; yint(i)=yd+lqb*sc*(k-1)+2*r*(k-1);end
   if j==3; xint(i)=mid+lqb*sc/2*xd+r; yint(i)=yd+lqb*sc*(k-1)+2*r*(k-1);end
   if j==4; xint(i)=mid+lqb*1.5*sc*xd+3*r; yint(i)=yd+lqb*sc*(k-1)+2*r*(k-1);end
   j=j+1;
   if j==5;k=k+1; j=1;end
end
```

Subroutine : 'contactseach'

Contact detection by direct round contact search.

```
function  [contl,Noc,Bcontl,Nob]=contactsearch(cor,r,sc,Nop,lqb,xmin,xmax,ymin,ymax,bbp);
% if lqb==0;sc=0;end
tol=1e-6;contdis=sc;k=1;
v=0;u=0;stage=2;
%=============================================
%contact search
%=============================================
for j=1:1:Nop;
   for i=1:1:Nop;
      if i~=j;
         radialdis=sqrt((cor(1,i)-cor(1,j))^2+(cor(2,i)-cor(2,j))^2)-2*r;
         if radialdis< contdis | abs(radialdis-contdis)<tol;
            if  (abs(radialdis-sc)<tol |(radialdis-sc)<0)&  radialdis>sc*bbp &
radialdis>0;stage=1;end
            if radialdis<0; stage=3;end
            cont(k,1)=j;cont(k,2)=i;cont(k,3)=stage;u=1;
         else
            cont(k,1)=0;cont(k,2)=0;cont(k,3)=0;
         end
      end
      k=k+1;
   end
end
i=1;
if u==1;n=numel(cont(:,1));
   for q=1:1:n
```

```
      if cont(q,1)~=0;
         contl(i,1)=cont(q,1);
         contl(i,2)=cont(q,2);
         contl(i,3)=cont(q,3);
         i=i+1;
      end
   end
end

% if iszeros(contl);
Noc=i-1;
if u==0; contl=0;end
%=============================================
% Boundary search
%=============================================
Bcont=zeros(1,4);
for i=1:1:Nop
   if cor(1,i)-r<=xmin; Bcont(i,1)=i;Bcont(i,2)=1;v=1;end
   if cor(2,i)-r<=ymin; Bcont(i,3)=i;Bcont(i,4)=2;v=1;end
   if cor(1,i)+r>=xmax; Bcont(i,1)=i;Bcont(i,2)=3;v=1;end
   if cor(2,i)+r>=ymax; Bcont(i,3)=i;Bcont(i,4)=4;v=1;end
end
i=1;
if v~=0;n=numel(Bcont(:,1));end
if v==0 ;Bcontl=0;Nob=0;return;end
for q=1:1:n;
   if Bcont(q,1)~=0 | Bcont(q,3)~=0;
      if Bcont(q,1)~=0
         Bcontl(i,1)=Bcont(q,1);
         Bcontl(i,2)=Bcont(q,2);
         i=i+1;
      end
      if Bcont(q,3)~=0
         Bcontl(i,1)=Bcont(q,3);
         Bcontl(i,2)=Bcont(q,4);
          i=i+1;
      end
   end
end
Nob=i-1;
```

Subroutine : 'newfil'

Evaluation of filling angle with a given separation distance

```
function [cosfa,cosfaca,sinfa,sinfaca]=newfil(ca,objx,objy,sc,v,r);
c0=(v-0.01)/(0.06097941)+0.61461;
c1=(v-0.01)/(-0.087133313)+(-0.38911);
c2=(v-0.01)/(0.116535025)+0.45302;
c3=(v-0.01)/(-0.665680473)+(-0.17792);
ds=sqrt((objx(1)-objx(2))^2+(objy(1)-objy(2))^2)-2*r;
ratio=ds/sc;
```

```
fa=c0+c1*ratio+c2*ratio^2+c3*ratio^3;
cosfa=cos(fa);cosfaca=cos(fa+ca);sinfa=sin(fa);sinfaca=sin(fa+ca);
```

Subroutine : 'contactforce'

Computation of interparticle force.

```
function
[Fx,Fy,Flt]=contactforce(bbp,r,cosfa,objx,objy,cosfaca,sinfa,sinfaca,Vlv,vis,Zx1,Zy1,Zx2,Zy2,E
E,rr,Vlp,sc,dt,c);
tol=1e-5;
ds=sqrt((objx(1)-objx(2))^2+(objy(1)-objy(2))^2);
nx=(objx(2)-objx(1))/ds;ny=(objy(2)-objy(1))/ds;
Zx=Zx1-Zx2;
Zy=Zy1-Zy2;
v2y=nx*Zx+ny*Zy;
ds=(ds-2*r);
if  (abs(ds-sc)<tol |(ds-sc)<0)&  ds>sc*bbp & ds>0
   Flt=lqbforce(r,cosfa,ds/2,cosfaca,sinfa,sinfaca,Vlv,vis,v2y);
   if Vlv==0;Flt=0;end;
   Fx=Flt*nx;
   Fy=Flt*ny;
end
if ds<sc*bbp
   Fnn=lqbforce(r,cosfa,(sc*bbp)/2,cosfaca,sinfa,sinfaca,Vlv,vis,v2y);
   dss=dt*abs(v2y);dds=sc*bbp+dss/100;
   Fn=lqbforce(r,cosfa,(dds)/2,cosfaca,sinfa,sinfaca,Vlv,vis,v2y);
   dFds=(Fn-Fnn)/dss;
   if (dss)==0;dFds=0;end
   if v2y<0;dFds=-dFds;end
   distance=sc*bbp-ds;
   Flt=Fnn+dFds*distance;
   if Vlv==0;Flt=0;end;
   Fx=Flt*nx;
   Fy=Flt*ny;
end
if ds<0;
   Fnn=lqbforce(r,cosfa,(sc*bbp)/2,cosfaca,sinfa,sinfaca,Vlv,vis,v2y);
   Flqbstop=Fnn+dFds*sc*bbp;
   if Vlv==0;Flqbstop=0;end;
   Flt=Flqbstop-((4/3)*(-ds)^(3/2)*EE/rr-sqrt(16*pi*Vlp*EE*(-ds)^(3/2))+v2y*c);
   Fx=Flt*nx;
   Fy=Flt*ny;
end
```

Subroutine : 'boundaryforce'

Compute reaction force from boundaries

```
function
[Fbx,Fby]=Boundaryforce(particle,boundary,xmin,xmax,ymin,ymax,x,y,E,pr,r,Vlp,c,Zx,Zy);
E1=E;E2=E;
pr1=pr;pr2=pr;
```

```
EE=E1*E2/(E2*(1-pr1^2)+E1*(1-pr2^2));
% Fn=lqbforce(0.1,0.9848,(dds)/2,0.1736,0.1736,0.9848,0.0725/1000,0.0012/1000,v2y);
if boundary==1;
   ds=xmin-(x-r);
   Fbx=(4/3)*(ds)^(3/2)*EE/r-sqrt(16*pi*Vlp*EE*(ds)^(3/2))-c*Zx;
   Fby=0;
end
if boundary==2;
   ds=ymin-(y-r);
   Fbx=0;
   Fby=(4/3)*(ds)^(3/2)*EE/r-sqrt(16*pi*Vlp*EE*(ds)^(3/2))-c*Zy;
end
if boundary==3;
   ds=xmax-(x+r);
%    if abs(ds)>0.001;fprintf('excessive ovelap');end
   Fbx=-((4/3)*(-ds)^(3/2)*EE/r-sqrt(16*pi*Vlp*EE*(-ds)^(3/2))+c*Zx);
   Fby=0;
end
if boundary==4;
   ds=ymax-(y+r);
%    if abs(ds)>0.001;fprintf('excessive ovelap');end
   Fby=-((4/3)*(-ds)^(3/2)*EE/r-sqrt(16*pi*Vlp*EE*(-ds)^(3/2))+c*Zy);
   Fbx=0;
End
```

Subroutine : 'circor'

Graphical output of each particle contour

```
function[ccor]=circor(x,y,r,pt);
% global xc yc
j=1;dp=360/pt;
for i=0:dp:360
   xc(j)=x+r*cos(i*pi()/180);
   yc(j)=y+r*sin(i*pi()/180);
   ccor(:,j)=[xc(j);yc(j)];
   j=j+1;
end
```

Subroutine : 'circor'

University of Wales Swansea

AN INVESTIGATION AND PROPOSED INTEGRATED INTERACTION LAW FOR MOIST AGGLOMERATE

CHEUK YIN KO, BEng
Thesis submitted for the degree of Master of Philosophy
2007

Summary

In process industries powders are frequently granulated in order to promote their handleability and flowability. During these operations, a liquid binder is usually mixed with the powders to increase their cohesiveness. For binder granulation processed, coalescence and collision of moist agglomerate during the mixing process is the main concern. This thesis considers the computer simulation of moist agglomerate collisions using the discrete element method (DEM). The study is confined to pendular state moist agglomerate, at which liquid bridge is presented as a pendular liquid bridge and interparticle force is modeled as the adhesive contact force, the static liquid bridge force and the dynamic liquid bridge force.

This thesis briefly described various algorithms developed by other researchers for modelling the contact force due to surface adhesion and particle deformation and the pendular static liquid bridge force between mono-sized spherical particles due to hydrostatic pressure deficiency and surface tension.

A theoretical study of the pendular dynamic liquid bridge force between mono-sized spherical particles has been made and it has been found that a numerical instability occures from a DEM simulation with a fine time step size. As a result, an interaction law is proposed and implemented into a DEM code, DEMC, by specifying a minimum separation distance, namely the 'breakdown distance' two particles. It essentially avoids an infinite value of dynamic liquid bridge force predicted by typical expressions derived from lubrication theory for the dynamic liquid bridge, when two particles just contact.

Two dimensional computer simulations of a 'two particles head-on collision test' and 'agglomerate free falling tests' are reported. The results from the former simulation test demonstrate the effectiveness of adding viscous binder to prevent disintegration. Results of the agglomerate free falling test show that a repulsive liquid bridge force occurs between a pair of particles just about to contact. The magnitude of this repulsive force increases with a decreasing breakdown distance. It is also found that an excessive repulsive force occurs for agglomerate with too small value of breakdown distance. As a result, a range of appropriate value of the breakdown distance is recommended such that an appropriate amount of viscous effect is involved from the liquid bridge to the agglomerate system.